PUBLISHED MONTHLY

Journal of

ELECTROANALYTICAL CHEMISTRY

International Journal Dealing with all Aspects of Electroanalytical Chemistry, Including Fundamental Electrochemistry

ELSEVIER

GENERAL INFORMATION

See also Suggestions and Instructions to Authors which will be sent free, on request to the Publishers.

Types of contributions

(a) Original research work not previously published in other periodicals.
(b) Reviews on recent developments in various fields.
(c) Short communications.
(d) Bibliographical notes and book reviews.

Languages

Papers will be published in English, French or German.

Submission of papers

Papers should be sent to one of the following Editors:
Professor J. O'M. Bockris, John Harrison Laboratory of Chemistry, University of Pennsylvania, Philadelphia 4, Pa. 19104, U.S.A.
Dr. R. Parsons, Department of Chemistry, The University, Bristol 8, England.
Professor C. N. Reilley, Department of Chemistry, University of North Carolina, Chapel Hill, N.C. 27515, U.S.A.

Authors should preferably submit two copies in double-spaced typing on pages of uniform size. Legends for figures should be typed on a separate page. The figures should be in a form suitable for reproduction, drawn in Indian ink on drawing paper or tracing paper, with lettering etc. in thin pencil. The sheets of drawing or tracing paper should preferably be of the same dimensions as those on which the article is typed. Photographs should be submitted as clear black and white prints on glossy paper.
All references should be given at the end of the paper. They should be numbered and the numbers should appear in the text at the appropriate places.
A summary of 50 to 200 words should be included.

Reprints

Twenty-five reprints will be supplied free of charge. Additional reprints can be ordered at quoted prices. They must be ordered on order forms which are sent together with the proofs.

Publication

The *Journal of Electroanalytical Chemistry* appears monthly and has six issues per volume and two volumes per year, each of approx. 500 pages.

Subscription price: £ 12.12.0 or $ 35.00 or Dfl. 126.00 per year; £ 6.6.0 or $ 17.50 or Dfl. 63.00 per volume; plus postage.
Additional cost for copies by air mail available on request.
For advertising rates apply to the publishers.

Subscriptions

Subscriptions should be sent to:

ELSEVIER PUBLISHING COMPANY, P.O. Box 211, Amsterdam, The Netherlands.

JOURNAL OF ELECTROANALYTICAL CHEMISTRY
VOL. 12 (1966)

JOURNAL
of
ELECTROANALYTICAL CHEMISTRY

INTERNATIONAL JOURNAL DEALING WITH ALL ASPECTS OF ELECTROANALYTICAL CHEMISTRY, INCLUDING FUNDAMENTAL ELECTROCHEMISTRY

VOL. 12 1966

ELSEVIER PUBLISHING COMPANY

AMSTERDAM

PRINTED IN THE NETHERLANDS

CONTROLLED CHRONOPOTENTIOMETRIC STRIPPING OF METALS DEPOSITED ON THE HANGING MERCURY-DROP ELECTRODE

WIKTOR KEMULA AND JERZY W. STROJEK
Department of Inorganic Chemistry, Warsaw University, Warsaw (Poland)
(Received December 11th, 1965)

At the present time, the determination of small concentrations (10^{-6}–10^{-10} mole/l) of some elements is very important, mainly in the production of semiconductors and for the control of the purity of reagents and substances used in radiochemistry.

The last few years have brought significant advances in the development of new instrumental methods, which are often simple and rapid. Polarography is such a method but it can be used only for solutions more concentrated than 10^{-6} mole/l.

The development of other methods has lowered the determination limit even more. The square-wave polarograph enables 10^{-7} *M* solutions to be analyzed. Lower concentrations down to 10^{-9} mole/l can be determined using a polarograph connected with a hanging mercury-drop electrode (HMDE) with preliminary accumulation of metals in the electrode by pre-electrolysis[1]. This method is very simple and very sensitive, but the precision is not high and the accuracy of the results obtained varies from 10–50%. In this method, concentrations are determined from the peaks of the anodic stripping currents of metals from the amalgams formed by pre-electrolysis. There are several reasons for these comparatively high errors. One is the difficulty of

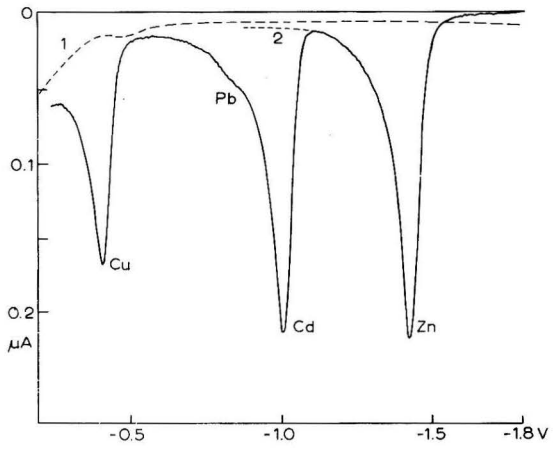

Fig. 1. Anodic chronovoltammetric stripping after 5-min pre-electrolysis time by −1.8 V. Background electrolyte, 0.1 *N* KNO_3 containing $8 \cdot 10^{-8}$ mole/l Cu^{2+}, $3 \cdot 10^{-9}$ mole/l Pb^{2+}, $8 \cdot 10^{-8}$ mole/l Cd^{2+} and $8.5 \cdot 10^{-8}$ mole/l Zn^{2+}. Stripping rate, 0.8 V/min.

the measurement of the "background" current from which the peak current is measured. The "background" current is due to the capacitive current of the discharging of the double layer of the hanging mercury electrode (which is especially significant when determining 10^{-7} mole/l or lower[2]) and also to the stripping current of the more electro-negative metals that have no time to be oxidized before the potential reaches the oxidation potential of the next metal present in the mercury drop.

Figure 1 represents a typical $I=f(U)$ curve obtained by anodic stripping of the metals accumulated in the hanging mercury drop, by cathodic pre-electrolysis. Curve 1 (dotted) represents schematically the current of the discharging of the double layer of the HMD electrode in 0.1 N KNO_3 solution. Curve 2 (dotted) shows the anodic current of zinc that would flow in the absence of cadmium ions in the solution and, consequently, cadmium atoms in the amalgam. It follows from this example, that the precise determination of anodic peak heights of cadmium and copper is possible only by applying certain corrections, while the determination of a very small quantity of lead is impossible.

THE PRINCIPLE OF THE NEW METHOD

A closer look at the processes that are taking place at the hanging mercury-drop electrode leads to the conclusion, that more accurate results can be obtained by measuring the total charge that flows during the anodic stripping instead of recording the instantaneous maximal anodic current.

The measurement of the charge corresponding to the stripping of some quantity of metal deposited initially at the hanging mercury drop is rather difficult because:

(i) the quantities of electricity flowing in such processes are in the range of 1 μC, and even lower, for concentrations lower than 10^{-7} mole/l;

(ii) the baseline with respect to which the integration has to be made is not a straight line;

(iii) the stripping time of the metal from the HMDE is rather long, and usually ranges from 1 to several minutes.

From conditions (i) and (iii) it follows that a high quality apparatus has to be used for charge measurement; its sensitivity must be high enough to enable the measurement of a hundredth part of 1 μC for full-scale deflection and its time constant should be in the range 10^4 sec. This is the reason why, in this work, the charge was not measured by means of a proper integration (relevant results will be published later), but by using some properties of the stripping process of deposited metals at the hanging mercury-drop electrode.

The shape of the peak of the $I=f(U)$ curve obtained by the chronovoltamperometric method is dependent on the rate of change of the applied potential, the initial metal concentration, the rate of metal diffusion from the bulk of the mercury drop to its surface, the rate of diffusion from the electrode of metal ions formed, the resistance of the circuit and the rate of the charge transfer in the reaction

$$Me(Hg) \rightarrow (Hg) + Me^{n+} + n\,e \qquad (1)$$

This last process is fast and the potential of the amalgam electrode is determined by the amalgam concentration and the concentration of metal ions in the solution according to the Nernst equation

$$E = E_0 + \frac{RT}{nF} \ln \frac{C_{Me^{n+}}}{C_{Me}} \quad (2)$$

An electrolytic cell with the HMD electrode (on which the metals have been deposited) can work as a cell depending on the transfer of the deposited metal into the solution.

If no current is consumed and the solution contains no oxygen or more electropositive metal ions, and the amalgam does not react with the solvent, the stripping process will not occur. If, under such conditions, after metal deposition on the hanging mercury drop, this electrode is connected to the reference electrode through a large resistor (more than 10^7 Ω, so that the stripping process is comparatively slow) the galvanic cell formed has a voltage which can be measured with an electrometer. Using such an arrangement, the initial stripping potential observed is that of the most electro-negative metal. This lasts as long as this metal is present in the electrode. Then the potential drops to the stripping potential of the next more electro-negative metal. When this metal is almost completely oxidized the potential drops to the stripping potential of the next more electro-positive metal and this is repeated until all the metals initially deposited are oxidized from the HMD electrode. The current intensity observed in the circuit of the applied constant resistor is proportional to the instantaneous voltage of the cell. Thus, the dependence of the voltage on the time, $U=f(t)$, is recorded, and the areas under each step correspond to the charges that flow during anodic stripping of the metals. The concentration measurements are simplified to the measurement of stripping times which are proportional to the length of the recorded step. This kind of measurement should be more precise than the peak-height measurement in the chronovoltammetric method. Diffusion, and some incidental resistance which in voltammetry with linearly changing potential can change the peak-height, have no effect on the stripping time.

During the stripping time, the potential of the indicator electrode is given by relation (2), so that stripping should be selective and simultaneous dissolution of different metals should not occur as in chronovoltammetry. The rate of the double-layer discharge is dependent on the resistance of the circuit and the potential. These parameters affect the steepness of potential changes on the second curve. Since the potentials at the beginning and the end of the horizontal part of each step are similar, the capacitive current is also similar.

To determine the concentrations of different ions on the basis of the recorded diagram, both the stripping times of metals and their voltage have to be taken into account. To some extent this complicates the comparison and evaluation of concentrations of different ions.

This method, which is characterized by constant resistance, can be modified in such a manner that the stripping current is the same for the stripping of all metals deposited in the HMDE. The concentrations of these ions will then be proportional only to their stripping times from the amalgam. This kind of stripping can be easily arranged if one inserts in the circuit, a current source with the voltage exceeding by two orders of magnitude the stripping voltage of the most negative metal and simultaneously increase in the same ratio (two orders of magnitude) the resistance of the circuit. Such an arrangement enables the anodic stripping to be carried out at constant current.

The experimental part of this work explores the potentialities of both these stripping methods and gives some preliminary results.

EXPERIMENTAL

Apparatus

To check the assumption given earlier in this paper, an analysis of a standard solution was carried out using both methods: (i) R = constant; (ii) I = constant.

The hanging mercury-drop electrode used had a surface area of 1.95 mm^2 and a capillary diameter equal to 0.0178 cm. A Hg–$HgNO_3$–KNO_3 electrode was used as external reference electrode. All experiments were carried out at 22°. The solutions were prepared from AnalaR reagents and doubly-distilled water. The electrolytically-generated hydrogen used was passed through hot palladium asbestos to ensure complete removal of oxygen[3]. During the electrolysis, the solutions were stirred with a magnetic stirrer. The diagram of the circuit for the recording of the stripping curves using method (i) is shown in Fig. 2. In this scheme, V denotes the dynamic electro-

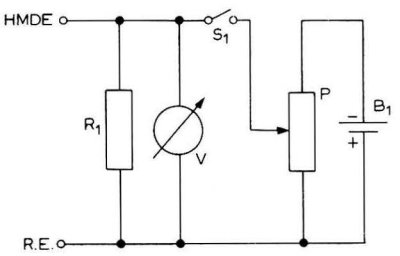

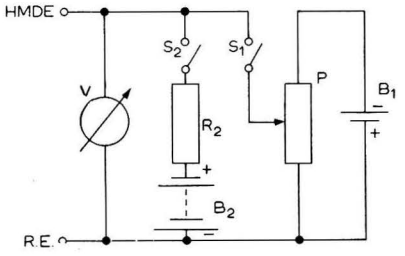

Fig. 2. Electrical circuit for R = const. stripping method. HMDE, hanging mercury drop electrode; RE, reference electrode; R_1, stripping resistor (10^8–10^9 Ω); V, electrostatic voltmeter; P, potentiometer for pre-electrolysis and stripping; B_1, 4-V battery; S_1, deposition current switch.

Fig. 3. Electrical circuit for I = const. stripping method. R_2, resistor fixing the stripping current; B_2, 50–200 V battery for stripping current; S_1, deposition current switch; S_2, stripping current switch.

meter with an input resistance 10^{15} Ω and recorder. The magnitude of the dissolution resistance, R, was dependent on the concentration of the ions in the solution and the deposition time.

Figure 3 is the schematic diagram of the circuit used for the recording of the stripping curves by method (ii).

Experiments

Using the three methods: R = constant, I = constant and $I = f(U)$ (method iii), the curves were recorded for the stripping of amalgams formed in the same solution.

The stripping curve obtained under the conditions of method (iii) is shown in Fig. 1. Before the electrolysis, the solution in the cell was de-aerated for at least 45 min, after which the HMD electrode was dipped into the solution. Under these conditions there was insufficient time for the mercury to be dissolved.

To investigate the stripping process of the amalgams using method (i), the metals investigated (Zn, Cd, Pb and Cu) were deposited initially at a constant poten-

tial of -1.8 V (the potential was applied by means of key S_1 in the stirred solution for 5 min) 30 sec after the stirring had been stopped (the time necessary for the solution to come to rest), the recorder, which followed the change of the voltage measured by voltmeter V, was switched on by disconnecting S_1. The curve shown in Fig. 4 was then recorded.

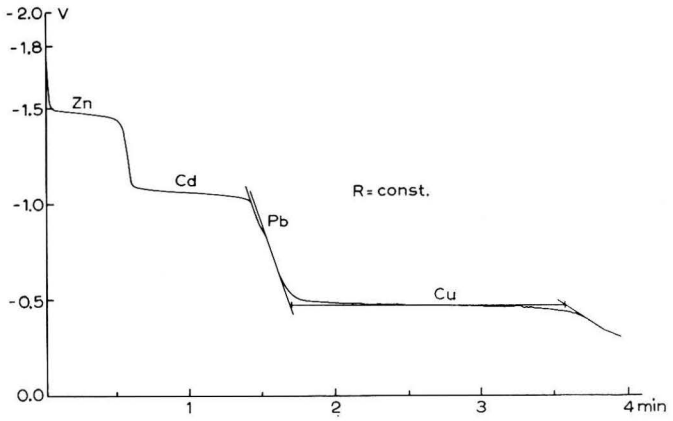

Fig. 4. Anodic stripping curve obtained by R = const. method. Pre-electrolysis time and soln. composition as in Fig. 1. $R_1 = 10^8\ \Omega$.

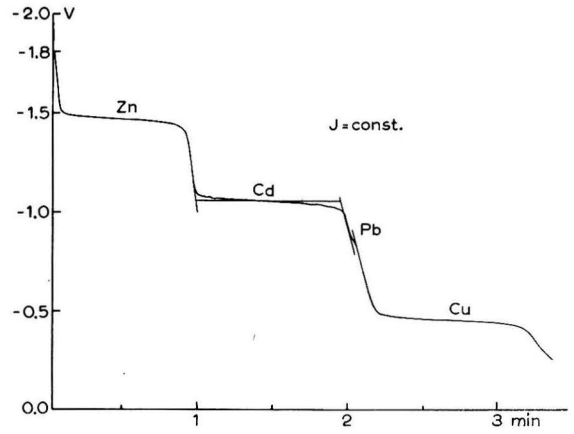

Fig. 5. Anodic stripping curve obtained by I = const. method. Pre-electrolysis time and soln. composition as in Fig. 1. $B_2 = 120$ V, $R_2 = 10^{10}\ \Omega$.

To investigate the stripping process under the conditions of method (ii), preliminary deposition (see the scheme in Fig. 3) was carried out by switching on S_1 with continuous stirring of the solution. After 5 min of deposition followed by 30 sec of rest, the recorder was switched on by S_2, disconnecting at the same time S_1. The curve recorded is given in Fig. 5.

TABLE 1

RESULTS CHARACTERIZING THE STRIPPING PROCESS OF METALS FROM AN AMALGAM, OBTAINED BY THREE DIFFERENT METHODS

Metal	*Chronovoltammetric (Method (iii))*		*R = const. (Method (i))*			*I = const. (Method (ii))*		
	Maximal stripping current (μA)	*Quantity of electricity (μC)*	*Stripping time (sec)*	*Stripping current (μA)*	*Quantity of electricity (μC)*	*Stripping time (sec)*	*Stripping current (μA)*	*Quantity of electricity (μC)*
Cu	0.150	1.18	112	0.23	2.58	58	0.42	2.44
Cd	0.206	1.70	49	0.52	2.55	58	0.42	2.44
Zn	0.213	1.89	30	0.72	2.16	51	0.42	2.14

DISCUSSION

The experiments carried out confirm the validity of the conclusions given in the introductory part of this paper. The curves obtained (Fig. 4, method (i) and Fig. 5, method (ii)) had well-defined steps so that the determination of the stripping time was easy and precise.

The sensitivity of these methods is evident if one compares the lead stripping step on these curves with that obtained by the chronovoltammetry method shown in Fig. 1.

The measurement of the stripping time was graphical and analogous to that used in polarography. The steep parts of the curve, more or less parallel to the potential axis, were extended and the line between these lines parallel to the time axis in the middle of the curve was taken as the stripping time.

The reproducibility of numerous experimental curves was good and the error did not exceed 2%. The accuracy of the stripping time determination varies from 1–5% depending on the length of step. The precision of the concentration determination by these methods was 2–10%. To obtain this accuracy, only reaction (1) should take place at the electrode. This condition is usually fulfilled, when there is no oxygen and no mercury ions in the solution. The presence of oxygen in the solution leads to uncontrolled stripping of the deposited metals, probably according to the equation

$$Me^{II}(Hg) + O + H_2O \rightarrow (Hg) + Me^{2+} + 2\ OH^- \qquad (3)$$

This reaction lowers the results or even makes proper results impossible by lowering the stripping time of metals.

Similarly, mercury ions react with the metals in the amalgam

$$Me^{II}(Hg) + Hg^{2+} \rightarrow Hg + Me^{2+} \qquad (4)$$

and, consequently, the content of the metals in the amalgam is lowered, and the stripping time is shortened. For this reason oxygen should be removed, and the use of an external reference electrode is advised. The HMD electrode should be dipped into the solution after de-aeration of the solution[4].

The other more electro-positive metal ions present in the solution can act in the same way as mercury ions with other more electro-negative metals deposited in the HMD electrode. For example, if zinc is deposited at the mercury electrode, and the solution contains cupric ions, the following reaction can take place:

$$Zn(Hg) + Cu^{2+} \rightarrow Cu(Hg) + Zn^{2+} \qquad (5)$$

and the quantitative result is dependent on the time of interaction. Consequently the stripping time for zinc would be shorter, and that of copper increased, owing to the uncontrolled substitution. To diminish the effect of such reactions, the ratio of the flux of dissolved ions to the flux of deposited ions should be as high as possible (about 100). This means that the deposition of metal should be carried out rather intensively in vigorously stirred solutions and the oxidation current should be comparatively high. The effect of ions present in the solution that can interact with the metals of the amalgam is decreased by carrying out the oxidation process in quiet solution.

The stripping time of a metal, *e.g.* Zn, depends on the value of the circuit resistance, R, or on the current, I. At the end of the stripping time a trace of the metal

remains in the amalgam depending on R and I, but is no longer potential-determining. In this case, it strips with the following more electropositive metal. This correction can be reduced by suitable choice of R and I.

It was said in the introduction that the process of metal stripping can be characterized by the quantity of electricity that flows in the time of metal stripping from the amalgam into the solution. This charge can be calculated from the curves obtained by the three methods mentioned (Figs. 1, 4 and 5). The graphs of the stripping of Cu, Cd and Zn from the amalgam obtained by methods (i) and (ii) were made under the same conditions (Figs. 4 and 5). The quantities of electricity recorded can be compared with the result obtained by the chronovoltammetric method. Table 1 contains all data necessary for this calculation. The quantity of electricity in the chronovoltammetric method was calculated from the area between the stripping curve and the base line. In methods (i) and (ii) these calculations were simpler; the stripping current was multiplied by the stripping time. The current in method (i) was calculated by multiplying the stripping resistance, R_1, by the mean stripping voltage of each type of ion. In method (ii), the current was measured directly. From these data it follows that the agreement of results is better in methods (i) and (ii); the results obtained by the chronovoltammetric methods were lower. It can be assumed, that at the given scan rate (0.8 V/min) only part of each metal was dissolved from the amalgam. This behaviour is most evident in the copper stripping.

SUMMARY

New schemes for R = constant and I = constant, of the stripping of amalgams formed by electrodeposition of metals at the HMDE have been described. Using these methods concentrations as low as 10^{-9} mole/l can be precisely (2–10%) determined. Especially recommended is the I = constant method, where the stripping times are proportional to the concentrations of deposited metals and, consequently, to the concentrations of these metal ions in the solution.

Further investigations concerned with the problem of exchange of ions and adaptation of methods for analytical purposes are in progress.

REFERENCES

1 W. KEMULA, in I. LONGMUIR (ed.), *Advances in Polarography*, Vol. 1, Pergamon Press, London, 1960, p. 105. W. KEMULA AND Z. KUBLIK, *Advan. Anal. Chem. Instr.*, 2 (1963) 123.
2 W. KEMULA AND J. W. STROJEK, *Chem. Anal. Warsaw*, 10 (1965) 1327.
3 W. KEMULA AND R. SIODA, *Chem. Anal. Warsaw*, 8 (1963) 629.
4 W. KEMULA, *Microchem. J.*, in press.

OHMIC DROP DISTORTION OF ANODIC STRIPPING CURVES FROM A THIN MERCURY-FILM ELECTRODE

W. T. DE VRIES AND E. VAN DALEN
Department of Chemistry, The Free University, Amsterdam (The Netherlands)
(Received September 14th, 1965)

INTRODUCTION

The theory of anodic stripping voltammetry with a plane, thin mercury-film electrode assumes the potential of the working electrode to be a linear function of time[1,2]. This theory is related to that of linear-sweep voltammetry under conditions of semi-infinite linear diffusion. It has been shown recently[3,4] that uncompensated ohmic drop, which makes the working electrode potential sweep non-linear, deforms the linear-sweep polarogram, and thus can cause errors in analytical measurements and in diagnosis of reaction kinetics.

The question then arises as to the effects of uncompensated ohmic drop on anodic stripping curves from a thin mercury-film electrode, and a study of these effects is presented below.

MODIFICATION OF BOUNDARY CONDITION; EQUATION FOR THE FLUX

The derivation of formulae will be illustrated using the exact solution[2] although for pairs of values of sweep rate and mercury-film thickness lying in the region where the approximate solution gives nearly correct results, this approximate solution can be used. However, derivation of the corresponding formulae will not be given here, as it is strictly analogous to the derivation of the exact solution.

The differential equations and the initial and boundary conditions are given in ref. 2 but the boundary condition expressing the linear potential change of the working electrode (ref. 2, eqn. (4)) should be changed to

$$C_O(0, t) = \theta\varepsilon(t) \cdot C_R(0, t) \,, \tag{1}$$

with

$$\varepsilon(t) = \exp\left[\sigma t - \frac{n^2 F^2}{RT} A\Omega q(t)\right]. \tag{2}$$

Derivation of the expression for $\varepsilon(t)$ is analogous to that of eqn. (3), ref. 4. A is the electrode area in cm^2, Ω the sum of the resistances that contribute to the uncompensated ohmic drop, and $q(t)$ the flux of electroactive species at the electrode surface in mol cm^{-2} sec^{-1}. The other symbols used in this paper have the meaning given earlier[2]. We have thus neglected the capacity current, and this will be justified below.

Taking into account the modification of this boundary condition, it is easily verified that the recursive current–potential curve equation is now given by:

$$q_j = \frac{\frac{3}{4}C^0\sqrt{\frac{\pi D_R}{\delta}}\left(1-\frac{1}{\varepsilon(j,q_j)}\right)-\left(1+\frac{1}{\theta\varepsilon(j,q_j)}\right)\sqrt{\frac{D_R}{D_O}}\,S_1-\frac{3}{2}S_2}{\frac{3}{2}(A_1-B_1)+1+\frac{1}{\theta\varepsilon(j,q_j)}\sqrt{\frac{D_R}{D_O}}} = \Phi(j,q_j)\,, \qquad (3)$$

with

$$\varepsilon(j,q_j)=\exp\left[j\sigma\delta-\frac{n^2F^2}{RT}A\Omega q_j\right], \qquad (4)$$

and where q_j is the flux at time $t=j\delta$ at the electrode surface[2].

From the forms of eqns. (2) and (3) it can be deduced that, given a pair of values of D_R and D_O, a distorted anodic stripping curve can be characterized by l, the mercury-film thickness, $n\times v$ (*i.e.*, n-times sweep rate) and $n(i_p'\Omega)$, n-times the maximal value of the appearing ohmic drop (i_p' is the peak current).

NUMERICAL CALCULATION OF DISTORTED ANODIC STRIPPING CURVES

Evaluation of eqn. (3) has been carried out by straightforward iteration[4], using q_{j-1} as the first approximation to be substituted into the right-hand side of eqn. (3). The iteration then follows the scheme

$$q_{j,0}=\Phi(j,q_{j,-1})\,,$$

$$q_{j,1}=\Phi(j,q_{j,0})\,,$$

$$q_{j,2}=\Phi(j,q_{j,1})\,,\ \text{etc.},$$

which process is continued until successive approximations differ very little. However, this method of computation is only applicable if

$$\left|D^1(j,q_j)\right|=\left|\frac{\mathrm{d}}{\mathrm{d}q_j}\Phi(j,q_j)\right|<1\,,$$

for only then will the series $q_{j,0}, q_{j,1}, q_{j,2}, \ldots$ converge to the limit q_j.

When straightforward iteration was not possible, the well-known Newton–Rhapson iteration method has been used[5]. This method was also used by NICHOLSON[3], and is to be preferred to our method of bisection used earlier[4]; moreover, since the convergence to the sought value, q_j, improves during the computation of successive approximations, the Newton–Rhapson method is sometimes more rapid than straightforward iteration, especially when $|D^1(j,q_j)|$ is not very small.

From the principle of the Newton–Rhapson method it follows that the following formula holds, when $q_{j,-1}$ is used as the first approximation:

$$q_{j,0}=q_{j,-1}-\frac{\Phi(j,q_{j,-1})-q_{j,-1}}{D^1(j,q_{j,-1})-1}\,,$$

and a better approximation to q_j is

$$q_{j,1} = q_{j,0} - \frac{\Phi(j, q_{j,0}) - q_{j,0}}{D^1(j, q_{j,0}) - 1},$$

and this process is continued until successive approximations differ very little.

The numerical calculations have been programmed in ALGOL-60 for computation with a digital computer in accordance with the above equations. Also, a program has been written based on formulae derived from the approximate solution[1], and this has been used for calculations with appropriate combinations of values of sweep rate and mercury-film thickness, where the approximate solution gives nearly correct results[2]. Copies of both programs are available from the authors on request. The values used for the various numerical constants are the same as those used earlier[1].

RESULTS AND DISCUSSION

(a) *Results of the calculations*

Figure 1 shows the rather exaggerated case of an anodic stripping curve (for a reaction $M^0 \rightarrow M^{2+} + 2e$) distorted by uncompensated ohmic drop with a maximal value of 33.6 mV. The curve (b) is plotted *versus* applied cell voltage, as it would appear when registered with an *X-t* recorder. The corresponding undistorted curve

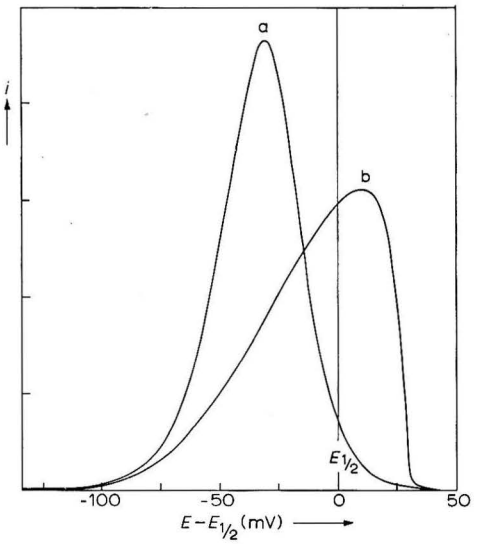

Fig. 1. Distortion of an anodic stripping curve by ohmic drop. Electrode reaction is $M^0 \rightarrow M^{2+} + 2e$. Sweep rate, 1/8 $Vmin^{-1}$; mercury-film thickness, 10 μ. (a), no ohmic drop; (b), appearing maximal ohmic drop 33.6 mV.

(a) is also shown. In this case, the *corrected* peak potential is shifted from -31.0 to -23.0 mV, and the width at half height is increased from 37.8 to 62.2 mV. The height of the distorted peak is 67.2% of that of the undistorted one, *i.e.*, a percentage decrease of 32.8.

It thus appears that the effect of uncompensated ohmic drop is qualitatively the same as in the case of linear-sweep voltammetry under conditions of semi-infinite linear diffusion. The height of the peak is decreased, the corrected peak potential is shifted towards more positive values, and the width is increased. The error in peak height as measured by percentage decrease in peak current, however, is much larger for a mercury-film electrode than for the case of semi-infinite linear diffusion ("normal" linear-sweep voltammetry). In the latter case, an uncompensated maximal ohmic drop of 33.6 mV for a two-electron electrode reaction causes a percentage decrease of 13.7; in the case depicted in Fig. 1 the error is thus 2.4 times larger.

The effect of uncompensated ohmic drop on peak current is shown in more detail in Fig. 2, where the ratio i_p'/i_p (i_p is the peak current in absence of ohmic drop) is plotted *versus* n-times maximal ohmic drop, for several values of l, the mercury-film thickness, and $n \times v$, n-times sweep rate. Also shown in the figures is the corresponding curve for the case of semi-infinite linear diffusion.

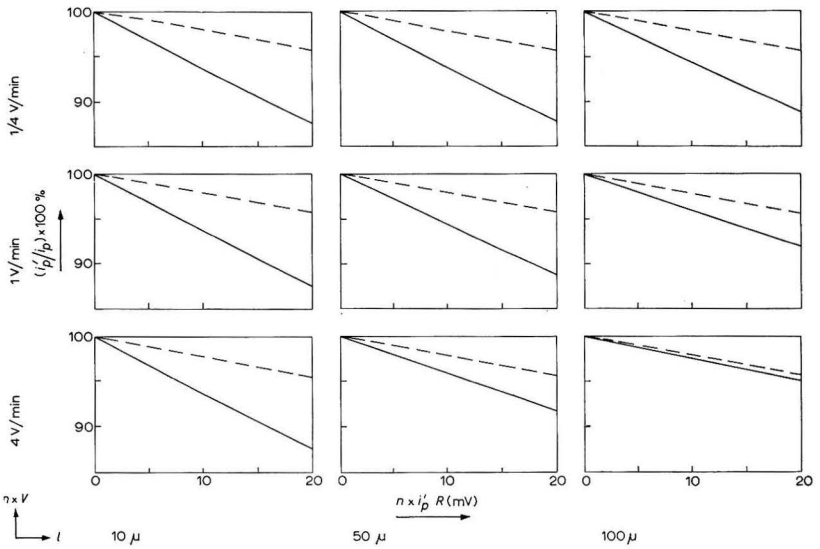

Fig. 2. Ratio i_p'/i_p plotted *vs.* n-times appearing maximal ohmic drop, for several values of l, the mercury-film thickness, and $n \cdot v$, n times sweep rate (——). The other curve in the figures (– – – –) pertains to the case of semi infinite linear diffusion.

It can be inferred that for slow sweep rates and thin mercury-films the percentage decrease in peak current can be 2.5–3 times larger than in "normal" linear-sweep voltammetry. As can be expected, the i_p'/i_p-curve for a mercury-film electrode approaches that for "normal" linear-sweep voltammetry with increasing l and/or v.

The effects of ohmic drop on peak potential and width at half height have the same trends as in "normal" linear-sweep voltammetry. However, anodic stripping voltammetry has not yet found extensive use for investigating electrode reaction kinetics, and it is doubtful whether it will ever find general use for such purposes. Therefore we have not presented these (rather minor) effects.

We have checked the results of our calculations in two ways. First, when such pairs of values of l and v were used that the resulting stripping peak was indistinguishable from the case of semi-infinite linear diffusion[2], the results of the ohmic drop calculations were the same, within computational error, as those reported earlier[4]. Secondly, also in the ohmic drop calculations, the exact and the approximate solutions agreed very well for not too high values of v and l (ref. 2, Fig. 4).

From the general properties of anodic stripping curves from a thin mercury-film electrode it is apparent that the characteristic advantages of a mercury-film electrode are only retained when the sweep rate is not too high, *e.g.*, below 4 V/min. Thus, the low sweep rates generally used in anodic stripping voltammetry cause the capacity current to be only a small fraction of the faradaic current due to the dissolution of the reduced metal, and this justifies our neglect of the capacity current in our theoretical treatment.

(*b*) *Practical considerations*

Because uncompensated ohmic drop can have a very large effect on the peak current, it is necessary to keep it small. In order to obtain reliable results, ohmic drop should preferably be smaller than $5/n$ mV, and certainly not be more than $10/n$ mV. In general, this objective can be easily achieved when a plane mercury-film electrode is used in a three-electrode arrangement[6], provided that the electrode area is not excessively small[4,7].

Calculation of the effects of ohmic drop on linear-sweep polarograms has not yet been accomplished for the case of semi-infinite spherical diffusion, nor for that of a mercury-plated spherical micro-electrode, or a very small mercury-drop electrode. When used in anodic stripping voltammetry, the latter two electrodes will be virtually depleted of reduced metal when oxidation is effected with slow potential scans. However, it can be safely assumed that in these two cases the effect of ohmic drop on peak current is also large, analogous to the case investigated above.

From this it can be concluded that a combination of a spherical (mercury-drop or mercury-plated) microelectrode and large peak currents will make it difficult to obtain measurements unaffected by uncompensated ohmic drop, because it is difficult to compensate for ohmic drop occurring in the solution around a spherical micro-electrode[7].

ACKNOWLEDGEMENTS

The authors wish to express their thanks to Dr. J. A. ZONNEVELD of the computation Department of the Mathematical Centre, Amsterdam, for making available the electronic computer XI for the lengthy numerical calculations.

This work has been carried out with financial support from the Netherlands Organization for the Advancement of the Pure Research (Z.W.O.).

SUMMARY

An exact treatment of the effect of uncompensated ohmic drop on anodic stripping curves from a plane, thin mercury-film electrode is given. The decrease in peak current caused by the ohmic drop can be 2.5–3 times larger than in the corre-

sponding case of semi-infinite linear diffusion ("normal" linear-sweep voltammetry). Practical implications of the results, as well as the case of spherical micro-electrodes, are discussed briefly.

REFERENCES

1 W. T. DE VRIES AND E. VAN DALEN, *J. Electroanal. Chem.*, 8 (1964) 366.
2 W. T. DE VRIES, *J. Electroanal. Chem.*, 9 (1965) 448.
3 R. S. NICHOLSON, *Anal. Chem.*, 37 (1965) 667.
4 W. T. DE VRIES AND E. VAN DALEN, *J. Electroanal. Chem.*, 10 (1965) 183.
5 H. MARGENAU AND G. M. MURPHY, *The Mathematics of Physics and Chemistry*, D. Van Nostrand Company, Inc., New York, 1956, p. 492.
6 W. M. SCHWARZ AND I. SHAIN, *Anal. Chem.*, 35 (1963) 1770.
7 W. B. SCHAAP AND P. S. MCKINNEY, *Anal. Chem.*, 36 (1964) 1251.

ADSORPTION ET IMPEDANCE FARADIQUE

I. ETUDE THEORIQUE

A. M. BATICLE ET F. PERDU
Laboratoire d'Electrolyse du C.R.N.S., 1, Place Aristide Briand, Bellevue, Seine et Oise (France)
(Reçu le 6 août, 1965)

INTRODUCTION

Il a été constaté expérimentalement que le déphasage courant–tension, en régime sinusoïdal, à l'interface électrode–solution, peut être supérieur à 45°, dans un grand domaine de basses fréquences, lorsque la réaction électrochimique se produit entre des espèces actives adsorbées à l'électrode. Lorsqu'il n'y a pas adsorption, spécifique ou non spécifique, des espèces actives, l'angle de phase est toujours inférieur à 45°.

L'introduction d'une étape d'adsorption dans la relation potentiel/courant a conduit quelques auteurs[1–7] à des impédances complexes quelque peu différentes les unes des autres. Dans ces études le calcul est toujours fait sur la base d'une isotherme d'adsorption, sauf refs. 6 et 7. Certains supposent que le transfert de charges se fait uniquement par l'intermédiaire des espèces électroactives dans l'état adsorbé[2,5,7], d'autres admettent un transfert de charges par l'intermédiaire de toutes les espèces, adsorbées ou non[1,3,4].

LAITINEN ET RANDLES[1], LLOPIS, FERNANDEZ-BIARGE ET PEREZ-FERNANDEZ[2] montrent que, moyennant certaines hypothèses simplificatrices, l'adsorption est représentée par une résistance et une capacité, toutes deux indépendantes de la fréquence, ajoutées différemment au schéma représentatif de la réaction. Les éléments d'impédance sont obtenus par approximations successives.

BARKER[3] a établi un schéma équivalent apériodique où l'adsorption est encore représentée par des capacités et des résistances indépendantes de la fréquence.

LORENZ ET SALIE[4] proposent un mécanisme très général et, dans des cas particuliers, utilisent des expressions de l'impédance globale $R_r - j/\omega C_r$, aux basses fréquences en se servant des limites des courbes $tg\,\theta = 1/\omega R_r C_r$ en fonction de $\omega^{\frac{1}{2}}$ et $(R_r - 1/\omega C_r)$ en fonction de $\omega^{-\frac{1}{2}}$, lorsque $\omega \to 0$.

KASTENING et ses collaborateurs[5] obtiennent un schéma représentatif analogue à celui de SENDA ET DELAHAY[7], dont les éléments ont des significations un peu différentes par suite des hypothèses de départ un peu différentes. N'utilisant que les valeurs expérimentales de $cotg\,\theta$, ces auteurs[5] sont amenés à négliger certains termes et à chercher le bon accord entre les valeurs expérimentales et les formes analytiques simplifiées.

SLUYTERS-REHBACH et ses collaborateurs[6] ayant observé un comportement anormal de l'impédance d'une cellule électrochimique en présence des ions Tl^+ sont

amenés à tenir compte de l'adsorption de ces ions par une capacité indépendante de la fréquence et fonction du potentiel, ajoutée à la capacité de double couche.

L'impédance proposée par SENDA ET DELAHAY[7] semble la plus générale, aucune hypothèse sur l'isotherme d'adsorption n'ayant été admise et l'adsorption des deux espèces actives ayant été examinée. Mais à notre connaissance, cette théorie n'a pas reçu de confirmation expérimentale.

Dans la première partie de ce travail, nous proposons la suite de calculs nécessaires pour passer des grandeurs mesurées à l'impédance théorique établie par SENDA ET DELAHAY. Nous montrons comment, à partir des valeurs expérimentales, il est possible de déterminer quels sont les processus coexistant à l'électrode, et de calculer les paramètres cinétiques de ces différents processus. Dans la deuxième partie qui sera publiée ultérieurement, nous utiliserons ces calculs pour exploiter nos résultats expérimentaux.

REPRÉSENTATION DE L'IMPÉDANCE D'UNE RÉACTION ÉLECTROCHIMIQUE

Considérons la réaction électrochimique $O+ne \rightleftarrows R$ qui s'effectue selon le schéma suivant:

$$C_R^0 \underset{\text{diffusion}}{\rightleftarrows} C_R^* \overset{\text{adsorption}}{\underset{\text{désorption}}{\rightleftarrows}} \Gamma_R \overset{\text{transfert}}{\underset{\text{de charges}}{\rightleftarrows}} \Gamma_O \overset{\text{désorption}}{\underset{\text{adsorption}}{\rightleftarrows}} C_O^* \underset{\text{diffusion}}{\rightleftarrows} C_O^0 \qquad (1)$$

Elle comprend trois processus partiels: diffusion, adsorption, transfert de charges. Nous admettons que le transfert de charges n'a lieu que par l'intermédiaire des espèces adsorbées, lorsque l'adsorption existe. Il a été montré par SENDA ET DELAHAY[7,8], que, dans ce cas, l'impédance faradique, à l'interface électrode solution, peut être représentée par le schéma de la Fig. 1. Pour cela deux hypothèses ont été nécessaires:

(a) les deux processus d'adsorption des espèces O et R sont indépendants;

(b) la variation de Γ avec le potentiel influe beaucoup moins sur le processus d'adsorption que sur le processus de transfert de charges.

L'indice, i, représentant une espèce active O ou R, les éléments du schéma de la Fig. 1 sont définis comme suit:

$$\text{(diffusion) } R_{di} = 1/\omega C_{di} = \sigma_i \omega^{-\frac{1}{2}} \qquad (2)$$

$$\sigma_i = RT/n^2F^2C_i^0\sqrt{2D_i} \qquad (3)$$

$$\text{(transfert de charges) } R_t = (RT/nF)(1/I_a^0) \qquad (4)$$

$$= RT/n^2F^2k_a^0(C_R^0)^\alpha(C_O^0)^{1-\alpha}$$

$$\text{(adsorption spécifique) } R_{ai} = (RT/n^2F^2)[1/(\partial\Phi_{ai}/\partial C_i^0)](1/C_i^0) \qquad (5)$$

$$1/\omega C_{ai} = (1/\omega)(RT/n^2F^2)[1/(\partial\Gamma_i/\partial C_i^0)](1/C_i^0) \qquad (6)$$

I_a^0 est le courant d'échange apparent de la réaction,
D_i est le coefficient de diffusion de l'espèce i,
Φ_{ai} est le flux de substance adsorbée,
C_i^0 est la concentration de l'espèce i au sein des phases,
Γ_i est la concentration superficielle de l'espèce i adsorbée.

Lorsqu'une seule espèce est adsorbée, le schéma se simplifie en annulant R_{ai} et C_{ai} correspondant à l'autre espèce.

En l'absence d'adsorption spécifique, la répulsion ou l'attraction électrostatique des ions dans la double couche par la surface chargée de l'électrode, sont représentées respectivement par des résistances R_{si} ou des capacités C_{si} placées comme les résistances ou les capacités d'adsorption mais dont les valeurs sont données par[8]:

$$R_{si} = (RT/n^2F^2)\ (1/C_i^0)\ (\xi_i/KD_i) \tag{7}$$

$$1/\omega C_{si} = (1/\omega)\ (RT/n^2F^2)\ (K/C_i^0\xi_i) \tag{8}$$

$1/K$ est l'épaisseur de la partie diffuse de la double couche,

ξ_i est une fonction de la charge de l'électrode, de la charge des ions électroactifs ainsi que de celle des ions de l'électrolyte-support.

La mesure de l'impédance d'une cellule électrochimique, en courant sinusoïdal, dans les conditions classiques, (électrolyte-support ajouté aux espèces électroactives, contre-électrode de très grandes dimensions) est représentée, pour chaque fréquence, par le circuit de la Fig. 2, dans lequel R_E et C_E sont respectivement la résistance de

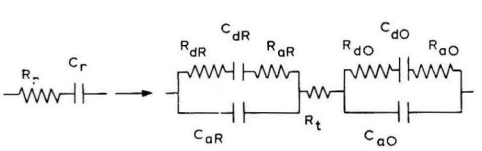

Fig. 1. Schéma représentatif de l'impédance faradique d'une réaction comprenant diffusion, adsorption des deux espèces O et R, transfert de charges.

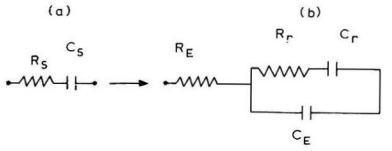

Fig. 2. Impédance globale mesurée.

l'électrolyte et des connexions, et la capacité de double-couche. Après soustraction de ces deux dernières valeurs, on obtient, pour chaque fréquence, les grandeurs R_r et C_r qui représentent l'impédance série équivalente au schéma de la Fig. 1, et que nous utilisons dans la suite de cet exposé.

Nous avons calculé les éléments de l'impédance série $R_r - j/\omega C_r$. En posant:

$$\begin{aligned} a_i &= \sigma_i\omega^{-\frac{1}{2}} + R_{ai} \\ b_i &= \sigma_i\omega^{-\frac{1}{2}} + 1/C_{ai}\omega \end{aligned} \tag{9}$$

nous avons obtenu:

$$R_r = R_t + \Sigma[a_i/(C_{ai}^2\omega^2)\ (a_i^2 + b_i^2)] \tag{10}$$

$$1/\omega C_r = \Sigma(1/\omega C_{ai}) - \Sigma[b_i/(C_{ai}^2\omega^2)\ (a_i^2 + b_i^2)] \tag{11}$$

et $\operatorname{cotg}\theta = R_rC_r\omega$: (12)

$$\operatorname{cotg}\theta = \frac{R_tC_{aO}^2C_{aR}^2\omega^2(a_R^2+b_R^2)(a_O^2+b_O^2) + a_OC_{aR}^2(a_R^2+b_R^2) + a_RC_{aO}^2(a_O^2+b_O^2)}{(\Sigma C_{ai})(C_{aO}C_{aR}\omega)(a_R^2+b_R^2)(a_O^2+b_O^2) - b_OC_{aR}^2(a_R^2+b_R^2) - b_RC_{aO}^2(a_O^2+b_O^2)}$$

Dans toutes les équations les sommes Σ sont étendues aux espèces O et R.

NATURE DES PROCESSUS PARTIELS DE LA RÉACTION: FORME DE LA COURBE cotg θ EN FONCTION DE $\omega^{\frac{1}{2}}$

La forme de la courbe cotg θ, en fonction de $\omega^{\frac{1}{2}}$, dépend à la fois de la nature des processus partiels de la réaction et des grandeurs relatives de ces différents processus. L'examen de l'expression (12) amène à dégager certaines formes caractéristiques qui permettront, à la vue des courbes expérimentales, de déterminer l'existence ou non des processus envisagés dans la réaction (1). Considérons l'expression (12) de cotg θ. Au voisinage de zéro et de l'∞, cette expression est équivalente aux premiers termes de son développement en série.

Lorsque $\omega \to 0$, on a:

$$\operatorname{cotg} \theta_{(\omega \to 0)} = 1 + \omega^{\frac{1}{2}}[(R_t + \Sigma R_{ai} - 2\Sigma C_{ai}\sigma_i^2) \cdot \Sigma (1/\sigma_i)] + 4\omega \Sigma[\sigma_i C_i(\sigma_i^2 C_{ai} - R_{ai}) \cdot \Sigma(1/\sigma_i)] \quad (13)$$

et la pente à l'origine de la courbe cotg $\theta/\omega^{\frac{1}{2}}$ est alors:

$$[\mathrm{d}(\operatorname{cotg} \theta)/\mathrm{d}(\omega^{\frac{1}{2}})]_{\omega \to 0} = (R_t + \Sigma R_{ai} - 2\Sigma \sigma_{ai}\sigma_i^2) \cdot \Sigma(1/\sigma_i) \quad (14)$$

Cette pente sera positive dans les cas ne comportant pas de termes réactifs C_{ai} ou C_{si}, et positive ou négative dans les autres cas selon que:

$$R_t + \Sigma R_{ai} \gtrless 2\Sigma C_{ai}\sigma_i^2 \quad (15)$$

Lorsque ω croît, aux fréquences moyennes, la courbe présentera une concavité positive s'il existe des termes réactifs C_{ai} ou C_{si}, et sera une droite dans les autres cas.

Aux très basses fréquences, lorsque la pente à l'origine est positive, la courbe cotg $\theta/\omega^{\frac{1}{2}}$ peut, dans certains cas, présenter un maximum, et, par suite, couper la droite cotg $\theta = 1$ en 0 et 1 ou 2 points différents de $\omega = 0$, selon les valeurs relatives des éléments d'impédance.

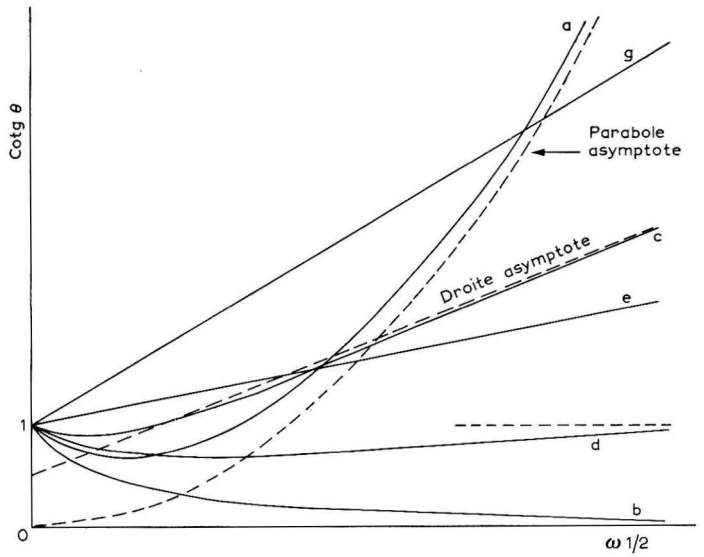

Fig. 3. Variations de cotg $\theta/\omega^{\frac{1}{2}}$ suivant la nature des processus existant à l'électrode.

Lorsque $\omega \to \infty$ les limites sont essentiellement différentes suivant les processus existants à l'éléctrode.

(a) Cas général comportant diffusion, adsorption spécifique des deux espèces actives O et R et transfert de charges (Fig. 3a).

$$\operatorname{cotg} \theta_{(\omega\to\infty)} = \omega[R_t/\Sigma(1/C_{ai})] + \omega^{-\frac{1}{2}}[R_t/\Sigma(1/C_{ai})^2] \cdot \Sigma[\sigma_i/R_{ai}{}^2C_{ai}{}^2] \tag{16}$$

La courbe cotg $\theta/\omega^{\frac{1}{2}}$, lorsque $\omega \to \infty$, admet pour asymptote la parabole (16') cotg $\theta = \omega R_t/\Sigma(1/C_{ai})$, passant par l'origine et d'axe $\omega = 0$.

(b) Diffusion, adsorption spécifique des deux espèces O et R, transfert de charges infiniment rapide: $R_t = 0$ (Fig. 3b).

$$\operatorname{cotg} \theta_{(\omega\to\infty)} = \omega^{-1}[1/\Sigma(1/C_{ai})] \cdot [1/\Sigma(R_{ai}C_{ai}{}^2)] \to 0 \tag{17}$$

Lorsque $\omega \to \infty$ la courbe cotg $\theta/\omega^{\frac{1}{2}}$ tend vers la droite cotg $\theta = 0$.

(c) Diffusion, adsorption spécifique d'une seule espèce, O par exemple, $C_{aR} = R_{aR} = 0$, transfert de charges (Fig. 3c).

$$\operatorname{cotg} \theta_{(\omega\to\infty)} = 1 - (R_t/\sigma_R{}^2C_{a0}) + (R_t/\sigma_R)\omega^{\frac{1}{2}} \tag{18}$$

Lorsque $\omega \to \infty$ la courbe cotg $\theta/\omega^{\frac{1}{2}}$ tend vers la droite définie par l'éqn. (18).

(d) Diffusion, adsorption spécifique d'une seule espèce, O par exemple, transfert de charges infiniment rapide: $R_{aR} = C_{aR} = R_t = 0$ (Fig. 3d).

$$\operatorname{cotg} \theta_{(\omega\to\infty)} = 1 - \omega^{-\frac{1}{2}}(1/\sigma_R C_{a0}) + \omega^{-1}(1/\sigma_R{}^2C_{a0}{}^2) \to 1 \tag{19}$$

La courbe cotg $\theta/\omega^{\frac{1}{2}}$ tend, pour $\omega \to \infty$, vers la droite cotg $\theta = 1$, par valeurs inférieures à 1.

(e) Diffusion et transfert de charges. Pas d'adsorption spécifique. $R_{aR} = C_{aR} = R_{a0} = C_{a0} = 0$ (Fig. 3e).

La courbe cotg $\theta/\omega^{\frac{1}{2}}$ est la droite d'éqn. (20), bien connue dans les mesures d'impédance faradique.

$$\operatorname{cotg} \theta = 1 + \omega^{\frac{1}{2}}(R_t/\Sigma\sigma_i) \tag{20}$$

(f) Diffusion et transfert de charges avec attraction électrostatique d'une ou des deux espèces O et R: $R_{a0} = R_{aR} = 0$, $C_{a0} = C_{s0}$, $C_{aR} = C_{sR}$.

$$\begin{aligned}\operatorname{cotg} \theta_{(\omega\to\infty)} = {} & \omega[R_t/\Sigma(1/C_{si})] + \omega^{\frac{1}{2}}R_t \cdot [\Sigma(1/\sigma_i C_{si}{}^2)]/2[\Sigma(1/C_{si})]^2 \\ & + R_t[\Sigma(1/\sigma_i C_{si})]^2/4[\Sigma(1/C_{si})]^2\end{aligned} \tag{21}$$

L'allure générale de la courbe cotg $\theta/\omega^{\frac{1}{2}}$ est la même que celle de la Fig. 3a mais la parabole asymptote d'éqn. (21) est différente de la parabole asymptote d'éqn. (16').

(g) Diffusion et transfert de charges avec répulsion électrostatique d'une ou des deux espèces O et R: $C_{a0} = C_{aR} = 0$ (Fig. 3g).

La courbe cotg $\theta/\omega^{\frac{1}{2}}$ est une droite dont la pente est différente de celle du cas (e):

$$\operatorname{cotg} \theta = 1 + \omega^{\frac{1}{2}}[(R_t + \Sigma R_{si})/\Sigma\sigma_i)] \tag{22}$$

Si $R_t = 0$, on a une droite de pente $\Sigma R_{si}/\Sigma\sigma_i$.

(h) Diffusion, attraction électrostatique d'une ou des deux espèces O et R, transfert de charges infiniment rapide: $R_{aR} = R_{a0} = R_t = 0$.

L'allure générale de la courbe est la même que celle de la Fig. 3b, mais pour $\omega \to 0$ la pente est toujours négative.

$$\operatorname{cotg} \theta_{(\omega\to\infty)} = \omega^{-\frac{1}{2}}[\tfrac{1}{2}\Sigma(1/C_{ai}\sigma_i{}^2)/\Sigma(1/C_{ai})] \to 0 \tag{23}$$

$$\operatorname{cotg} \theta_{(\omega\to 0)} = 1 - \omega^{\frac{1}{2}}[(2\Sigma C_{ai}\sigma_i{}^2)/\Sigma\sigma_i)] \tag{24}$$

La comparaison des courbes de la Fig. 3 et des courbes expérimentales permettra donc de déterminer la nature des phénomènes intervenant dans la réaction étudiée.

CALCUL DES PARAMÈTRES CINÉTIQUES DES PROCESSUS PARTIELS DE LA RÉACTION

Si l'expression analytique de $\cot g\,\theta$ nous a permis de différencier qualitativement un certain nombre de processus participant à la réaction, elle ne peut être utilisée pour séparer tous les paramètres de la réaction. Cette détermination pourra s'effectuer à l'aide des éléments de l'impédance série équivalente, R_r et $1/\omega C_r$, en utilisant leurs valeurs aux différentes fréquences (Fig. 4). Aux très hautes et très basses fréquences, lorsque $\omega \to 0$ ou $\omega \to \infty$, les expressions de R_r et $1/\omega C_r$ sont équivalentes à leurs développements limités. Nous examinerons successivement les cas (a)–(h) définis ci-dessus.

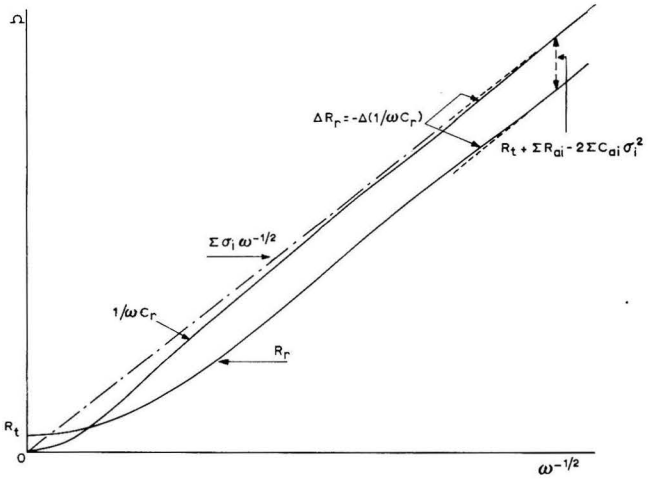

Fig. 4. Variations de R_r et $1/\omega C_r$ en fonction de $\omega^{-\frac{1}{2}}$ pour une réaction comportant diffusion, adsorption des deux espèces O et R, transfert de charges.

A. Détermination de la résistance de transfert de charges R_t et du courant d'échange $I_a{}^0$ de la réaction

Cette valeur est à déterminer dans les cas (a), (c), (e), (f), (g).

Dans les cas (a) et (c), c'est-à-dire adsorption spécifique d'une ou des deux espèces O et R, on a:

$$R_{r(\omega\to\infty)} = R_t + \omega^{-2}\,\Sigma(1/R_{ai}C_{ai}{}^2) \tag{25}$$

et la courbe R_r en fonction de ω^{-2} présente une partie rectiligne que l'on peut extrapoler à $\omega^{-2} = 0$ pour déterminer R_t.

Dans le cas (e), lorsqu'il n'y a que diffusion et transfert de charges, les courbes R_r et $1/\omega C_r$ en fonction de $\omega^{-\frac{1}{2}}$ sont des droites de pente $\Sigma\sigma_i$ et l'écart constant entre

les deux droites est, pour toutes les fréquences:

$$R_t = R_r - 1/\omega C_r \tag{26}$$

Dans le cas (f), diffusion et transfert de charges avec attraction électrostatique d'une ou des deux espèces O et R, lorsque $\omega \to \infty$ on a:

$$R_{r(\omega\to\infty)} = R_t + \omega^{-\frac{1}{2}} \Sigma(\tfrac{1}{2}\sigma_i C_{si}^2) \tag{27}$$

et la courbe R_r en fonction de $\omega^{-\frac{1}{2}}$ présente une partie rectiligne que l'on peut extrapoler à $\omega^{-\frac{1}{2}} = 0$ pour obtenir R_t.

Dans le cas (g), diffusion et transfert de charges avec répulsion électrostatique d'une ou des deux espèces O et R, les courbes R_r et $1/\omega C_r$ sont des droites parallèles. L'écart constant entre les droites est:

$$R_r - 1/\omega C_r = R_t + \Sigma R_{si} \tag{28}$$

Dans ce cas, la valeur de R_t ne peut être obtenue (*cf.* note) qu'après soustraction des termes R_{si}, qu'on ne peut déterminer expérimentalement, mais qu'il faut calculer d'après les équations établies par SENDA ET DELAHAY[7].

B. Détermination de l'impédance de diffusion et des coefficients de diffusion D_O et D_R

Dans tous les cas lorsque $\omega \to 0$, les courbes R_r et $1/\omega C_r$ en fonction de $\omega^{-\frac{1}{2}}$ présentent des parties linéaires de pente:

$$\Sigma \sigma_i = (R_t/\sqrt{2}n^2F^2)(1/C_O^0 D_O^{\frac{1}{2}} + 1/C_R^0 D_R^{\frac{1}{2}}) \tag{30}$$

Lorsque $\omega \to 0$, on a en effet pour $R_{r(\omega\to 0)}$ l'éqn. (29) ci-dessous et pour $1/\omega C_{r(\omega\to 0)}$:

$$(1/\omega C_r)_{(\omega\to 0)} = \omega^{-\frac{1}{2}} \Sigma \sigma_i \tag{31}$$

En travaillant avec deux concentrations C_O^0 et une concentration C_R^0, ou inversement, l'utilisation de l'éqn. (30) permet le calcul de D_O et D_R.

C. Détermination de l'impédance d'adsorption

Nous reprenons les différents cas définis plus haut.

(*a*) *Diffusion, adsorption spécifique des deux espèces, transfert de charges.* Il s'agit de déterminer les deux capacités C_{ai} et les deux résistances R_{ai}. Pour cela cinq équations sont utilisables.

Lorsque $\omega \to \infty$ les quatre éléments de l'impédance d'adsorption sont liés par l'éqn. (25) et l'équation:

$$(1/C_r)_{(\omega\to\infty)} = \Sigma(1/C_{ai}) - \omega^{-\frac{1}{2}} \Sigma(\sigma_i/R_{ai}^2 C_{ai}^2) \tag{32}$$

A partir de ces deux relations il est possible de déterminer graphiquement les valeurs numériques des expressions suivantes:

Note: L'extrapolation à $\omega^{-\frac{1}{2}} = 0$ de la partie rectiligne à basse fréquence de la courbe $R_r/\omega^{-\frac{1}{2}}$, ne déterminera R_t que dans le seul cas (e), diffusion et transfert de charges. En effet, il faut remarquer que l'expression générale de R_r à basse fréquence est:

$$R_{r(\omega\to 0)} = R_t + \Sigma R_{ai} - 2\Sigma C_{ai}\sigma_i^2 + \omega^{-\frac{1}{2}}\Sigma\sigma_i \tag{29}$$

En particulier, lorsqu'il y a attraction électrostatique des ions, cette extrapolation conduit à une valeur apparente de R_t trop faible, $(R_t - 2\Sigma C_{ai}\sigma_i^2)$, et lorsqu'il y a répulsion électrostatique une valeur apparente de R_t trop grande, $(R_t + \Sigma R_{si})$.

pente de la courbe $R_{r(\omega\to\infty)}$ en fonction de ω^{-2}:

$$\Sigma(1/R_{ai}C_{ai}^2)=n \tag{33}$$

Limite et pente de la courbe $(1/C_r)_{\omega\to\infty}$ en fonction de $\omega^{-\frac{1}{2}}$:

$$\Sigma(1/C_{ai}) = m \tag{34}$$

$$\Sigma(\sigma_i/R_{ai}^2C_{ai}^2) = s \tag{35}$$

Lorsque $\omega\to 0$, à très basses fréquences, les deux courbes R_r et $1/\omega C_r$, en fonction de $\omega^{-\frac{1}{2}}$, sont des droites de même pente $\Sigma\sigma_i$ et l'écart constant entre les deux droites, pour chaque ω, est:

$$(R_r-1/\omega C_r)_{(\omega\to 0)} = R_t+\Sigma R_{ai}-2\Sigma C_{ai}\sigma_i^2 = p \tag{36}$$

Cette valeur numérique p peut être obtenue graphiquement d'une autre façon. On peut représenter $1/\omega C_r$ en fonction de R_r. Lorsque $\omega\to 0$, cette courbe est une droite de pente 1, dont l'extrapolation à $1/\omega C_r=0$ coupe l'axe des R_r au point: $R_r=p$.

Lorsque ω croît, dans un petit domaine de basses fréquences, les deux courbes $R_r/\omega^{-\frac{1}{2}}$ et $(1/\omega C_r)/\omega^{-\frac{1}{2}}$ s'écartent symétriquement des droites de pente $\Sigma\sigma_i$. L'écart de chaque courbe par rapport à la droite correspondante, pour chaque valeur de ω considérée dans ce domaine, est:

$$\Delta R_r = -\Delta(1/\omega C_r)=2\Sigma[\sigma_i C_{ai}(\sigma_i^2C_{ai}-R_{ai})]\omega^{\frac{1}{2}}=q \tag{37}$$

La résolution des éqns. 33–37 permet le calcul des quatre éléments de l'impédance d'adsorption (*cf. A*ppendice).

(*b*) *Diffusion, adsorption spécifique des deux espèces, transfert de charges infiniment rapide.* Le calcul du cas (a) est utilisé en posant $R_t=0$ dans l'éqn. (36), seule p étant une fonction de R_t.

(*c*) *Diffusion, adsorption spécifique d'une seule espèce, transfert de charges.* Il est alors possible d'éviter les extrapolations utilisées dans les deux premiers cas et d'obtenir un calcul simple à partir des valeurs de R_r et $1/\omega C_r$ associées pour chaque fréquence.

Supposons l'espèce O seule adsorbée, $C_{aR}=R_{aR}=0$, et posons:

$$\begin{aligned} A &= R_r-R_t-\sigma_R\omega^{-\frac{1}{2}} \\ B &= 1/\omega C_r-\sigma_R\omega^{-\frac{1}{2}} \end{aligned} \tag{38}$$

En combinant les éqns. (9), (10) et (38) on obtient, pour chaque fréquence, les valeurs C_{aO} et R_{aO}, par les équations:

$$(1/\omega C_{aO})^2(\sigma_O\omega^{-\frac{1}{2}}-B)+(1/\omega C_{aO})(A^2+B^2-2B\,\sigma_O\omega^{-\frac{1}{2}})+\sigma_O\omega^{-\frac{1}{2}}(A^2+B^2)=0 \tag{39}$$

$$R_{aO}=[1/A]\cdot[(1/\omega C_{aO})(B-\sigma_O\omega^{-\frac{1}{2}})+\sigma_O\omega^{-\frac{1}{2}}(B-A)] \tag{40}$$

L'adsorption de l'espèce R seule conduit à intervertir les indices O et R dans les éqns. (38), (39) et (40).

(*d*) *Diffusion, adsorption spécifique d'une seule espèce, transfert de charges infiniment rapide.* Il suffit de poser $R_t=0$ dans la première des éqns. 38 et d'utiliser les éqns. (38), (39) et (40).

(*f*) *et* (*h*) *Diffusion et transfert de charges avec attraction électrostatique d'une ou des deux espèces* O *et* R. Si les deux espèces sont attirées dans la double-couche, on a: $R_{a\mathrm{R}}=R_{a\mathrm{O}}=0$, $C_{a\mathrm{R}}=C_{s\mathrm{R}}$, $C_{a\mathrm{O}}=C_{s\mathrm{O}}$. Les éqns. (36) et (37) se simplifient:

$$R_r-R_t-1/\omega C_r=-2\Sigma C_{si}\sigma_i^2=\mathrm{p}' \tag{41}$$

$$\Delta R_r=-\Delta(1/\omega C_r)=2\Sigma(\sigma_i^3 C_{si}^2)\omega^{\frac{1}{2}}=\mathrm{q}' \tag{42}$$

Et l'éqn. (34) reste valable:

$$\Sigma(1/C_{si})=\mathrm{m}$$

La résolution des éqns. (41), (42) et (34) donne les valeurs de $C_{s\mathrm{O}}$ et $C_{s\mathrm{R}}$.

Si une seule espèce, O par exemple, est attirée, la seule éqn. (41) donne immédiatement $C_{s\mathrm{O}}$.

Si le transfert est infiniment rapide $R_t=0$, les éqns. (34), (41) et (42) sont utilisées. Il faut remarquer que dans ces deux cas l'éqn. (29) s'écrit:

$$R_r(\omega\to 0)=R_t-2\Sigma(C_{si}\sigma_i^2)+\omega^{-\frac{1}{2}}\Sigma\sigma_i \tag{43}$$

De sorte que l'extrapolation à fréquence infinie de la portion linéaire ($\omega\to 0$) de la courbe $R_r/\omega^{-\frac{1}{2}}$, conduit à une valeur apparente de R_t trop faible. Il faut utiliser l'extrapolation mentionnée ci-dessus, éqn. (27).

(*g*) *Diffusion et transfert de charges avec répulsion électrostatique d'une ou des deux espèces* O *et* R: $C_{a\mathrm{O}}=C_{a\mathrm{R}}=0$, $R_{ai}=R_{si}$. Comme on l'a vu pour le calcul de la résistance de transfert, les grandeurs R_{si} ne peuvent être obtenues que par le calcul direct (7).

Il est important de noter que les valeurs expérimentales ne permettent pas toujours d'utiliser le calcul général proposé. En effet, les domaines de fréquences, dans lesquels les extrapolations pour $\omega\to\infty$ ou $\omega\to 0$ sont valables, dépendent des valeurs relatives des différents paramètres. En particulier, le domaine d'extrapolation à fréquence infinie sera d'autant plus repoussé vers les hautes fréquences que les résistances $R_{a\mathrm{O}}$, $R_{a\mathrm{R}}$ et R_t seront plus petites, c'est à dire que les vitesses d'adsorption et de transfert de charges seront plus grandes. Par contre, si ces vitesses sont très faibles, ce sera le domaine d'extrapolation basses fréquences qui sera repoussé vers les fréquences très petites. Or le domaine de fréquences utilisable dans les mesures de l'impédance faradique se trouve limité habituellement entre 10 Hz et 100 kHz.

Il est rare cependant que les différents éléments de l'impédance faradique interviennent dans le processus électrochimique avec la même importance. Certains facteurs sont alors négligeables et peuvent même être masqués. Le calcul est ramené à l'un des cas particuliers de résolution plus facile. Dans la deuxième partie expérimentale de ce travail les limitations de la méthode apparaîtront clairement.

D. Application: détermination de la capacité de double-couche en présence d'une réaction électrochimique simple, diffusion et transfert de charges, et calcul du courant d'échange de la réaction

Dans toutes les mesures d'impédance faradique il est indispensable de connaître la résistance de l'électrolyte R_E et la capacité de la double-couche C_E, qu'il faut séparer de l'impédance globale de la cellule seule mesurable. Inversement, il n'est pas

possible de déterminer la capacité de couche-double en présence d'une réaction, puisque la mesure donne toujours l'impédance globale de la cellule. Si l'on a affaire à une réaction simple ne comportant que les processus de transfert de charges et de diffusion, une seule expérience à fréquence variable permettra de déterminer tous les termes de l'impédance globale mesurée, en adaptant le calcul exposé plus haut.

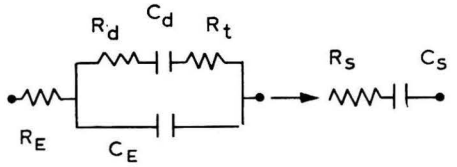

Fig. 5. Schéma de l'impédance globale mesurée d'une réaction ne comportant que diffusion et transfert de charges.

Le circuit représentatif de l'impédance complexe équivalente est alors celui de la Fig. 5, dans lequel:

$$R_d = 1/C_d\,\omega = \Sigma\,\sigma_i\omega^{-\frac{1}{2}} = \sigma_d\omega^{-\frac{1}{2}} \tag{44}$$

$R_s - j/\omega C_s$ étant l'impédance série globale mesurée. Les équations établies plus haut pour le cas d'une réaction avec adsorption d'une seule espèce active sont directement utilisables, en considérant l'analogie entre la première maille du circuit de la Fig. 1 et le circuit de la Fig. 5 (Note).
En effectuant le changement de variables:

$$\begin{array}{ll} \sigma_R = 0 & \sigma_0 \sim \sigma_d \\ R_t \sim R_E & \\ R_{a0} \sim R_t & C_{a0} \sim C_E \\ R_r \sim R_s & C_r \sim C_s \end{array}$$

l'éqn. (25) permet la détermination de R_E par extrapolation de R_s/ω^{-2} à fréquence infinie.

$$R_s(\omega \to \infty) = R_E + \omega^{-2}(1/R_t C_E^2) \tag{45}$$

Le calcul de R_t et C_E est effectué à chaque fréquence en utilisant les éqns. (38) ,(39) et (40) qui s'écrivent alors:

$$A' = R_s - R_E$$

$$B' = 1/\omega C_s \tag{46}$$

$$(1/\omega C_E)^2(\sigma_d\omega^{-\frac{1}{2}} - B') + (1/\omega C_E)(A'^2 - B'^2 - 2B'\sigma_d\omega^{-\frac{1}{2}}) + \sigma_d\omega^{-\frac{1}{2}}(A'^2 + B'^2) = 0 \tag{47}$$

$$R_t = [1/A'][(1/\omega C_E)(B' - \sigma_d\omega^{-\frac{1}{2}}) + \sigma_d\omega^{-\frac{1}{2}}(B' - A')] \tag{48}$$

SUMMARY

From measurements of the faradaic impedance of an electrochemical reaction with sinusoidal current it is possible to determine the partial processes of this reaction

Note: La comparaison de ces deux schémas montre que, dans le cas de l'adsorption d'une seule espèce réagissante, il est possible d'adapter certaines applications graphiques de SLUYTERS et de ses collaborateurs[9].

and to calculate the different kinetic parameters. The processes considered are: diffusion; charge transfer; adsorption of the reacting species. The calculation can be adapted to the determination of the double-layer capacity of an electrode in presence of a reaction controlled by diffusion and charge transfer.

RÉSUMÉ

A partir des mesures en courant sinusoïdal de l'impédance faradique d'une réaction électrochimique il est possible de déterminer les processus partiels de cette réaction et de calculer les différents paramètres cinétiques. Les processus envisagés sont: diffusion, transfert de charges, adsorption des espèces réagissantes. Le calcul peut s'adapter à la détermination de la capacité de double-couche d'une électrode en présence d'une réaction contrôlée par la diffusion et le transfert de charges.

APPENDICE

Résolution du système d'équations 33–37

La résolution des éqns. (33)–(37) conduit à l'équation ci-dessous du 8° degré en C_{a0} qui peut être résolue avec un ordinateur:

$$m^4n\sigma_0^6 \cdot C_{a0}^8 + m^3\sigma_0^4 A.C_{a0}^7 + m^2\sigma_0^3 B.C_{a0}^6 + m\sigma_0 C.C_{a0}^5 + D.C_{a0}^4 + E.C_{a0}^3 + F.C_{a0}^2 + G.C_{a0} + H = 0 \qquad (49)$$

en posant:

$$A = m(np - m^2) - 2(e + \sigma_0)dn$$

$$B = m[3(\sigma_0 + d)\sigma_0 m - (3d + \sigma_0)np] + 6d^2en$$

$$C = (5\sigma_0^2 + 3e\sigma_R)dmnp + (m^3 - 2\sigma_R dn)m^2q + (\sigma_R m^2 - \sigma_0 np - mnq)m^2p + \sigma_R e^2m^3 + (n - 16m)\sigma_0^2 dm^2 + 2d^2[\sigma_0\sigma_R^2 - (e + \sigma_0)de]n$$

$$D = 3\sigma_0\sigma_R m^2 n(p^2 + 2dq) - (3\sigma_0\sigma_R + d^2)m^4p + (3\sigma_0 + e)m^3npq - (5\sigma_0 + d)m^5q - np^4q^2 - [d^2(d^2 - 12\sigma_0^2) - \sigma_0^3(d + 2\sigma_0)]m^3 + (d^2e^2 - \sigma_0^2\sigma_R^2)d^2n - [d^2e + \sigma_0(\sigma_0 + 2e)(\sigma_R + d)]dmnp$$

$$E = (4d^2 + 3\sigma_0\sigma_R)m^3p - 3[\sigma_0\sigma_R p + (\sigma_0 + e)mq]mnp + (d^2 + \sigma_0\sigma_R)denp + [4m^2nq + (9\sigma_0 + 5d)m^3 - 6\sigma_0\sigma_R dn]mq - [\sigma_0 d(8e + 10d) + 3e(d^2 - \sigma_0\sigma_R)]dm^2$$

$$F = (\sigma_0 + 3e)mnpq - [6nq + (5d + 3\sigma_0)m]m^2q - (2d + \sigma_0)(2d + \sigma_R)m^2p + \sigma_0\sigma_R(p^2 + 2dq)n + 2(\sigma_0 d + 2\sigma_0 e + 2ed)d^2m$$

$$G = m[4nq^2 + (7d + 2\sigma_0)mq + 4d^2p] - e(2d^3 - npq)$$

$$H = -d(2mq + dp) - nq^2$$

$$d = \sigma_0 + \sigma_R \qquad e = \sigma_0 - \sigma_R$$

BIBLIOGRAPHIE

1 H. A. LAITINEN ET J. E. B. RANDLES, *Trans. Faraday Soc.*, 51 (1955) 54.
2 J. LLOPIS, J. FERNANDEZ-BIARGE ET M. PEREZ-FERNANDEZ, *Transactions of the Symposium on Electrode Processes, Philadelphia, 1959*, rédigé par E. YEAGER, John Wiley and Sons, New York, 1961, p. 221.
3 G. C. BARKER, *Transactions of the Symposium on Electrode Processes, Philadelphia, 1959*, rédigé par E. YEAGER, John Wiley and Sons, New York, 1961, p. 325.
4 W. LORENZ ET G. SALIE, *Zt. Physik. Chem. Leipzig*, 218 (1961) 259.
5 B. KASTENING, H. GARTMANN ET L. HOLLECK, *Electrochim. Acta*, 9 (1964) 741.
6 M. SLUYTERS-REHBACH, B. TIMMER ET J. H. SLUYTERS, *Rec. Trav. Chim.*, 82 (1963) 553.
7 M. SENDA ET P. DELAHAY, *J. Phys. Chem.*, 65 (1961) 1580.
8 P. DELAHAY, *Advances in Electrochemistry and Electrochemical Engineering*, Interscience Publishers, New York, 1961, p. 233.
9 J. H. SLUYTERS, *Rec. Trav. Chim.*, 79 (1960) 1092; M. REHBACH ET J. H. SLUYTERS, *Rec. Trav. Chim.*, 81 (1962) 301.

THE EFFECT OF ANTIMONY AND DIFFERENT ANIONS ON THE POTENTIAL OF LEAD

E. M. KHAIRY*, A. A. ABDUL AZIM AND K. M. EL SOBKI
Laboratory of Electrochemistry and Corrosion, National Research Centre, Dokki, Cairo (U.A.R.)
(Received June 23rd, 1965)

Metallic lead used for technical purposes, including lead accumulators, is invariably contaminated with antimony. It has been frequently pointed out that the presence of antimony in lead generally decreases its corrosion resistance[1-4]. RUETSCHI AND CAHAN[5] investigated the anodic corrosion of lead and lead–antimony alloys in sulphuric acid under conditions of oxygen evolution. They observed that at constant current corrosion increased slightly, whereas at constant potential corrosion increased strongly with increasing antimony concentration. VAISBERG, KRIVOLAPOVA AND KABANOV[6] reported that the time–potential curves of the Pb–Sb electrode polarised at $2 \cdot 10^{-4}$ A/cm^2, exhibited arrests corresponding to the reaction:

$$Sb + H_2O = SbO^+ + 2\,H^+ + 3\,e$$

KATO[7] found that antimony alloyed with lead (1–10% Sb) lowered the hydrogen overvoltage of the latter. CROATTO AND DA VIA[8] reported that throughout the eutectic region a linear relation was obtained between the composition of the alloy and the current density required to contribute a given overvoltage in 6 *N* KOH solutions.

The aim of the present work is to investigate the effect of varying antimony inclusions on the pH–potential relationship of lead in the absence and presence of different amounts of chloride and sulphate ions. Three different lead–antimony alloys were chosen to represent under-eutectic, approximately eutectic, and over-eutectic states with respect to both metals.

EXPERIMENTAL

Johnson-Matthey spectroscopically pure lead (99.995%) and antimony (99.995%) were used to prepare the alloys. Alloying was carried out in a Tamman furnace using alumina crucibles. The melt was cast in the form of rods in sand moulds. Three samples were thus prepared which gave the following analyses: alloy I, 92% Pb, 8% Sb; alloy II, 89% Pb, 11% Sb; alloy III, 50.7% Pb, 49.3% Sb.

Before measurements, the specimens were polished by abrasion with very fine emery paper, and then rubbed with a soft cloth. They were then thoroughly washed with distilled water and rinsed with the electrolyte. The potential was measured with a high impedance valve voltmeter using as reference a saturated calomel half-cell. The experiments were performed at 25°.

Two series of buffers, A and B, were used. In series A (Clark and Lubs) the

* Chemistry Department, Faculty of Science, Cairo University.

solution of pH 1.65 was an HCl–KCl mixture. The solutions of pH 2.2–3.8 were acid potassium phthalate–HCl and those of pH 4.0–6.2 were acid potassium phthalate–sodium hydroxide. For pH 7.0–10.3, potassium dihydrogen phosphate–sodium hydroxide mixtures were used and for pH 10.7–11.7 mixtures of 0.2 *M* disodium hydrogen phosphate and 0.2 *M* sodium hydroxide. Series B were universal buffer mixtures of pH-values ranging from 2.0 to 11.6. These were prepared from 0.12 *M* solutions of acetic, phosphoric and boric acids by adding appropriate amounts of 0.12 *M* sodium hydroxide.

Measurements were also made under anaerobic conditions; oxygen-free nitrogen was employed to de-aerate and saturate the solutions. Some of these experiments were carried out in solutions of buffers of series A, prepared to contain, in addition to the normal constituents, varying concentrations of chloride and/or sulphate ions.

RESULTS AND DISCUSSION

Behaviour in solutions of varying pH in air

A general feature of the alloys under examination is that in all solutions except those of pH 4 (series A), the potentials show little variation with time up to the attainment of steady values after 2–3 h. At pH 4, the steady state is approached after about 24 h from considerably more negative potentials. In the alkaline range (pH 10.7–11.7), the potentials are reached from more negative values and show considerable drift with time. Whereas the potentials attained in the phthalate buffer pH 6.03 are remarkably steady with time, the corresponding values obtained in the phosphate buffer pH 6.14 belonging to the same series (A), are much less negative and manifest considerable drift with time towards still less negative values attained overnight. This difference in behaviour is also observed in the pH range 5.2–6.2, between potentials obtained in series A and those obtained in series B of buffers.

In Fig. 1 (A and B) are shown the E_H–pH curves representing the behaviour of the three alloys in the two buffer series, respectively. It can be seen that the potentials show little variation with pH in the extreme acid range (< pH 2.5). Unlike the potentials attained in the phthalate buffers of about pH 5–6 (series A), the values obtained at pH 4.2 move up towards the reported value for the Sb/Sb_2O_3 potential[9]. This phenomenon is more pronounced with increase of antimony in the alloy. The tendency of the potential to acquire the Sb/Sb_2O_3 value is demonstrated still more clearly in series B in the pH range 3.5–5.

The steady-state potentials established in the pH range of about 6–11 in the two series, vary more or less linearly with pH. They follow the relation

$$E = E_0' - 0.059 \text{ pH} \qquad (1)$$

with E_0' equal to 0.270 V in series A and 0.250 in series B, the latter value coinciding with the theoretical value of 0.248 V for the reversible Pb/PbO system.

It may be noted that at pH-values 1.56, 2.13 and 3.5 (series A) containing 0.147, 0.061 and 0.020 molar concentrations of Cl^- ions, respectively, the behaviour is that of an electrode of the first kind (Pb/Pb^{2+}) rather than that of a $Pb/PbCl_2$ electrode. This may be deduced from the fact that by calculating the activity of Pb^{2+} ions using the relation

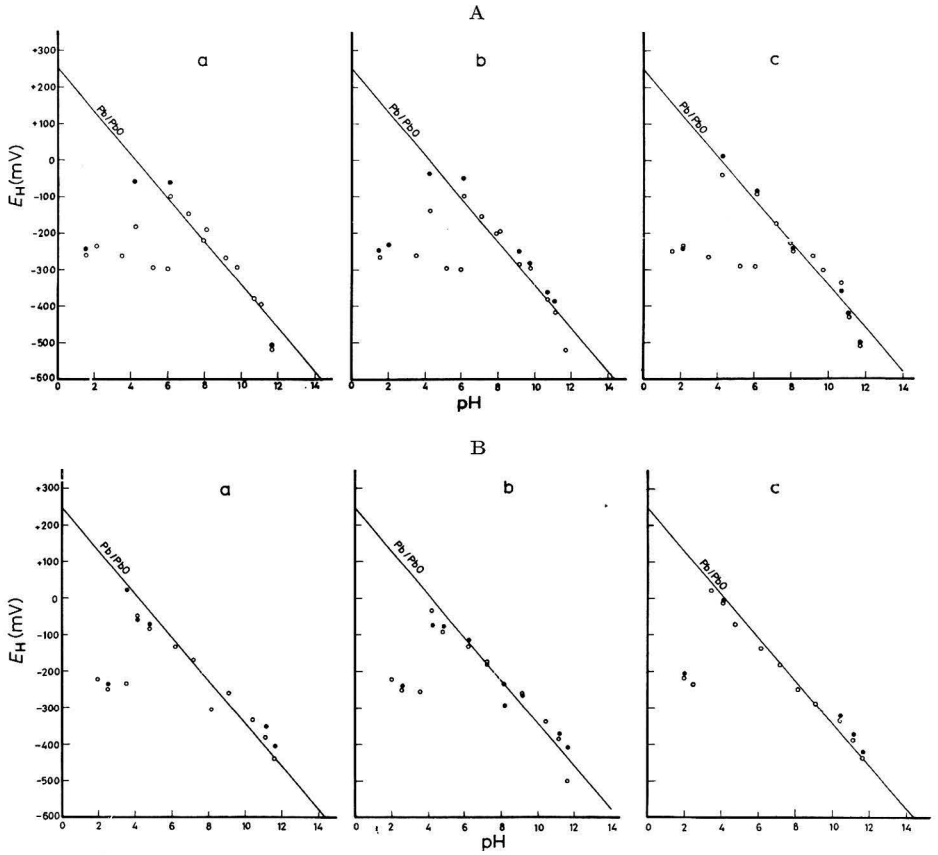

Fig. 1. The relation between potential and pH in aerated buffer solns. for Pb–Sb alloys containing: (a), 8%; (b), 11%; (c), 49.3% Sb. (A), series A; (B), series B.

$$E_H = -0.126 + 0.03 \log a_{Pb^{2+}} \quad (2)$$

values for $a_{Pb^{2+}} = 10^{-4}$, $10^{-3.7}$ and $10^{-4.6}$ M for the three solutions, respectively, are obtained for the 11% Sb-alloy. Multiplication of these values by the activities of the chloride ions in the above solutions yields the ionic products: 10^{-6}, $5 \cdot 10^{-7}$ and $8 \cdot 10^{-9}$, which lie below the solubility product of $PbCl_2$ ($1.6 \cdot 10^{-5}$)[10].

Above pH 3.5, the behaviour of the alloys tends to be determined either by antimony or by lead, functioning in each case as electrodes of the second kind. In spite of the fact that the E_0'-values for the systems Pb/PbO and Sb/Sb_2O_3 are close to each other (0.248 and 0.250 V, respectively), the curves in Fig. 1 (A and B) give some indication of the electrodic behaviour of the alloy with increasing antimony content in the different buffers. Thus, at pH 4 in series A and at pH 3.5–5 in series B, the electrochemical behaviour of the alloy becomes more dominated by antimony and the effect is greater the larger the proportion of this constituent in the alloy. It may be recalled in this connection that lead–antimony alloys give an eutectic at a 13% Sb-content. If examined microscopically, alloys I and II (8 and 11% Sb) would reveal dark dendrites of lead whereas alloy III may show primary antimony crystals

together with the eutectic. If either of the three alloys is dipped in the acid phthalate buffer pH 4, or in universal buffers pH 3.5–5, local action processes would take place between the bare metal parts acting as anodic areas and the parts with adsorbed oxygen acting as cathodic areas. Lead would eventually suffer limited corrosion yielding Pb^{2+} ions, the oxide being unstable at such a low pH. The antimony surface, however, would become oxidised, with subsequent shift of electrode potential towards that of the nobler Sb/Sb_2O_3 couple.

The potentials recorded in phthalate buffers of pH 5.20 and 6.03 (series A), which are more or less equal, correspond to a Pb^{2+} ion activity of about $2 \cdot 10^{-6}$ M. The molar concentration of the acid phthalate ion in the above buffer solutions is 0.05. The ionic product of Pb^{2+} and acid phthalate ions is, therefore, equal to $5 \cdot 10^{-9}$. This value is somewhat greater than the value of $3 \cdot 10^{-9}$ obtained by titrating lead nitrate solution with acid potassium phthalate until precipitation starts. It may be assumed that the potential observed within the pH range of about 5–6 is determined by a Pb/Pb hydrogen phthalate, rather than by the Sb/Sb_2O_3, couple. At pH 4.2, on the other hand, the lead hydrogen phthalate is presumably soluble and hence the predominance of the Sb/Sb_2O_3 potential.

The linear E_H–pH relation extending over the pH range 6–11 suggests the presence of a surface film of PbO which is stable in solutions open to air.

That the potential observed at pH 11.7 deviates from the linear relation extending from pH ~ 6 to 11 may be explained by assuming that $Pb(OH)_2$ tends, because of its amphoteric properties, to dissolve, yielding plumbite ions and, consequently, the potential shifts towards more negative values.

Behaviour in air-free solutions of varying pH

The potentials obtained in de-aerated solutions are reproducible and attain steady states shortly after immersion; these extend overnight with little drift towards

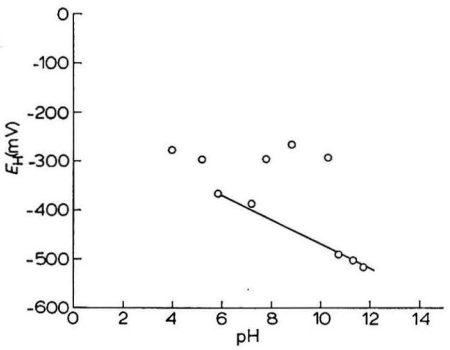

Fig. 2. The relation between potential and pH for a Pb–Sb alloy (11% Sb) in de-aerated buffer solns. (series A).

less negative values. Consideration of the relation between steady-state potentials and pH (Fig. 2) reveals that the absence of dissolved oxygen alters the behaviour of the alloys in many respects. Thus, appreciably more negative steady-state potentials are achieved at pH 4.2 than in aerated solutions. The electrode behaviour corresponds to a Pb/Pb^{2+}, rather than to an Sb/Sb_2O_3, couple. This may be explained on the prem-

ise that the cathodic reaction of the local action process is restricted in the absence of dissolved oxygen to the discharge of Pb^{2+} and/or H^+ ions on the antimony surface. It should be noted that the observed potential is comparable with that obtained with spectroscopically pure lead at the same pH[11].

The behaviour of the electrode in the phosphate buffers pH 5.85–7.20 is also notable as regards the role of dissolved oxygen. Thus, whereas the potentials obtained in aerated solutions lie close to the Pb/PbO potential, appreciably more negative values are attained in anaerobic conditions. By using the equilibrium constant[11], $8.7 \cdot 10^{-12}$, of the reaction

$$PbHPO_4 \rightleftharpoons Pb^{2+} + HPO_4^{2-}$$

the standard free energy change, ΔF°, of $PbHPO_4$ is calculated to be -282.3 kcal/mole. Using this value and the corresponding one for $H_2PO_4^-$, the standard potential, E_0, of the reaction

$$Pb + H_2PO_4^- = PbHPO_4 + H^+ + 2\,e$$

is found to be -0.239 V at 25°. The potential of the electrode in the above media, E_H, is, therefore, given by

$$E_H = -0.239 - 0.0296 \log H_2PO_4^- - 0.0296\ pH \qquad (3)$$

Substituting $H_2PO_4^-$ by 0.05 M prevailing in the above buffer solutions, eqn. (3) transforms to

$$E_H = -0.239 + 0.038 - 0.0296\ pH$$
$$= -0.201 - 0.0296\ pH$$

This gives -0.375 and -0.417 V for the electrode potential at pH 5.85 and 7.2, respectively. These values compare satisfactorily with the observed potentials, indicating that the electrode potential is governed by the $Pb/PbHPO_4$ system. Further evidence for this is given by the slope of the pH–potential curve which agrees satisfactorily with the theoretical value. Further, the potentials obtained in phosphate buffers pH 10.7–11.1 lie on the same line as those above, indicating the predominance of the $Pb/PbHPO_4$ couple.

The potentials given by the alloys in the pH range covered by the borate buffers (pH 7.8–10.3) differ from those in aerated solutions and are almost pH-independent. It is difficult to reconcile these values with a pure metal–metal oxide potential. The fact that the borate concentration is constant suggests the establishment of an oxy-borate layer of lead[12], rather than an oxide film. In the presence of dissolved oxygen, the enhanced local action process leads eventually to the formation of PbO and the electrode potential would then respond to variations of pH as a Pb/PbO couple.

Behaviour in air-free buffer solutions containing varying amounts of Cl^- or SO_4^{2-} ions

Solutions containing varying concentrations of Cl^- and SO_4^{2-} ions were buffered at pH-values 4, 7 and 10. Buffer solutions chosen from the Clark and Lubs series, were prepared containing these ions in addition to the original constituents.

In chloride solutions buffered at pH 4, the behaviour of the alloys depends on the halide concentration as well as the antimony content of the alloy. Thus, at chloride ion concentrations greater than 0.05 M the potentials are only 15–20 mV more nega-

tive than the calculated values for the system $Pb/PbCl_2$ at the respective pCl values. At decreasing chloride ion concentrations the potential lies nearer to that obtained in the absence of these ions (Fig. 3a). However, with increase in antimony content, there is a tendency towards the Sb/Sb_2O_3 potential. This is clearly demonstrated by the pCl–potential curves obtained with the 49% alloy (Fig. 3b) where antimony is present as a separate phase. The Sb/Sb_2O_3 potential is gradually approached as the

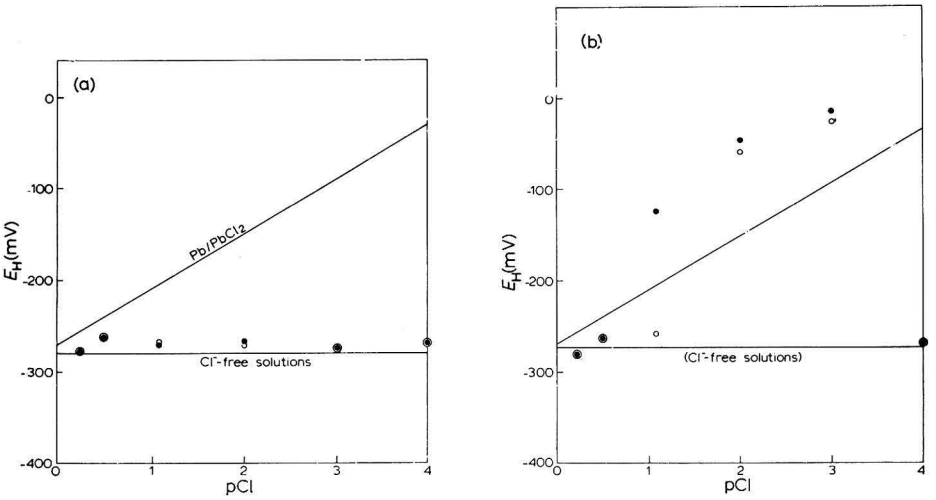

Fig. 3. The relation between pCl and potential for Pb–Sb alloys in de-aerated potassium hydrogen phthalate–sodium hydroxide buffer, pH 4. (a), 8% Sb; (b), 49.3% Sb; (○), 1st steady state; (●), 2nd steady state.

pCl of the solution exceeds 1, until it is attained at pCl 3. At the latter pCl, the potentials measured for the two alloys tend also, though to a less extent, to approach the value characteristic of the massive antimony electrode. This behaviour may be explained by assuming that in the presence of appropriate concentrations of Cl^- ions, a $PbCl_2$ layer is established on the electrode surface, and the potential is determined by the $Pb/PbCl_2$ system. At chloride ion concentrations insufficient to form such a layer, their only effect is to enhance the dissolution of both alloy metals, under which conditions an Sb_2O_3 layer might be formed, shifting the potential towards that of the much less negative Sb/Sb_2O_3 value.

The behaviour of the alloy in sulphate solutions buffered at pH 4 reveals that at pSO_4 values $\leqslant 2$, the potentials are identical with those measured in sulphate-free buffer solutions. At higher concentrations, the first steady-state potentials agree fairly well with those calculated for the $Pb/PbSO_4$ system at the respective sulphate ion activity. The second steady-state values, on the other hand, are shifted towards more positive values. This shift, which is dependent on the antimony content of the alloy, approaches the Sb/Sb_2O_3 potential more readily at lower $[SO_4^{2-}]$. This potential is attained by the 49.3% Sb electrode at a sulphate ion concentration of 10^{-1} M (Fig. 4). The formation of a lead sulphate film on the surface of the alloys leads to the establishment of local action cells, whereby OH^- ions accumulate in the vicinity of exposed metal parts leading to oxide formation. Of the two oxides which would

probably form, only Sb_2O_3 is thermodynamically stable. It should be pointed out, however, that the above local action process is more enhanced at a relatively higher porosity of the sulphate layer. This explains why the antimony oxide potential is more readily approached in the 0.1 than in the 0.5 *M* sulphate solution.

In sulphate and chloride solutions buffered at about the neutral point, the picture obtained is rather interesting. Although the solutions are free from dissolved oxygen, the potentials established indicate oxide formation even at $[Cl^-]$ or $[SO_4^{2-}]$ as low as 10^{-4} *M* (*cf.* representative Figs. 5 and 6). It has already been shown that in anaerobic conditions and in the absence of sulphate and chloride ions, a $Pb/PbHPO_4$ couple controls the behaviour of the alloys at pH 7. It may, thus, be supposed that Cl^- and SO_4^{2-} ions are preferentially adsorbed on the surface of the metal compared with HPO_4^- ions. Exposed metal parts acting as micro-anodes become gradually oxidised when a sufficient concentration of OH^- ions is furnished at the metal surface.

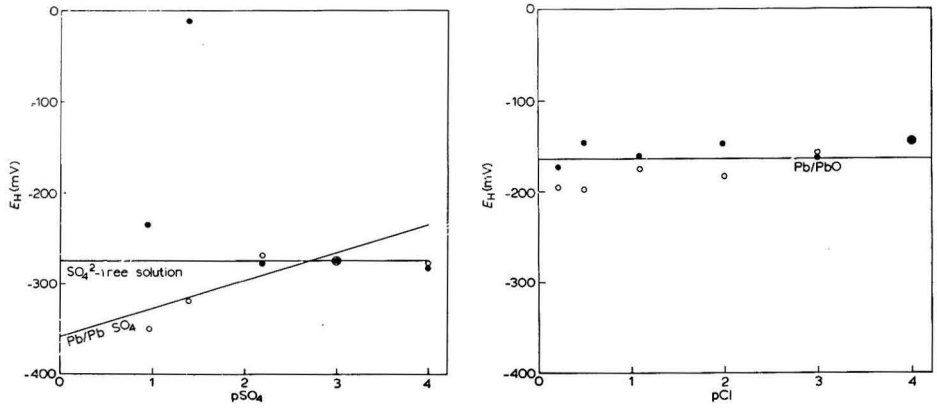

Fig. 4. The relation between pSO_4 and potential for a Pb–Sb alloy in de-aerated potassium hydrogen phthalate–sodium hydroxide buffer, pH 4. (○), 1st steady state; (●), 2nd steady state.

Fig. 5. The relation between pCl and potential for a Pb–Sb alloy (11% Sb) in de-aerated potassium dihydrogen phosphate–sodium hydroxide buffer, pH 7. (○), 1st steady state; (●), 2nd steady state.

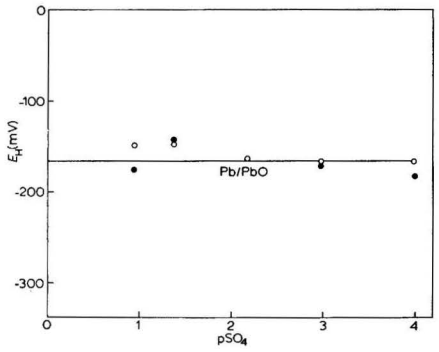

Fig. 6. The relation between pSO_4 and potential for a Pb–Sb alloy (11% Sb) in de-aerated potassium dihydrogen phosphate–sodium hydroxide buffer, pH 7. (○), 1st steady state; (●), 2nd steady state.

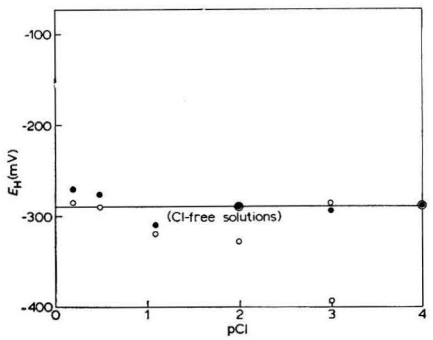

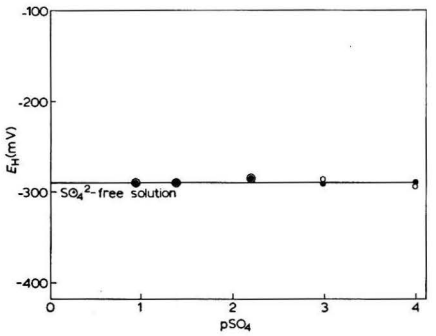

Fig. 7. The relation between pCl and potential for a Pb–Sb alloy (49.3% Sb) in de-aerated boric acid–sodium hydroxide buffer, pH 10. (○), 1st steady state; (●), 2nd steady state.

Fig. 8. The relation between pSO_4 and potential for a Pb–Sb alloy (49.3% Sb) in de-aerated boric acid–sodium hydroxide buffer, pH 10.

In Figs. 7 and 8 are shown two representative curves obtained with the 49.3% Sb alloy in the chloride and sulphate solutions buffered at about pH 10. It is clear that the steady-state potentials, usually attained overnight, lie close to the values obtained in absence of the anions. This indicates that the corrosion of the electrode surface is chiefly governed by OH^- ions in these alkaline solutions.

SUMMARY

Electrode potential measurements with three Pb–Sb alloys (8–49.3% Sb) in aerated buffer solutions show that in acid phthalate buffer, pH ~ 4, and in universal buffers, pH 3.5–5, the Sb/Sb_2O_3 potential predominates to an extent that increases with increase of Sb in the alloy. At lower pH-values, the behaviour corresponds to a Pb/Pb^{2+} potential, and in the pH range 6–11 the Pb/PbO couple determines the electrochemical behaviour of the alloys. PbO tends to dissolve in more alkaline solutions yielding plumbite ions.

Experiments under anaerobic conditions demonstrate the marked effect of dissolved oxygen on the electrochemical behaviour of the alloys. The local action process leading to the formation of Sb_2O_3 or PbO at the appropriate pH is materially *restricted*. The potential is influenced by anion effects, *e.g.*, phosphate ions in neutral and alkaline solutions and borate ions in alkaline solutions, in which cases the alloys behave as electrodes of the second kind. In the presence of Cl^- or SO_4^{2-} ions, the antimony potential is approached in acid solutions (pH ~ 4). The Pb/PbO potential predominates in neutral solutions, revealing decided corrosive actions of Cl^- and SO_4^{2-} ions.

REFERENCES

1 J. C. Olsen, M. H. Quell and W. G. Holley, *Trans. Am. Inst. Chem. Eng.*, 18 (1926) 19.
2 D. W. Jones, *J. Soc. Chem. Ind.*, 47 (1928) 161 T.
3 G. Osterheld and A. Portmann, *Helv. Chim. Acta*, 24, Engi Vol. (1941) 389.

4 V. P. MASHOVETS AND A. Z. LYANDRES, *Zh. Prikl. Khim.*, 21 (1948) 441.
5 P. RUETSCHI AND B. D. CAHAN, *J. Electrochem. Soc.*, 105 (1958) 369.
6 E. S. VAISBERG, E. V. KRIVOLAPOVA AND B. N. KABANOV, *Zh. Prikl. Khim.*, 32 (1959) 2354.
7 Y. KATO, *J. Electrochem. Soc. Japan*, (1932) 120.
8 U. CROATTO AND M. DA VIA, *Gazz. Chim. Ital.*, 73 (1943) 117.
9 A. RIAD TOURKY AND A. A. MOUSSA, *J. Chem. Soc.*, (1948) 752.
10 W. M. LATIMER, *Oxidation Potentials*, Prentice-Hall, New York, 1959, pp. 150–157.
11 L. A. SHALABY, Ph.D. Thesis, Cairo University, 1962.
12 J. W. MELLOR, *A Comprehensive Treatise on Inorganic and Theoretical Chemistry*, Vol. V, Longmans, New York, 1946, p. 106.

A CELL WITH SOLID MICROELECTRODE WITH PERIODICAL RENEWAL OF THE DIFFUSION LAYER

DANILO COZZI, GIORGIO RASPI AND LAMBERTO NUCCI
Institute of Analytical Chemistry, University of Pise (Italy)
(Received August 13th, 1965)

This new cell with a platinum microelectrode (other electrode materials may also be used) may be considered an improved version of the cell with a bubbling platinum electrode, previously described[1-4]. The operation of the latter microelectrode is based on the periodical movement of the solution, caused by the bubbling of nitrogen gas, which allows the renewal of the electrolyte on the platinum surface: the electrode

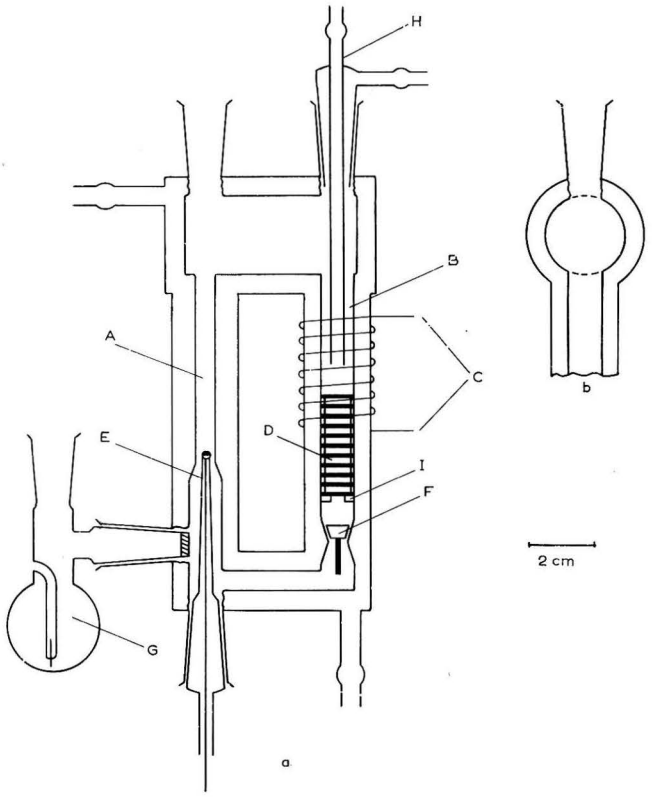

Fig. 1. Polarographic cell diagram: (a), front view; (b), side view. (A), Electrode compartment; (B), cylinder in which the piston runs; (C), magnet coil; (D), finned Teflon piston; (E), hemispherical platinum electrode; (F), frustum-conical valve with platinum stabilizer tail; (G), reference electrode; (H), de-aeration tube; (I), Teflon diaphragm.

can give a pulse current that may be easily measured with the methods used in the classical polarography. In the cell studied in this work, it is still the periodical movement of the electrolyte on the platinum microelectrode that causes a pulse current, but here the renewal of the electrolyte is caused by the displacement of a piston. The cell, made of pyrex glass, is shown diagrammatically in Fig. 1; the hemispherical platinum electrode (E) (this is the most suitable shape[4]) is placed in compartment (A) and must be perfectly centred in the tube (A). A Teflon-finned piston, containing an iron nucleus, runs with a close fit in the cylinder (B) which is to be considered the "cell-heart": it is pulse fed by the magnetic field produced by the external magnet coil (C) consisting of 520 turns of enamel-insulated copper wire with a diameter of 0.7 mm. The frustum-conical valve (F) is also Teflon built and has a platinum stabilizer tail. In non-operating conditions, the piston has the position shown in Fig. 1 and the valve lies in its seat. A Teflon diaphragm (I) is forced between the valve and the piston in compartment (B); this supports the piston and also limits the sliding speed of the solution. The movement of the piston is limited above, by the end of the de-aeration tube (H). The salt bridge of the reference electrode (G) is

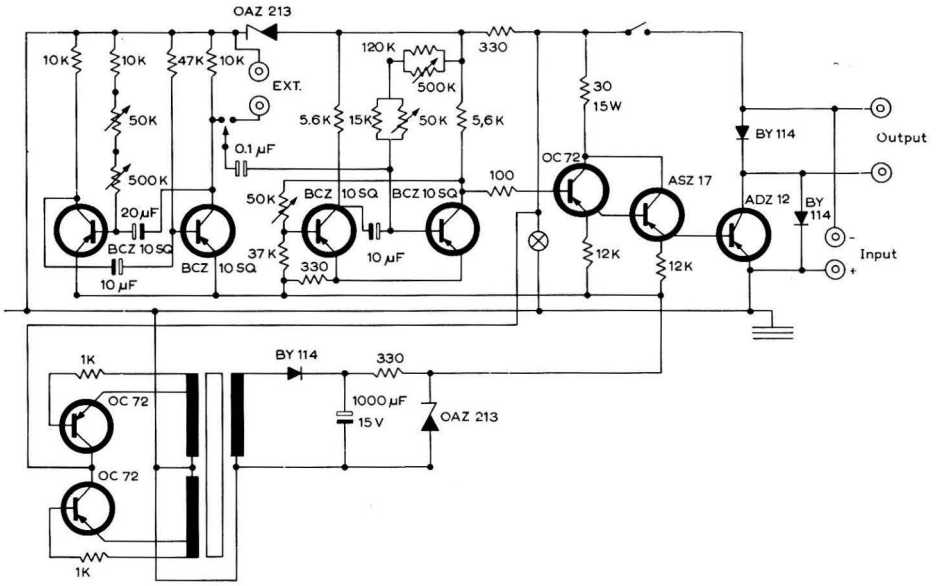

Fig. 2. Electronic switch scheme.

inserted through the side hole. The magnet coil (C) is connected to a storage battery through the electronic switch, as shown in the scheme of Fig. 2; it allows variation of both the frequency and the pulse period over a wide range. Its characteristics are: frequency: from one pulse in 1 sec to one pulse in 12 sec; closure period: from 0.1 sec to 1 sec; power supply: min. 14 V, max. 24 V in d.c.; piloted current: 10 A on 24 V.

Cell operating conditions

In order to establish the operating conditions of the cell, it is useful to take into consideration a complete cycle starting from the rest position of the piston. When

the current, controlled by the electronic switch, flows through the coil (C), a magnetic field is produced: it moves the piston upwards. During the whole period of rising, the valve (F) remains open allowing the passing of the solution drawn up by the piston: at every impulse the platinum electrode is supplied with a fresh electrolyte flow which ends as soon as the Teflon piston hits the end of the tube (H). After the stroke, the valve closes immediately excluding back flow of the electrolyte from tube (B) to tube (A) during the down movement of the piston which takes place as soon as the current, feeding the coil, is cut off. The speed of fall is comparatively slow due to the very small difference between the inner and the outer diameters of the glass tube and the Teflon piston, respectively. As a result of these piston displacements, a current may be registered the output of which (similar to the one obtained by the bubbling platinum electrode) is schematically reproduced in Fig. 3. Zero time is at the beginning

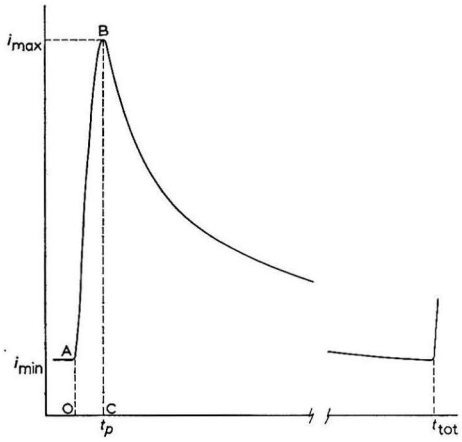

Fig. 3. Typical i–t curve during cell operation.

of the electrode washing, which is completed at time t_p. In the period between 0 and t_p, the solution is in motion while in the period t_p–t_{tot} it is stationary. During the washing, the current intensity increases from the value, i_{min}, to the value, i_{max}, owing to the rapid thinning of the diffusion layer; during the stationary period, the current intensity diminishes as the thickness of the diffusion layer on the electrode progressively increases. At t_{tot} time it reaches the value, i_{min}. The washing period is very short: it represents 1–3 hundredths of the stationary period. Under this condition, also, the quantity of current is small in comparison with that of the stationary period. The quantity of current, Q_1, during the first period, is represented by the area OABC, and it may be calculated, without any great error, as the area of the triangle having height $\overline{BC}$ and base $\overline{OC}$. Consequently

$$Q_1 = \frac{i_{max} \cdot t_p}{2} \tag{1}$$

The quantity, Q_2, may be calculated by the spherical diffusion equation, considering that in this period the electrode is in a stationary electrolyte:

$$i = a + \frac{b}{t^{\frac{1}{2}}} \tag{2}$$

where

$$a = \frac{nFADC}{r}, \quad b = \frac{nFAD^{\frac{1}{2}}C}{\pi^{\frac{1}{2}}}$$

integrating between t_p and t_{tot}, *i.e.*,

$$Q_2 = \int_{t_p}^{t_{tot}} \left(a + \frac{b}{t^{\frac{1}{2}}}\right) dt \tag{3}$$

This is possible on condition that at every instant between t_p and t_{tot} eqn. (2) is verified (the time is measured from the beginning of the electrode washing).
From eqns. (1) and (3):

$$Q = Q_1 + Q_2 = \left(a + \frac{b}{t_p^{\frac{1}{2}}}\right)\frac{t_p}{2} + \int_{t_p}^{t_{tot}} \left(a + \frac{b}{t^{\frac{1}{2}}}\right) dt$$

From this, integrating, it is seen that:

$$Q = a\left(t_{tot} + \frac{t_p}{2}\right) + b\,(2\,t_{tot}^{\frac{1}{2}} - 1.5\,t_p^{\frac{1}{2}})$$

and neglecting $t_p/2$ compared with t_{tot}:

$$Q = at_{tot} + b(2\,t_{tot}^{\frac{1}{2}} - 1.5\,t_p^{\frac{1}{2}})$$

Dividing by t_{tot}, we obtain the average current intensity:

$$\frac{Q}{t_{tot}} = \bar{\imath} = a + \frac{b}{t_{tot}}\,(2\,t_{tot}^{\frac{1}{2}} - 1.5\,t_p^{\frac{1}{2}}) \tag{4}$$

Equation (2) was verified with the cell operating as follows:

I. The piston strokes were experimented at the values: 2, 5, 8, 11 mm, corresponding to the displacement of solution with regard to the electrode, of 0.52—1.3—2.1—2.9 cm.

II. The diaphragm opening, which limits the solution translation speed, was experimented at the values 2, 3, 4 mm (the minimum opening of the valve seat is 5 mm).

III. The magnetic field intensity necessary to give the piston an impulse sufficient to cause its rapid displacement is obtained with a current above 2.0 A. Intensities of 2.6—4.4—6.1 A were experimented.

IV. The impulse length was established in 0.15–0.2 sec allowing both a whole piston stroke and the valve closure before the beginning of the piston downstroke.

V. The piston-seal results from the difference of 0.1 mm between the diameter of the tube (B) and that of the Teflon piston; this value ensures both a good seal during the upstroke and a not too slow downstroke. For the sake of simplicity we excluded a valve in the piston because there is an iron nucleus within it.

VI. The impulse frequency was established at 2.5—3.5—4.5—6—8 sec.

Results and discussion

The solution used for the measurements is the same as previously described[2-4]: 0.1 *N* NaOH containing $1 \cdot 10^{-3}$ *M* $K_4Fe(CN)_6$ thermostatted at $25 \pm 0.1°$.

An AME polarograph and a Metrohm Polarecord type E261 were used for the

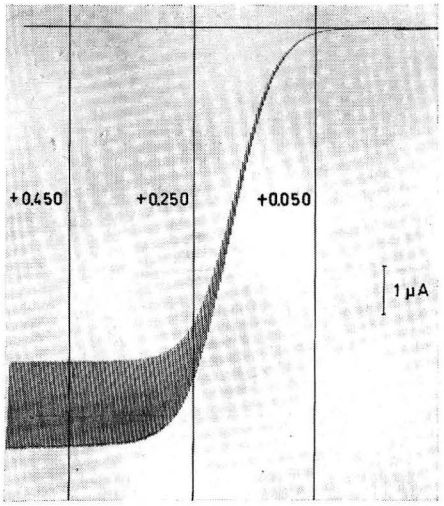

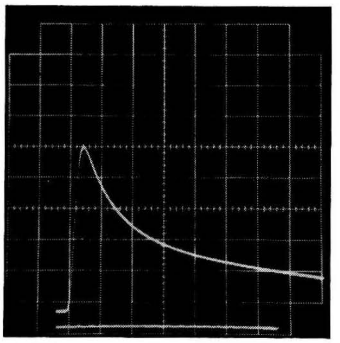

Fig. 4. Polarographic wave of $1 \cdot 10^{-3}$ *M* $K_4Fe(CN)_6$ in 0.1 *N* NaOH registered with the cell. The potential values are referred to a S.C.E.

Fig. 5. Instantaneous current–time curve of $1 \cdot 10^{-3}$ *M* $K_4Fe(CN)_6$ in 0.1 *N* NaOH registered with the electrode steadily polarized at +0.450 V (S.C.E.). Ordinates 10 μA/div; abscissae 50 msec/div.

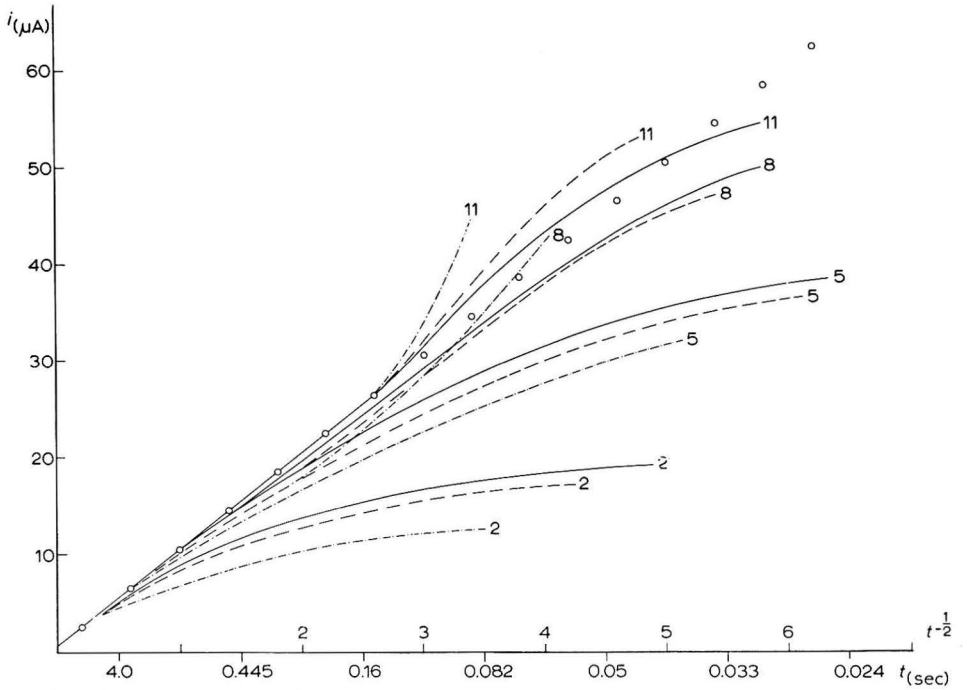

Fig. 6. Instantaneous current intensity plot as a function of t and of $t^{-\frac{1}{2}}$ obtained with a diaphragm diameter of 3 mm. Excitation intensity of the magnet coil: (——), 6.1 A; (– – – –), 4.4 A; (– · – · – ·), 2.66 A. The values (○) reproduce the theoretical behaviour obtained from eqn. (2). The number by the side of each curve represents the piston stroke in mm.

measurements of the average limiting diffusion currents and a Tektronix type 502 cathode ray oscilloscope for the oscilloscopic investigation. The platinum electrode is hemispherical with a diameter of 1.875 mm and an effective surface of 6.74 mm^2.

The voltammetric curve registered in the potential range −0.150 to +0.550 V (S.C.E.) is reproduced in Fig. 4. The instantaneous currents resulting from the electrode steadily polarized at +0.450 V (S.C.E.) are reproduced in Fig. 5. The results obtained with the cell operating under different conditions are reproduced in Figs. 6 and 7 where the calculated (○) and experimental (—, – – –, – · – · –) instantaneous current values between t_p and t_{tot} are plotted against $t^{-\frac{1}{2}}$. The results obtained with a diaphragm opening of 2 mm are not reported because the renewal of the diffusion layer proved quite insufficient.

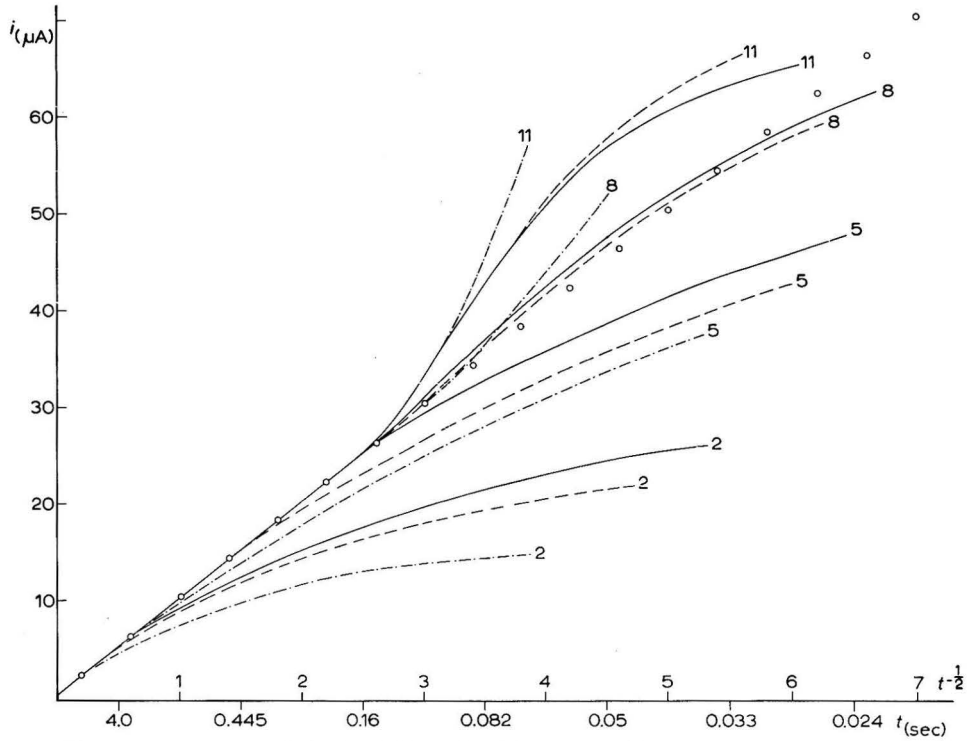

Fig. 7. Instantaneous current intensity plot as a function of t and of $t^{-\frac{1}{2}}$ obtained with a diaphragm diameter of 4 mm. Excitation intensity of the magnet coil: (——), 6.1 A; (– – – –), 4.4 A; (– · – · –), 2.66 A. The values (○) reproduce the theoretical behaviour obtained from eqn. (2). The number by the side of each curve represents the piston stroke in mm.

The curves reproduced in Fig. 6, regarding the cell with a diaphragm opening of 3 mm, show that the intensities of diffusion obtained with piston strokes of 2 and 5 mm are lower than the calculated values. This is because there is a depletion of depolarizer on the electrode surface owing to an incomplete renewal of the diffusion layer. The intensity values obtained with a piston stroke of 8 mm and coil excitation intensities of 2.66 and 4.1 A, show considerable improvement. They agree with the calculated values only after 1 sec from the beginning of the washing. For times less

TABLE 1

Section	*Excitation intensity (A)*	t_p *(msec)*	i_{pol} *(μA)*	i_{calc} *(μA)*	*Error (%)*	t_{tot} *(sec)*	*Diaphragm diameter (mm)*	*Piston stroke (mm)*
(A)	6.1	31	11.85	11.95	−0.8	2.51	3	8
		30	10.01	10.27	−2.5	3.54		
		30	9.03	9.22	−2.2	4.50		
		25	7.96	8.12	−1.9	6.05		
		18	6.98	7.20	−3.0	8.03		
(B)	2.66	96	11.63	11.15	+4.3	2.51	3	11
		87	9.80	9.75	+0.5	3.54		
		92	8.67	8.79	−1.3	4.50		
		83	7.80	7.80	0.0	6.05		
		82	6.85	6.92	−1.0	8.03		
	4.4	46	11.90	11.72	+1.5	2.51		
		45	9.97	10.11	−1.4	3.54		
		42	8.98	9.12	−1.6	4.50		
		41	7.90	8.01	−1.4	6.05		
		41	7.00	7.07	−1.0	8.03		
	6.1	32	12.12	11.93	+1.6	2.51		
		30	10.25	10.27	−0.2	3.54		
		30	9.15	9.22	−0.7	4.50		
		30	8.02	8.08	−0.7	6.05		
		35	7.10	7.10	0.0	8.03		
(C)	6.1	25	12.12	12.04	+0.6	2.51	4	5
		24	10.46	10.39	+0.7	3.51		
		22	9.20	9.26	−0.6	4.56		
		24	7.98	8.09	−1.3	6.07		
		25	7.05	7.15	−1.4	8.03		
(D)	2.66	52	11.70	11.60	+0.8	2.51	4	8
		50	10.08	10.09	−0.1	3.51		
		50	8.83	9.02	−2.1	4.56		
		46	7.77	7.95	−2.3	6.07		
		49	6.84	7.03	−2.7	8.03		
	4.4	25	12.18	12.04	+1.1	2.51		
		26	10.38	10.36	+0.2	3.51		
		27	9.02	9.21	−2.0	4.56		
		25	7.91	8.09	−2.2	6.07		
		25	6.93	7.15	−3.1	8.03		
	6.1	24	12.35	12.05	+2.5	2.51		
		22	10.65	10.41	+2.3	3.51		
		25	9.43	9.24	+2.0	4.56		
		22	8.18	8.11	+0.9	6.07		
		22	7.20	7.15	+0.7	8.03		
(E)	2.66	72	12.35	11.37	+8.6	2.51	4	11
		67	10.45	9.94	+5.1	3.51		
		65	9.22	8.92	+3.2	4.56		
		61	8.02	7.87	+1.9	6.07		
		61	6.99	6.98	+0.1	8.03		
	4.4	37	12.57	11.82	+6.3	2.51		
		32	10.65	10.28	+3.6	3.51		
		32	9.32	9.16	+1.7	4.56		
		31	8.10	8.04	+0.7	6.07		
		32	7.15	7.11	+0.6	8.03		
	6.1	29	12.83	11.96	+7.3	2.51		
		27	10.90	10.34	+5.3	3.51		
		25	9.54	9.24	+3.2	4.56		
		25	8.23	8.09	+1.7	6.07		
		27	7.20	7.12	+1.1	8.03		

than 1 sec, some differences between calculated and experimental current values still exist, but they are smaller than in the preceding cases. If the coil excitation intensity is 6.1 A, the current values become equal to the calculated values soon after 0.16 sec. As the time during which the experimental values are different from the calculated values is here very short, the experimental average limiting current agrees well enough with the values calculated by eqn. (4) (Table 1, section A). The currents measured when the piston stroke is 11 mm are equal to the calculated values only after 1 sec. The values of the experimental average limiting current reproduced in Table 1, section B, are in good agreement with the calculated values. The curves reproduced in Fig. 7, for the cell with a diaphragm opening of 4 mm in diameter, again show that the diffusion intensities, obtained with a piston stroke of 2 mm, are clearly lower than the calculated values. With a piston stroke of 5 mm, good results are obtained only when the coil is fed by a current of 6.1 A (Table 1, section C). Good results are obtained when the piston stroke is 8 mm, independently of the amount of current feeding the coil (Table 1, section D). The instantaneous currents approximately agree with the calculated values from t_p (0.025 sec) to 0.12 sec becoming identical with the calculated values between 0.12 sec and t_{tot} (2.5–8 sec). When the piston stroke is 11 mm (Table 1, section E), there may be some discrepancies both between the values of the experimental and calculated average intensities and between those of the experimental and calculated instantaneous intensities from t_p to 0.15 sec. The experimental values become higher than the calculated values; this is due to the setting up of a turbulent flow condition on the electrode surface.

Considering that the piston stroke, the diaphragm opening, and the excitation intensity may be varied over a wide range, without any remarkable difference between the experimental and calculated currents, the results can be considered satisfactory. Particularly, in comparison with the bubbling platinum electrode, this new cell apparatus shows very good operating characteristics:

(1) The diffusion limiting current may be calculated, with good agreement, through the simple expression of spherical diffusion, introducing a new parameter t_p, corresponding to the washing period of the electrode.

(2) With this cell, it is possible to achieve, periodically, total washing of the electrode and the complete renewal of the diffusion layer. The "renewal fault" is eliminated because the electrode is supplied by a fresh electrolyte flow unlike the bubbling electrode (and also the dropping mercury electrode) where only a small electrolyte quantity undergoes electrolysis.

(3) Between two consecutive pulsations, the electrode operates in a stationary electrolyte. On the contrary, in the bubbling electrode, there is always a very slow solution movement which causes small and unavoidable variations in the current especially when the bubbling period is rather long.

(4) It is possible to extend the voltammetric study to volatile compounds, as the cell may be kept quite closed.

(5) It allows many possibilities of regulation.

This new cell is particularly interesting in the study of many electrochemical processes characterized by a high redox potential. It was employed in the study of halogen–halide redox couples, and in the oxidation and reduction of sulphites, hydrogen peroxide and peroxides. We shall deal with the results obtained in future publications.

ACKNOWLEDGEMENT

The authors are greateful to the National Research Council of Italy for financial support.

SUMMARY

A new cell with a platinum microelectrode is described: the diffusion layer is renewed by the periodical movement of the electrolyte caused by the displacement of a piston. A magnetic field causes the piston displacement. The diffusion current intensities, both instantaneous and average, may be calculated with a good agreement by the simple equation of spherical diffusion. The cell allows many possibilities of regulation both in the period of the electrode washing and in that during which the electrode is in the stationary electrolyte. Moreover, the flow speed of the solution may be easily regulated. This new cell is particularly interesting for the study of many electrochemical processes characterized by a high redox potential.

REFERENCES

1 D. Cozzi and P. G. Desideri, *J. Electroanal. Chem.*, 4 (1960) 301.
2 D. Cozzi, G. Raspi and L. Nucci, *Atti Soc. Toscana Sci. Nat. Pisa, Proc. Verbali Mem., Ser. A*, 70 (1963) 121.
3 D. Cozzi, G. Raspi and L. Nucci, *J. Electroanal. Chem.*, 6 (1963) 267.
4 D. Cozzi, G. Raspi and L. Nucci, *J. Electroanal. Chem.*, 6 (1963) 275.

"METALLKOMPLEX" ELEKTRODEN. I. DIE $Ag|[Ag(NH_3)_2]^+$, NH_3 ELEKTRODE, ANGEWENDET BEIM STUDIUM DER KOMPLEXEN AMMONIAKATE EINIGER ZWEIWERTIGEN METALLE

CONSTANTIN LUCA, VASILE MAGEARU UND GRIGORE POPA
Bukarester Universität, Chemische Fakultät, Bukarest (Rumänien)
(Eingegangen am 14 September, 1965)

EINLEITUNG

Die potentiometrischen Methoden die beim Studium der Bildungsgleichgewichte der Komplexverbindungen angewendet werden, verwenden hauptsächlich Metallelektroden erster Ordnung. Nur eine kleine Zahl solcher Elektroden erlauben genaue Messungen. In sehr wenigen Fällen wurden Elektroden zweiter Ordnung, die in Bezug auf das Anion eines schwerlöslichen Salzes reversibil sind, hierfür verwendet.

Um das Feld der analytischen Methoden zu erweitern und die Versuchsmöglichkeiten im Bereich der Komplexverbindungen in Lösungen zu vergrössern, haben wir einen neuen Elektrodentypus zweiter Ordnung untersucht, wo statt der schwerlöslichen Verbindung, eine komplexe schwach ionisierte Verbindung steht. Diese Elektroden können in folgender Weise geschrieben werden

$$Me|[Me\ L_n]^{(a-nb)+}, L^{b-} \qquad (1)$$

und sind in Bezug auf den Liganden L^{b-} reversibil, welcher das Komplex $[MeL_n]^{(a-nb)+}$ mit dem Metallion Me^{a+} bildet. Die Rolle des Liganden L kann durch verschiedene Anionen oder neutrale Moleküle eingenommen werden.

Wenn sich auch Ionen eines anderen Metalles in der Lösung befinden, welche Komplexe mit dem Liganden L bilden, dann kann ihre Konzentration im Gleichgewicht mit Hilfe einer entsprechenden Elektrode erster Ordnung bestimmt werden und somit können die Bildungsgleichgewichte der Komplexe des zweiten Metallions mit dem Liganden L untersucht werden.

THEORETISCHER TEIL

Betrachten wir das Halbelement

$$Ag|Ag^+, L^{b-} \qquad (2)$$

wo L ein neutrales Molekül oder ein Anion ist, welches mit den Silberionen eine Komplexverbindung bildet

$$Ag^+ + 2\ L^{b-} \rightleftarrows [AgL_2]^{(2b-1)-} \qquad (3)$$

Die Konstante des Gleichgewichtes (3) kann wie folgt geschrieben werden

$$K = \frac{a_{Ag^+} \cdot a_L^{2b-}}{a_{[AgL_2]^{(2b-1)-}}} \tag{4}$$

Das Potential der Silberelektrode des Halbelementes (2) wird durch die Nernstsche Formel ausgedrückt

$$E = E^0_{Ag^+} + \frac{RT}{F} \ln a_{Ag^+} \tag{5}$$

Setzt man in die Beziehung (5) aus Gleichung (4) die Aktivitäten der Ag^+ Ionen, so ergibt sich

$$E = E^0_{Ag^+} + \frac{RT}{F} \ln \frac{K \cdot a_{[AgL_2]^{(2b-1)-}}}{a_L^{2b-}} \tag{6}$$

Wenn die totale Ag^+ Ionenkonzentration im Verhältnis zur Konzentration des Liganden L, sehr klein ist, ($[Ag^+]/[L^{b-}] \simeq 10^{-6}$) und gleichzeitig die Gesamtkonzentration der Ag^+ Ionen in einer Versuchsreihe konstant gehalten wird, dann wird praktisch auch die Konzentration der Komplexverbindung $[AgL_2]^{(2b-1)-}$ beim Gleichgewicht konstant bleiben. Folglich ist der Zähler aus der Beziehung (6) konstant und kann in den ersten Teil der Beziehung eingeschlossen werden, der ebenfalls konstant ist. Somit erhält man

$$E = E^0_{[AgL_2]^{(2b-1)-}} - \frac{2RT}{F} \ln a_L{}^{b-} \tag{7}$$

Aus der Beziehung (7) geht hervor, dass das Potential E durch die Aktivität des Liganden L bestimmt wird. Die Silberelektrode wird dadurch eine Elektrode zweiter Ordnung, die reversibel in Beziehung zum Liganden ist.

Der Ausdruck $E^0_{[AgL_2]^{(2b-1)-}}$ aus der Beziehung (7) stellt das Standardpotential der somit erhaltenen Elektrode zweiter Ordnung dar, der auch in folgender Form geschrieben werden kann

$$Ag\,|\,[Ag\,L_2]^{(2b-1)-},\ L^{b-} \tag{8}$$

Die Elektroden wurden aus Silber angefertigt, erstens weil Silberelektroden bei gleichen Arbeitsbedingungen immer vollkommen gleiche Potentiale geben und sich nicht polarisieren, zweitens bilden die Ag^+ Ionen mit einer grossen Anzahl neutraler Molekeln oder Anionen sehr stabile lösliche Komplexe. Ausserdem bilden sich in der Lösung, wenn man mit sehr kleinen Konzentrationen an Ag^+ Ionen arbeitet, in allen Fällen nur Komplexe vom Typus 1:2, der Form $[AgL_2]^{(2b-1)-}$.

Um die "Metall-Komplexe" Elektroden für Konzentrationsbestimmungen des Liganden L im Gleichgewicht benützen zu können, muss als erstes das Standardpotential der Elektrode $E^0_{[AgL_2]^{(2b-1)-}}$ bestimmt werden. Dieses hängt vom Wert des Standardpotentials der Silberelektrode $E^0_{Ag^+}$, von der Bildungskonstanten des Komplexes $[AgL_2]^{(2b-1)-}$ und von der Konzentration der Komplexionen in Lösung ab, demnach von der gesamten Konzentration an Silberionen, was mit folgender Beziehung ausgedrückt werden kann

$$E^0_{[AgL_2]^{(2b-1)-}} = E^0_{Ag^+} + \frac{RT}{F} \ln K \cdot a_{[AgL_2]^{(2b-1)-}} \tag{9}$$

Praktisch kann man, um das Standardpotential $E^0_{[AgL_2]^{(2b-1)-}}$ nicht vorher bestimmen oder berechnen zu müssen, auch nach einer der folgenden Varianten arbeiten.

(a) wenn die Bildungskonstante des Komplexes $[AgL_2]^{(2b-1)-}$ genau bekannt ist.

Man stellt zwei galvanische Elemente der Form

$$\begin{array}{ll} 1 & Ag\,|\,Ag^+\,|\,KNO_3\ (gesättigt)\,|\,KCl,\ Hg_2Cl_2\,|\,Hg \\ 2 & Ag\,|\,Ag^+,\ L^{b-}\,|\,KNO_3\ (gesättigt)\,|\,KCl,\ Hg_2Cl_2\,|\,Hg \end{array} \qquad (10)$$

auf. Die elektromotorischen Spannungen dieser zwei Elemente, deren Diffusionspotential einen konstanten Wert hat, kann folgendermassen geschrieben werden

$$E_1 = E^0_{Hg|Hg_2Cl_2} - (E^0_{Ag^+} + \frac{RT}{F} \ln a_{Ag_1{}^+}) \qquad (11)$$

$$E_2 = E^0_{Hg|Hg_2Cl_2} - (E^0_{Ag^+} + \frac{RT}{F} \ln a_{Ag_2{}^+}) \qquad (12)$$

Die Differenz dieser Gleichungen ergibt

$$\Delta E = E_2 - E_1 = \frac{RT}{F} \ln \frac{a_{Ag_1{}^+}}{a_{Ag_2{}^+}} \qquad (13)$$

Aus Gleichung (13), mit Berücksichtigung der Gleichung (4), erhält man, wenn immer mit sehr kleinen Konzentrationen an Gesamtgehalt an Silber gearbeitet wird, und diese Konzentrationen in den Elementen 1 und 2 ebenfalls gleich sind, übergehend zum dekadischen Logarithmus folgendes

$$pK = \frac{\Delta E}{0.05915} - 2\lg a_{L^{b-}} \qquad (14)$$

wo $pK = -\lg K$. Die Beziehung (14) ist gültig, wenn

$[L^{b-}] \gg [Ag^+]$ und folglich $a_{Ag_1{}^+} \simeq a_{[AgL_2]^{(2b-1)-}}$.

Aus Beziehung (14) kann nun die Beziehung abgeleitet werden, die die Berechnung der Aktivitäten des Liganden im Element 2, bei Gleichgewicht, erlaubt

$$\lg a_{L^{b-}} = \frac{pK}{2} - \frac{\Delta E}{0.11831} \qquad (15)$$

Die Bildungskonstanten der Silberkomplexen mit verschiedenen Liganden wurden mit grosser Genauigkeit in einer Reihe von Arbeiten bestimmt[1-10].

Es muss darauf hingewiesen werden, dass die Konstante K aus Gleichung (15) die thermodynamische Konstante der Bildung des Komplexes sein muss. Wenn in die Beziehung (15) der Wert der scheinbaren Konzentrationskonstanten eingesetzt wird, so erhält man die Konzentration des Liganden im Element 2 und nicht die Aktivität.

(b) wenn der Wert der Konstanten K nicht bekannt ist.

Man stellt zwei galvanische Elemente folgender Form auf

$$\begin{array}{ll} 3 & Ag\,|\,Ag^+,\ L^{b-}(C_s)\,|\,KNO_3\ (gesättigt)\,|\,KCl,\ Hg_2Cl_2\,|\,Hg \\ 4 & Ag\,|\,Ag^+,\ L^{b-}(C_x)\,|\,KNO_3\ (gesättigt)\,|\,KCl,\ Hg_2Cl_2\,|\,Hg \end{array} \qquad (16)$$

in welchem C_s eine bekannte Konzentration des Liganden darstellt. Das Element 3 wird hiermit Vergleichselement.

Wird nun die elektromotorische Spannung dieser zwei Elemente gemessen, so kann die Konzentration des Liganden im Element 4, also C_x bestimmt werden. Zu diesem Zweck wird die Differenz der elektromotorischen Spannungen dieser zwei Elemente mit Berücksichtigung der Gleichung (7) aufgeschrieben.

$$\Delta E = \frac{2RT}{F} \ln (a_{L^{b-}})_s - \frac{2RT}{F} \ln (a_{L^{b-}})_x \tag{17}$$

woraus

$$\lg(a_{L^{b-}})_x = \lg(a_{L^{b-}})_s - \frac{\Delta E}{0.11831} \tag{18}$$

Die Beziehung (18) erlaubt die Bestimmung der Konzentration oder der Aktivität des Liganden ohne die Bildungskonstante des Komplexes $[AgL_2]^{(2b-1)-}$ zu kennen. Die Elemente 3 und 4 können ebenfalls zu einer Konzentrationskette reduziert werden, so dass der Wert ΔE nun direkt erhalten wird.

Bei Reihenmessungen kann ein mit Hilfe des Elementes 3 geeichtes Elektrometer verwendet werden, welches ähnlich geeicht wird wie laufend die pH-Meter. Somit kann der Konzentrationswert des Liganden in der Untersuchungslösung direkt auf der Skala des Messinstrumentes abgelesen werden.

BESTIMMUNG DER BILDUNGSKONSTANTEN DER KOMPLEXEN Zn(II), Co(II) UND Ni(II)-AMMONIAKATE

Um die Verwendungsmöglichkeiten der Metallkomplexelektroden beim Studium der Bildungsgleichgewichte der Komplexverbindungen verschiedener Elemente zu untersuchen, haben wir die Bildungkonstanten der komplexen Zn(II), Co(II) und Ni(II) Ammoniakate bestimmt.

Zu diesem Zweck haben wir eine Metallkomplexelektrode der Form

$$Ag\,|\,[Ag(NH_3)_2]^+,\ NH_3 \tag{19}$$

benützt und eine Arbeitsweise verfolgt, die die Anwendung der Bjerrumschen Methode[11] für die Berechnung der aufeinanderfolgenden Bildungskonstanten der komplexen Ammoniakate gestattet. Zu diesen Zweck wurden die Elemente aufgebaut

$$\begin{aligned} &5 \quad Ag\,|\,[Ag(NH_3)_2]^+,\ NH_3\,|\,KNO_3\ (\text{gesättigt})\,|\,KCl,\ Hg_2Cl_2\,|\,Hg \\ &6 \quad Ag\,|\,[Ag(NH_3)_2]^+,\ NH_3,\ Me^{2+}\,|\,KNO_3\ (\text{gesättigt})\,|\,KCl,\ Hg_2Cl_2\,|\,Hg \end{aligned} \tag{20}$$

wo die Gesamtmenge an Silberionen in beiden Elementen gleich und sehr klein ist ($\sim 10^{-6}$).

Das Element 6 enthält zusätzlich gegenüber dem Element 5 eine bekannte Menge Metallionen des Metalles dessen Komplexe mit Ammoniak untersucht werden. Veränderlich waren die Ammoniakmengen, wobei eine Titriertechnik angewendet wurde, bei der das gleiche Volumen Lösung in beide Elemente zugefügt wurde. Das Element 5 dient folglich als Eichelement, welches den Wert der elektromotorischen Spannung des Elementes in Abwesenheit der Me^{2+} Ionen gibt, also den der Gesamt-

konzentration an Ammoniak. (Die kleine Menge Ammoniak die im Silberkomplex eingeschlossen ist, ist praktisch vernachlässigbar).

Im Element 6 wird ein Teil des Liganden für die Bildung der Komplexen $[Me(NH_3)_n]^{2+}$ verbraucht, während die Konzentration des Liganden beim Gleichgewicht in Gegenwart der Me^{2+}-Ionen aus dem elektromotorischen Spannungen der zwei Elemente, mit Hilfe der Beziehung (18) berechnet werden kann.

Wenn nun die Gesamtkonzentration der Me^{2+} Ionen und des Liganden beim Gleichgewicht bekannt ist, können für eine Reihe von Gesamtkonzentrationen des Liganden die Bildungskurven nach BJERRUM[11] der Form $\bar{n}$—p[L] gezogen werden. Danach können die aufeinanderfolgenden Bildungskonstanten der untersuchten Komplexe berechnet werden.

EXPERIMENTELLER TEIL

Für die Bestimmung der Bildungskonstanten der komplexen Zn(II), Co(II) und Ni(II) Ammoniakate wurden Lösungen verwendet, die aus Salzen mit dem Reinheitsgrad p.a. Merck und bidestilliertem Wasser hergestellt wurden.

TABELLE 1

EXPERIMENTELLE DATEN DES KOMPLEXEN Zn(II) AMMONIAKATES

$C_{Zn^{2+}}$	C_{NH_3}	$-\Delta E$ (V)	$[NH_3]$	$p[NH_3]$	$\bar{n}$
0.092920	0.01033	0.1471	0.0006147	3.21131	0.104
0.089545	0.04977	0.1768	0.0016735	2.77636	0.537
0.085650	0.09521	0.1838	0.0027963	2.5534	1.079
0.082081	0.13687	0.1869	0.0037883	2.4216	1.621
0.078800	0.17520	0.1849	0.0052660	2.2785	2.156
0.075773	0.21057	0.1784	0.0068630	2.1637	2.688
0.072961	0.24333	0.1658	0.0101053	1.9955	3.196
0.070353	0.27375	0.1425	0.0177551	1.7506	3.781
0.067930	0.30206	0.1074	0.0384201	1.4154	3.882
0.065663	0.32850	0.0817	0.0677211	1.1693	3.971
0.063551	0.35322	0.0513	0.1054100	0.9772	3.899

TABELLE 2

EXPERIMENTELLE DATEN DES KOMPLEXEN Co(II) AMMONIAKATES

$C_{Co^{2+}}$	C_{NH_3}	$-\Delta E$ (V)	$[NH_3]$	$p[NH_3]$	$\bar{n}$
0.20996	0.00145	0.0507	0.000549	3.2599	0.090
0.17390	0.11195	0.1521	0.006044	2.2186	0.608
0.16666	0.21458	0.1353	0.015998	1.7959	1.192
0.16000	0.30910	0.1170	0.032731	1.4850	1.727
0.15381	0.39615	0.1012	0.050645	1.2955	2.246
0.14293	0.55181	0.0759	0.128610	0.8907	2.961
0.13333	0.68666	0.0597	0.218401	0.6607	3.513
0.12503	0.80473	0.0471	0.325951	0.4868	3.830
0.11762	0.90882	0.0404	0.418603	0.3782	4.169
0.11111	1.00141	0.0341	0.520312	0.2837	4.333
0.10000	1.15875	0.0255	0.710400	0.1485	4.483
0.08701	1.34348	0.0300	0.934901	0.0292	4.696

TABELLE 3

EXPERIMENTELLE DATEN DES KOMPLEXEN Ni(II) AMMONIAKATES

$C_{Ni^{2+}}$	C_{NH_3}	$-\Delta E$ (V)	$[NH_3]$	$p[NH_3]$	$\bar{n}$
0.092307	0.03961	0.1942	0.000954	3.0205	0.420
0.090909	0.07803	0.1886	0.002092	2.6794	0.835
0.088235	0.15147	0.1676	0.006070	2.2167	1.647
0.085710	0.22071	0.1380	0.015625	1.8062	2.393
0.083333	0.28533	0.1124	0.033010	1.4813	3.028
0.081081	0.34797	0.0907	0.061045	1.2143	3.538
0.078947	0.40658	0.0734	0.099420	1.0025	3.890
0.075000	0.51500	0.0531	0.185910	0.7307	4.388
0.071421	0.61310	0.0411	0.278650	0.5549	4.682
0.068180	0.70250	0.0343	0.363800	0.4392	4.967
0.060000	0.92700	0.0220	0.607810	0.2162	5.321
0.057703	0.99038	0.0195	0.681240	0.1667	5.357

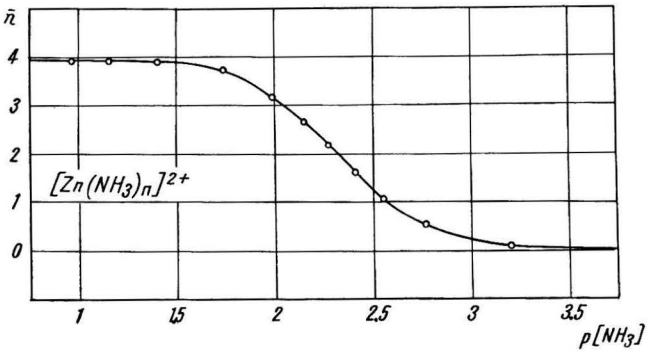

Abb. 1. Bildungskurwe der Zn(II)-Ammoniakat.

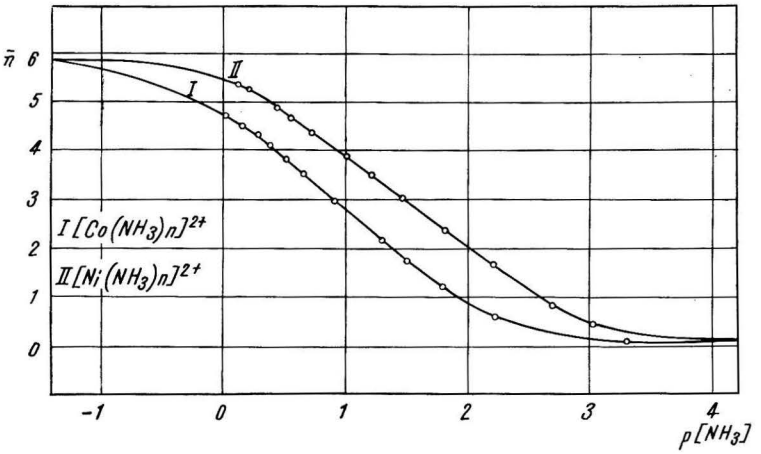

Abb. 2. Bildungskurwen der Co(II) und Ni(II)-Ammoniakate.

Die Ionenstärke aller Lösungen wurde mit NH_4NO_3 beim Werte 2 M konstant gehalten.

Die Messungen wurden mit Hilfe einer potentiometrischen Brücke, mit einer Genauigkeit von ± 0.1 mV, bei einer Temperatur von $25° \pm 0.1°$ ausgeführt. Nachdem nun die Gesamtkonzentration der Me^{2+} Ionen bekannt ist und die Konzentration des Liganden im Gleichgewicht mit der Metallkomplexelektrode $Ag|[Ag(NH_3)_2]^+, NH_3$ gemessen wurde, konnten die Werte für die Bjerrumsche Funktion der Komplexbildung berechnet werden (Tabelle 1, 2, 3).

Die graphischen Darstellungen der Bildungskurven zeigten eine gute Übereinstimmung mit den Daten aus der Fachliteratur[11] bei welchen die Ammoniakkonzentration im Gleichgewicht mit der Glasselektrode bestimmt wurde. Als Beispiel sind die Bildungskurven der untersuchten komplexen Ammoniakate in den graphischen Darstellungen 1 und 2 gegeben.

Von der Gleichung der Bildungskurve

$$\bar{n} + (\bar{n}-1)[L]k_1 + (\bar{n}-2)[L]^2K_2 + \ldots + (\bar{n}-N)[L]^NK_N = 0 \qquad (21)$$

ausgehend, können verschiedene Berechnungsvarianten[11,12,13] für die aufeinanderfolgenden Bildungskonstanten der untersuchten Komplexe angewendet werden.

Die mit Hilfe der Bjerrumschen[11] Formel (22) berechneten sukzessiven Konstanten sind in der Tabelle 4 zusammengefasst.

$$k_n = \left(\frac{1}{[L]}\right)_{\bar{n}=n-\frac{1}{2}} \cdot \frac{1 + \sum_{t=1}^{t=n-1} \frac{1+2t}{[L]^t \cdot k_{n-1} \cdot k_{n-2} \ldots k_{n-t}}}{1 + \sum_{t=1}^{t=N-n} (1+2t)[L]^t \cdot k_{n+1} \cdot k_{n+2} \ldots k_{n+t}} \qquad (22)$$

TABELLE 4

DIE BILDUNGSKONSTANTEN DER KOMPLEXEN Zn(II), Co(II) UND Ni(II)-AMMONIAKATE IN NH_4NO_3-LÖSUNG, 2 M, BEI 30°

	Werte bestimmt mit der "Metallkomplexelektrode"					
n	$p[NH_3]_{\bar{n}=n-\frac{1}{2}}$			$lg\ k_n$		
	Zn	*Co*	*Ni*	*Zn*	*Co*	*Ni*
1	2.811	2.317	2.951	2.325	2.08	2.715
2	2.442	1.634	2.283	2.292	1.52	2.20
3	2.205	1.126	1.734	2.357	1.166	1.708
4	1.884	0.667	1.217	2.389	0.736	1.237
5		0.117	0.683		0.252	0.797
6		(−0.70)	(−0.05)		−0.59	0.14
	Werte bestimmt mit der Glaselektrode[11]					
1	2.874	2.325	2.995	2.37	2.11	2.795
2	2.512	1.630	2.265	2.44	1.63	2.24
3	2.270	1.130	1.728	2.50	1.05	1.73
4	1.84	0.683	1.211	2.15	0.76	1.19
5		0.108	0.671		0.18	0.75
6		−0.75	(−0.14)		−0.62	0.03

In den ersten Kolonnen sind auch die Annäherungswerte der sukzessiven Bildungskonstanten der untersuchten Komplexe, die von den graphischen Darstellungen der Bildungskurven entnommen wurden, gegeben

$$k_n = \left(\frac{1}{[L]}\right)_{\bar{n}=n-\frac{1}{2}} \tag{23}$$

Bei den Co(II) und Ni(II)-Komplexen konnten die Konstanten K_6 nicht aus den Bildungskurven erhalten werden weil eine zu hohe Konzentration des Amoniaks notwendig gewesen wäre (~ 7 M). Sie wurden jedoch mit Hilfe der Beziehung (24) nach BJERRUM[11] berechnet.

$$k_n = \frac{1}{[L]} \cdot \frac{\sum_{t=0}^{t=n-1} \frac{\bar{n}-n+1+t}{[L]^t \cdot k_{n-1} \cdot k_{n-2} \ldots k_{n-t}}}{\sum_{t=0}^{t=N-n} (n-\bar{n}+t)[L]^t \cdot k_{n+1} \cdot k_{n+2} \ldots k_{n+t}} \tag{24}$$

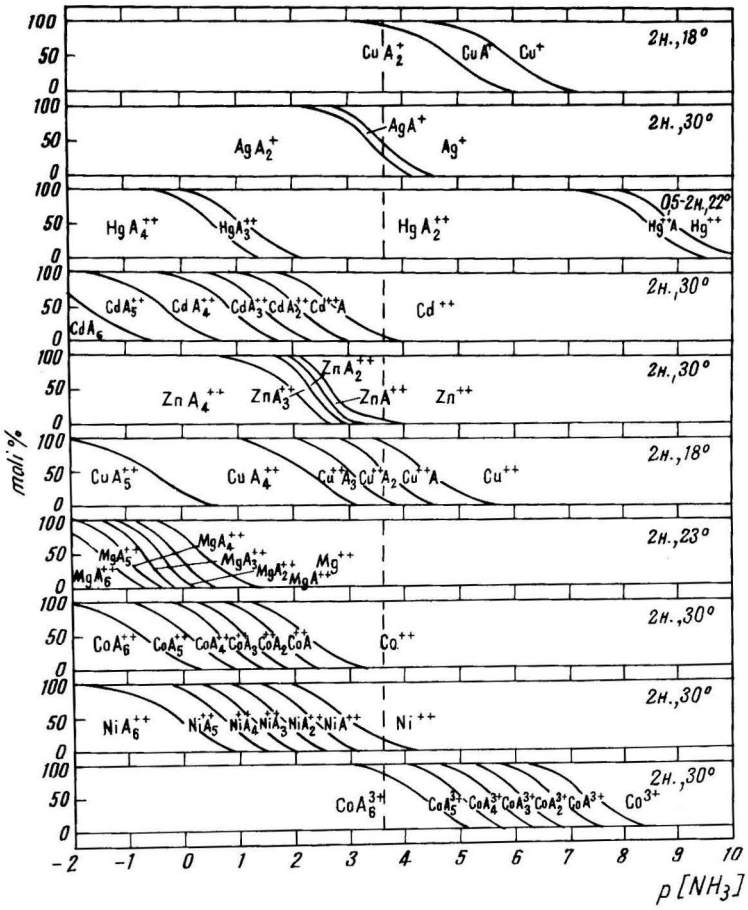

Abb. 3. Existenzbereiche einiger Komplex-Ammoniakate.

Es wird eine sehr gute Übereinstimmung zwischen den Werten der Bildungskonstanten die mit Hilfe der Metallkomplexelektroden und den Werten die mit Hilfe der Glaselektroden bestimmt wurden, festgestellt, wie aus Tabelle 4 hervorgeht.

Die Verwendungsmöglichkeiten der $Ag|[Ag(NH_3)_2]^+$, NH_3 Elektrode für die Bestimmung der Bildungskonstanten der komplexen Ammoniakate der Metallionen, ist vom Verhältnis der Stabilität dieser Komplexe gegenüber dem Silberammoniakat, abhängig. Aus Abb. 3 in welcher die Existenzbereiche einiger komplexen Ammoniakate dargestellt sind, geht hervor, dass diejenigen Komplexe untersucht werden können, deren Existenzkurven sich links von der punktierten Senkrechten, die das Bildungsgebiet des Silberammoniakates markiert, befinden.

Die Vorteile bei der Verwendung der Metallkomplexelektroden im Vergleich mit anderen Elektroden bestehen in folgendem.

(a) Man arbeitet mit galvanischen Elementen mit einem kleinen elektrischen Innenwiderstand, wodurch eine genauere Messung der elektromotorischen Spannung möglich ist.

(b) Es bedarf keiner elektronischen Apparatur für die Messung der elektromotorischen Spannung.

(c) Die Aktivität des Liganden im Gleichgewicht wird direkt bestimmt, während bei der Verwendung der Glaselektrode, diese Aktivität aus der Aktivität der Wasserstoffionen berechnet wird (also indirekt).

(d) Die Anwendungsmöglichkeiten sind mannigfaltig, wobei auch Komplexe mit Liganden untersucht werden können, die nicht Säuren oder Basen sind.

(e) Sie können bedeutende Dienste bei der Untersuchung der Komplexverbindungen in nichtwässrigen Medien und teilwässrigen Medien bringen, wo andere Elektrodentypen (insbesondere die Glaselektrode) schwer zu verwenden sind.

ZUSAMMENFASSUNG

Es wird ein neuer Elektrodentypus, unter dem Namen "Metallkomplex" Elektrode, untersucht, deren Potential von der Aktivität des Liganden in der Lösung einer Komplexverbindung abhängt.

Diese Elektroden ermöglichen die direkte potentiometrische Bestimmung einer grossen Zahl von Anionen oder neutralen Molekeln, desgleichen erlauben sie die Untersuchung der Bildungsprozesse der Komplexverbindungen sowie auch die Bestimmung der Gleichgewichtskonstanten.

In dieser Arbeit wurde die $Ag|[Ag(NH_3)_2]^+$, NH_3 Elektrode untersucht und die Möglichtkeit ihrer Verwendung bei der Bestimmung der sukzessiven Bildungskonstanten der komplexen Zn(II), Co(II) und Ni(II)-Ammoniakate, wobei eine sehr gute Übereinstimmung mit den Daten aus der Fachliteratur zu verzeichnen ist.

Dieser Elektrodentypus bietet eine Reihe von Vorteilen im Vergleich mit andern Elektroden, sowohl bei analytischen Bestimmungen als auch bei der Untersuchung der Bildungsreaktionen vieler komplexer Verbindungen.

LITERATUR

1 G. Popa, C. Luca und V. Magearu, *J. Chim. Phys.*, 60 (1963) 355.
2 G. Popa, C. Luca und V. Magearu, *J. Chim. Phys.*, 62 (1965) 449.

3 C. LUCA, V. MAGEARU UND G. POPA, *Analele Univ. Bucuresti, Ser. Stiint. Nat., Chim.*, unter Druck.
4 A. M. GOLUB UND V. V. SCOPENKO, *Zh. Neorgan. Khim.*, 1 (1961) 140.
5 V. ARMEANU UND C. LUCA, *Z. Physik. Chem.*, 214 (1960) 81.
6 V. ARMEANU UND C. LUCA, *Z. Physik. Chem.*, 217 (1961) 389.
7 P. SPACU UND C. LUCA, *Analele Univ. Bucuresti, Ser. Stiint. Nat., Chim.*, 11 (1962) 105.
8 R. GAUGUIN, *J. Chim. Phys.*, 42 (1945) 28.
9 G. SCHWARZENBACH, *Helv. Chim. Acta*, 33 (1950) 974.
10 J. E. PRUE UND G. SCHWARZENBACH, *Helv. Chim. Acta*, 33 (1950) 985.
11 J. BJERRUM, *Metal ammine formation in aqueous solution*, Haase, Copenhagen, 1957.
12 S. FRONAEUS, *Acta Chem. Scand.*, 5 (1951) 859.
13 H. OLERUP, Dissertation, Lund, 1944.

AN AMPEROMETRIC METHOD OF END-POINT LOCATION IN CONSTANT-CURRENT COULOMETRY

W. A. ALEXANDER AND D. J. BARCLAY
Department of Pure and Applied Chemistry, University of Strathclyde, Glasgow, C.1. (Great Britain)
(Received August 18th, 1965)

DISCUSSION

Amperometric end-point detection methods are widely used in coulometric titrimetry[1]. The technique, which involves a plot of current through the indicating electrode(s), requires that the electrochemical reaction at the indicator electrode must involve negligible amounts of the substance being determined. In the method here described, the indicating current is part of the working current, and this restriction is no longer necessary—the indicating current may be as high as 1% or more of the total constant current.

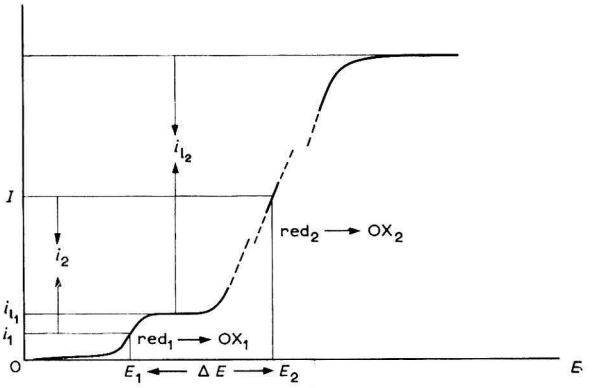

Fig. 1. Idealised current/potential curves for system containing red_1 and red_2.

Consider the coulometric titration of red_1 with ox_2 electrogenerated from the precursor, red_2. The idealised current/potential constant curve for this system is shown[2] in Fig. 1, where i_{l_1} and i_{l_2} represent limiting currents for the systems shown and i_1 and i_2 represent currents less than the limiting current for these systems. It is seen that the total constant current (I) is composed of two parts, i_1 corresponding to the reaction

$$red_1 - n_1 e = ox_1 \qquad (1)$$

and i_2 corresponding to the reaction

$$red_2 - n_2 e = ox_2 \qquad (2)$$

If now the current (I) is divided between two working electrodes (1 and 2, Fig. 2) by the resistances R_1 and R_2, there results a voltage difference, ΔE, between the two electrodes. By suitable adjustment of R_1 and/or R_2, ΔE can be maintained constant as the titration proceeds and the current through electrode (1) can be made to correspond to i_1 in Fig. 1, *i.e.* only reaction (1) takes place at electrode (1), and this current is directly proportional to the concentration of red_1.

The potential of an anodically polarised electrode immersed in a stirred solution of an oxidant and a reductant related by the equation $ox + ne = red$ is given by[3]:

$$E = E_{\frac{1}{2}} + \frac{RT}{nF} \ln \frac{i}{i_1 - i} \tag{3}$$

where

$$E_{\frac{1}{2}} = E^0 + \frac{RT}{nF} \ln \frac{D_O \delta_R f_R}{D_R \delta_O f_O} \tag{4}$$

where

i_1 = limiting diffusion current of reductant;
D_O and D_R = diffusion coefficients of oxidant and reductant, respectively;
δ_O and δ_R = extent of diffusion layers for oxidant and reductant, respectively;
f_O and f_R = activity coefficients of oxidant and reductant, respectively.

Expressions of this form hold for both reversible and irreversible systems, provided a steady state is attained at this electrode. This can be achieved by using ionic solutions of high concentration and ensuring regular stirring. For reactions (1) and (2), it is readily seen that if the distance between the two electrodes is small, so that the iR drop between them is negligible, then:

$$\Delta E = \Delta E_{\frac{1}{2}} - \frac{RT}{nF} \ln \frac{i_1}{i_{1_1} - i_1} + \frac{RT}{nF} \ln \frac{i_2}{i_{1_2} - i_2} \tag{5}$$

If, now, ΔE is maintained constant, $i_2 \leqslant 99\%$ of I, and i_{1_2} is high (due to the addition of a large excess of red_2) then $i_1/i_{1_1} - i_1$ will remain constant during the titration, *i.e.*, i_1 will remain proportional to the concentration of red_1.

The limit stated for i_2 is approximate only; for example, for a total constant current of 100 mA and a value of i_{1_2} of about 10 times this current, the voltage fluctuation due to the last term in eqn. (5) would not exceed $0.3/n_2$ mV, and the indicating current would start at 1 mA.

It would be desirable to hold the potential of the indicating electrode (E_1) on

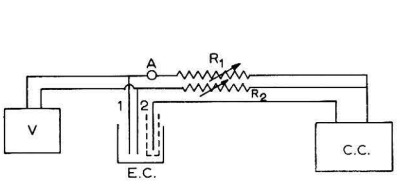

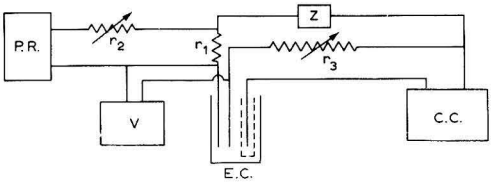

Figs. 2 and 3. Circuit diagrams. C.C., constant supply unit, in this case, a version of that used by GLASS AND MOORE[8] was utilised; R_1 and R_2, 0–5 kΩ wire-wound variable resistors; E.C., electrolysis cell (see text); A, variable range ammeter; V, valve voltmeter (Pye Dynacap); P.R., pen recorder, 0–10 mV scale, chart speed 1 in./min. (Honeywell Brown); Z, zener diode (Mullard, 9 V); r_1, 20 Ω wire-wound resistor; r_2, 20 kΩ variable wire-wound resistor; r_3, 1 kΩ variable resistor.

the plateau of the first wave in Fig. 1. This, however, is not practical due to:

(i) the plateau being not nearly so well-defined under the experimental conditions as that shown in the idealised case in Fig. 1;

(ii) the potential being very sensitive to current changes in this range.

For these reasons, the potential chosen will normally lie on the rising portion of the first wave and zero current will not correspond to zero concentration of red_1. This latter difficulty is overcome by pre-titrating the generating electrolyte (after addition of an amount of the ion to be determined) to a finite value of the indicating current and then titrating the sample to the same end-point.

EXPERIMENTAL

The above discussion should apply generally to coulometric titrations where the species involved in the two electrode reactions give rise to concentration-dependent limiting current phenomena. In the present work, the systems studied are listed in Table 1 together with the details of the generating electrolyte. The electrolysis cell was of capacity 200 ml and of conventional design; the usual volume contained in an experiment was 65 ml. The auxiliary electrode (bright platinum) was contained in a glass sleeve with a sintered-glass partition. The electrolyte in this compartment contained acid of the same nature and concentration as that in the titration cell. The two working electrodes immersed in the latter were bright platinum wires (20 s.w.g., length 2 cm) placed close together, and the solution stirred with a magnetic or mechanical stirrer. All reagents were of analytical reagent-grade; solutions were deoxygenated and the titrations were carried out in an atmosphere of nitrogen.

TABLE 1

Titrand	*Generated titrant*	*Titrant precursor*	*Composition of generating electrolyte*	*Ref.*
Fe(II)	Ce(IV)	Ce(III)	satd. $Ce_2(SO_4)_3$, 3 *M* H_2SO_4	5
Fe(II)	Cl_2	Cl^-	2 *M* HCl, 0.05 *M* $CuSO_4$	6
As(III)	Br_2	Br^-	1 *M* KBr, 0.1 *M* H_2SO_4	4

After some preliminary work with the hand-operated circuit (Fig. 2), the modification shown in Fig. 3 was finally adopted. This employs a Zener diode (z) to maintain ΔE constant. The pen-recorder responds to the voltage changes over the low resistance, r_1. This measures the current through electrode (1), and the electrolysis time. If the current through electrode (2) remains substantially constant, then ΔE should not change during the experiment by more than the change in the small voltage drop over r_1.

PROCEDURE

This involves a preliminary pre-titration to determine an arbitrary end-point followed by the actual titration to the same end-point.

An aliquot of the titrand was transferred to the generating electrolyte as given in Table 1. Stirring was started, and the nitrogen atmosphere established. The current

and pen-recorder were switched on and r_3 (Fig. 3) adjusted to give the required ΔE between the two electrodes, and a suitable reading on the pen-recorder. ΔE-values were determined experimentally before commencing the pre-titration. The latter was allowed to proceed until the indicating current fell to a few microamperes. This value was noted, and the generating current switched off. A fresh aliquot of the titrand was added to this pre-titrated solution, and the procedure repeated until the current fell to the noted value—the time for this being given by the pen-recorder.

RESULTS

Results for the three systems listed in Table 1 are given in Table 2. The plots of current *vs.* time showed slight curvature corresponding to the early part of the titration, but were linear for at least the last half of the titration. It was observed that ΔE did alter during the titration, often rather more than could be accounted for by the simple theory outlined above. For example, in the titration of iron(II) by electrogenerated chlorine, ΔE altered (decreased) by approximately 0.06 V. Since the initial indicating current was approximately 0.5 mA, and the value of r_1 was approximately 20 Ω, the theoretical alteration in ΔE should have been of the order of 0.01 V.

TABLE 2

RESULTS USING CIRCUIT SHOWN IN FIG. 3

Titrand	*Generated titrant*	*Equivs. taken* ($\times 10^4$)	*No. of determinations*	*ΔE*		*Generating current (approx. mA)*	*Indicator current*		*Recovery (equivs.* $\times 10^4$)	*Stand. deviation (%)*
				Initial	*Final*		*Initial (μA)*	*Final (μA)*		
Fe(II)	Ce(IV)	1.03	10	0.60	0.52	10	70	2	1.04	0.96
Fe(II)	Cl_2	9.60	10	0.60	0.54	100	650	10	9.57	0.42
Fe(II)	Cl_2	9.60	10	0.60*	0.60	100	650	10	9.56	0.43
As(III)**	Br_2	1.05	10	0.11*	0.11	10	100	5	1.04	0.96

* r_3 operated manually to keep ΔE constant.
** Platinised platinum indicating electrode used.

Deviation from the initial selected value of ΔE during the titration was, in some cases, corrected by manipulation of r_3. When this was done (marked by asterisk in Table 2) the current/time plot was linear throughout. In such cases, the titration could have been interrupted at an early stage and the result obtained by extrapolation. If a titration is continued until complete, the same result is obtained whether ΔE is maintained constant by hand manipulation or not.

It should be noted that in the amperometric end-point location method given by MYERS AND SWIFT[4] for the coulometric titration of arsenic(III) with bromine, the end-point is indicated by the diffusion current of the latter, and not of arsenic(III) as in this work. Under conventional amperometric end-point location conditions, the slowness of the arsenic(III)/arsenic(V) reaction precludes its use as an indicator system. Further, the conventional amperometric end-point technique in coulometry is stated as being confined to micro-coulometric titrations due to possible interference with the indicating system by parasitic current at high working current intensities[7].

The technique described in this paper should be applicable to both macro- and micro-determinations. The actual concentration range studied was 10^{-4}–10^{-2} M.

SUMMARY

An amperometric end-point determination for constant-current coulometric titrations has been investigated in which the voltage between two working electrodes having the same polarity with respect to the solution, is kept constant. The two electrodes share the constant current; the lesser fraction of the current through one electrode is recorded—this current being a linear function of the concentration of the ion being determined. An advantage of this method over a conventional amperometric method, is that there is no loss of current efficiency due to electrolysis at the indicator electrode, and consequently the indicating current can be monitored continuously and be very much greater than that used in the conventional method; *i.e.*, end-point detection in titrations involving species that are slowly oxidised or reduced electrochemically under normal amperometric conditions is facilitated.

REFERENCES

1 K. Abresch and I. Claasen, *Coulometric Analysis*, Chapmann and Hall, London, 1965, Part 1, chap. 4.
2 G. Charlot, J. Badoz-Lambling and B. Trémillon, *Electrochemical Reactions*, Elsevier Publishing Co., Amsterdam, 1962, p. 253.
3 P. Delahay, *New Instrumental Methods in Electrochemistry*, Interscience Publishers Inc., New York, 1954, p. 220.
4 R. J. Myers and E. H. Swift, *J. Am. Chem. Soc.*, 70 (1948) 1047.
5 N. H. Furman, C. E. Cooke and C. N. Reilley, *Anal. Chem.*, 23 (1951) 945.
6 P. Farrington, W. P. Schaeffer and J. M. Dunham, *Anal. Chem.*, 33 (1961) 1318.
7 Ref. 1, p. 47.
8 J. R. Glass and E. J. Moore, *Anal. Chem.*, 32 (1960) 1265.

SHORT COMMUNICATIONS

Characterization of bacterial pigments by single-sweep polarography

A satisfactory description of the chemical nature of a considerable number of pigments of micro-organisms, in particular, bacteria, cannot be found in the literature.

Chromatography and spectrophotometry may not yield sufficient data for identification of a bacterial pigment. With the exception of bacterial chlorophylls and some carotenoids, involved methods of analytical chemistry are needed for a positive identification of the pigment, and these are time-consuming and very often impractical for the micro-biologist.

Polarography has been used for investigating some bacterial pigments[1-3], but the application of modern polarographic techniques, which use very sensitive instruments, still awaits development.

A study was therefore initiated in this laboratory to determine the possibility of characterizing bacterial pigments by means of single-sweep polarography. This study was prompted by the fact that unsuccessful attempts had previously been made at determining the structure of the red pigment of a bacterium isolated from a culture of a marine flagellate.

Experimental

Bacterial pigments. Prodigiosin, obtained from a strain of *Serratia marcescens*, violacein obtained from a strain of *Chromobacterium violaceum*, and the red pigment of a marine bacterium, previously associated with the flagellate *Cryptomonas erosa Ehrenberg*, were used in this investigation. The β-carotene used in this study was obtained from a chemical supplier.

The organisms were grown on nutrient agar containing 0.3% yeast extract. For the marine bacterium, 75% sea-water was used in place of distilled water.

Cells from the surface growth of large agar plates were suspended in distilled water and centrifuged. The sedimented cells were washed with distilled water, centrifuged again, the supernatant liquid discarded, and the pigment extracted with either methanol or acetone. The pigment of *Chromobacterium violaceum* and the marine bacterium were extracted with methanol while acetone was used for *Serratia marcescens*.

The pigment solutions were then passed through a millipore micro-filter assembly (using Whatman #50 filter paper as the filtering disc) to remove any residual bacterial cells after centrifugation, and finally isolated through evaporation of the methanol or acetone solution in a rotary evaporator at room temperature. The pigments were not purified by chromatography.

Solutions of all pigments for the polarographic studies were prepared from the dry pigment. A methanol solution of the marine bacterium was used to obtain an absorption spectrum of the pigment. A Perkin-Elmer recording spectrophotometer was used in this work.

Polarography. A Davis Differential Cathode-Ray Polarotrace and a Moseley 2D X-Y recorder were used to record the polarographic data.

The supporting electrolyte used for the polarographic studies was aqueous

McIlvaine buffer, with enough methanol added to make the final solution 50% methanol and 50% buffer, by volume. One milliliter of a $1 \cdot 10^{-4}$ g/ml methanol solution of the dry pigment was added to 1 ml of the buffer solution in a 5-ml polarographic cell. The solution was then purged with oxygen-free nitrogen for 3 min and polarographed from 0 to −2.0 V. The nitrogen was passed over copper at 450° and then through a 50% methanol solution before entering the polarographic cell.

The polarographic measurements were made at 25° ± 0.10° with a dropping mercury electrode that had a drop time of 7 sec in distilled water and $m = 5.4$ mg per drop. Redistilled mercury was used as the anode and all current peak potential values are referred to the mercury pool.

Results and discussion

The marine bacterium investigated in these studies is a small non-motile gram-negative rod that at times has a cocco-bacillary appearance; its pigment is non-diffusible and has a pink tinge. When extracted in the dry state, it has a waxy appearance and a dark red color. The pigment does not have the purple tinge of prodigiosin and the color of the solution does not change with pH. It is insoluble in water but soluble in most organic solvents.

A test for carotenoids, using sulfuric acid[4] on the cellular material, did not yield a characteristic blue color; however, a blue color appeared when the same test was made with the dry pigment.

An absorption spectrum of the pigment in the visible range showed a peak at 475 mμ. This peak did not appear to offer much help in characterizing the pigment, as prodigiosin also produces an absorption peak at approximately the same wave-length. A number of polarographic studies were then carried out to test the possibility of using this method as a means of characterizing the pigment.

TABLE 1

SINGLE-SWEEP POLAROGRAPHIC DATA FOR β-CAROTENE AND PIGMENT OF MARINE BACTERIUM (50% METHANOL–50% BUFFER)

Pigment ($5.0 \cdot 10^{-5}$ *g/ml*)	*pH*	*Waves observed*		*Remarks*
		Peak voltage	*Peak current*[a]	
β-Carotene	3.0	−1.45	—	Poorly defined
	4.0	−1.56	53.0	Single wave
	5.0	−1.61	43.0	Single wave
	6.0	−1.68	16.0	Single wave
	7.0	—	—	No wave
	8.0	—	—	No wave
Marine bacterium	4.0	−1.46	63.0	Single wave
	5.0	−1.52	53.0	Single wave
	6.0	−1.62	26.0	Single wave
	7.0	—	—	No wave
	8.0	—	—	No wave

[a] $10 \cdot 10$ to the $\frac{1}{2}$-in. graph-paper divisions

Tables 1 and 2 show the results obtained, in the pH-range 3–8 for each of the four pigments, by single-sweep polarography. It can be seen in Table 2 that at pH 4.0,

TABLE 2

SINGLE-SWEEP POLAROGRAPHIC DATA FOR PRODIGIOSIN AND VIOLACEIN (50% METHANOL–50% BUFFER)

Pigment ($5.0 \cdot 10^{-5}$ *g/ml)*	*pH*	*Waves observed*		*Remarks*
		Peak voltage	*Peak current*[a]	
Prodigiosin	4.0	−1.30	25.0	Double wave
		−1.39	10.0	
	5.0	−1.26	7.0	Double wave
		−1.44	26.0	
	6.0	−1.25	3.0	
		−1.43	12.0	Triple wave
		−1.51	4.0	
	7.0	—	—	No wave
	8.0	—	—	No wave
Violacein	4.0	−0.85	20.0	Single wave
		−1.19	8.0	Single wave
		−1.43	3.0	Single wave
		−1.69	37.0	Single wave
	5.0	−0.86	16.0	Single wave
		−1.70	24.0	Single wave
	6.0	−0.91	17.0	Single wave
		−1.71	12.0	Single wave
	7.0	−0.93	18.0	Single wave
		−1.70	—	Poorly defined
		−1.96	45.0	Single wave
	8.0	−0.98	42.0	Single wave
		−1.40	46.0	Single wave
		−1.95	54.0	Poorly-defined

[a] $10 \cdot 10$ to the $\frac{1}{2}$-in. graph-paper divisions

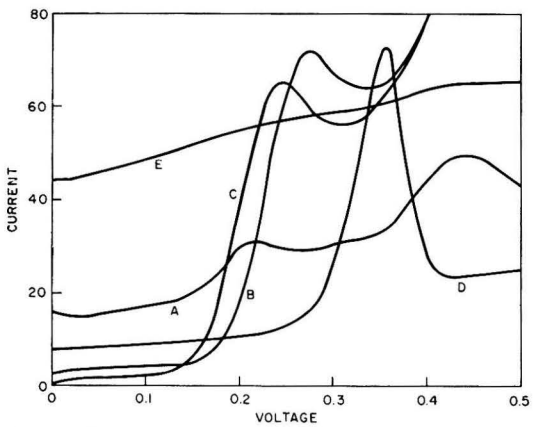

Fig. 1. Single-sweep polarograms of prodigiosin and violacein (pH 10): (S), prodigiosin; (V), violacein. Starting potential: (A), −0.85 (S); (B), −1.50 (S); (C), −1.50 (V); (D), −0.50 (V); (E), −0.90 V (V).

solutions of both prodigiosin and violacein give well-defined peaks around −1.0 to −1.4 V, while solutions of β-carotene and the pigment of the marine bacterium, respectively, do not produce polarograms in this voltage range. Prodigiosin also exhibits two smaller waves at −1.30 and −1.39 V, respectively, while violacein shows

a single well-defined polarogram with a peak at −0.85 V. The only waves observed for β-carotene and the pigment of the marine bacterium occurred in the region of −1.5 to −1.6 V. These waves are caused by the reduction of hydrogen ion in the supporting electrolyte and not by the reduction of the pigment. It can be seen from Table 1, that as the pH approaches 7, the peak potential becomes more negative and the peak current becomes less. At pH 7.0 the wave can no longer be seen. The McIlvaine buffer solution in the pH range 3–7 shows the same wave, with the peak potentials and peak currents the same as with the buffered solutions of these two pigments.

Solutions of violacein exhibit well-defined polarograms at pH 8 (Tables I and II) and at pH 10 (Fig. 1). Prodigiosin solutions do not produce waves at pH 8. Thus, one can characterize violacein in a solution containing these two pigments, in this manner. This wave was found to be linear in the range $1 \cdot 10^{-4}-1 \cdot 10^{-5}$ g/ml of violacein and could be used for quantitative studies. Prodigiosin showed a characteristic two-peaked polarogram at pH 10 (Fig. 1). This was not observed with any other pigment studied and should be useful in characterization and quantitative studies with this pigment.

From the observed single-sweep polarographic data obtained in this study, it appears that the chemical nature of the marine bacterium is more nearly like that of β-carotene than either prodigiosin or violacein. β-Carotene has previously been reported to be non-reducible polarographically[5]. The results of this study also showed β-carotene to be non-reducible at the dropping mercury electrode over the voltage range 0 to −2.0 V. The pigment of the marine bacterium was found to be non-reducible over this voltage range. Prodigiosin and violacein apparently contain easily reducible groups within their structure and thus exhibit several characteristic polarographic waves, while the red pigment of the marine bacterium does not appear to contain easily reducible groups.

From the results of this preliminary study, it is suggested that single-sweep polarography, because of its sensitivity and simplicity, can be a valuable tool for the characterization and study of bacterial pigments; however, a considerable amount of data needs to be gathered before the technique can be applied efficiently to the identification of the vast array of substances in biological pigments.

Chemistry Division,
U. S. Naval Ordnance Test Station,
China Lake, Calif. (U.S.A.)

G. C. WHITNACK
GIORGIO SOLI

1 C. CATTANEO AND G. SARTORI, *Arch. Sci. Biol. Bologna*, 27 (1941) 361.
2 C. CATTANEO, G. SARTORI AND M. MORELLINI, *Gazz. Chim. Ital.*, 77 (1947) 381.
3 H. P. KAUFMANN, D. SCHWEITZER AND P. WIERTZ, Deutsche Ges. Fettwissenschaft, Vortragstagung Dusseldorf, 1952.
4 V. B. D. SKERMAN, *A Guide to the Identification of the Genera of Bacteria (Carotenoid Pigments*, pp. 158–159), The Williams and Wilkins Company, Baltimore, Md., 1959.
5 M. BREZINA AND P. ZUMAN, *Polarography in Medicine, Biochemistry and Pharmacy*, Interscience Publishers, New York, 1958, pp. 381–2.

Received November 1st, 1965

Electrochemical behaviour of cadmium

Studies of the electrochemistry of the Cd(II)/Cd(Hg) system by polarography have been characterized by two features:

(1) Frequently, "anomalous" behaviour has been reported, *i.e.*, behaviour indicating that the electrode process has a mechanism more complex than an electron-transfer step combined with solely diffusive mass transport.

(2) Results obtained in different investigations have not generally been in accordance. In ostensibly similar systems, anomalies have sometimes been reported; even in the absence of anomalies, reported values for the kinetic parameters (rate constant k, transfer coefficient α) have generally differed.

It is proposed to show here that all reported observations are explicable by taking into account that mass transport is influenced by electrical migration of cadmium ions within the diffuse double layer.

Previous experimental results

Reported values for the kinetic parameters of the electron-transfer reaction involving cadmium ions at a mercury electrode have not been concordant. Work published up to 1960 has been reviewed and discussed in a recent monograph[1]. Later experimental work has continued to show conflicting and unexplained features: RANDLES[2] observed a difference in the rate constant (k) by a factor of 2 when using cadmium amalgam or pure mercury electrodes; and rate constants in sulphate solutions were much smaller than those in chloride or nitrate solutions (one feature in which all published work shows at least qualitative agreement). BIEGLER AND LAITINEN[3] obtained results which were partly in agreement with those of RANDLES[2] for perchlorate solutions, but differed in some respects, *e.g.*, in the variation of rate constant with potential, which is a measure of the transfer coefficient (α). Further, BIEGLER AND LAITINEN[3] obtained results in chloride and nitrate solutions that did not accord with those of BAUER, SMITH AND ELVING[4]. The latter found phase angles exceeding 45° ("anomalous"), the former found angles $=45°$ for chloride and $<45°$ for nitrate ("normal"). SLUYTERS-REHBACH AND SLUYTERS[5] have reported a k-value in 1 M potassium chloride at 25° as >12 cm sec^{-1}, in qualitative accord with the results of BIEGLER AND LAITINEN[3] but considerably faster than found by BARKER[6]. Observations made using the technique of second-harmonic a.c. polarography (defined and reviewed by BAUER[7]) have also demonstrated that the Cd(II)/Cd(Hg) system shows behaviour that is "anomalous" (SMITH[8] and BAUER AND FOO[9]).

Theory for mass transport influenced by attraction in the diffuse double layer

The ratio of measured to apparent (corrected for electrostatic effects) rate constants for the type of electrode process under discussion depends on the potential ϕ^0 at the outer Helmholtz plane in the manner shown in Fig. 1 (for quantitative results, see MATSUDA[10], MATSUDA AND DELAHAY[11], RANGARAJAN[12], NARAYANAN AND RANGARAJAN[13]). It is apparent that for a particular value of ϕ^0, the measured rate constant is infinite; for smaller values of ϕ^0 it is positive (phase angle $<45°$ in faradaic-admittance studies) and for larger values it is negative (phase angle $>45°$).

This "critical" value of ϕ^0 depends on the true exchange-current-density(*i.e.*, on the concentrations of the oxidant and reductant and on the transfer coefficient) and on the nature (number of charges carried by the ions) and concentration (affecting the double-layer thickness) of the supporting electrolyte. Therefore, in a system where

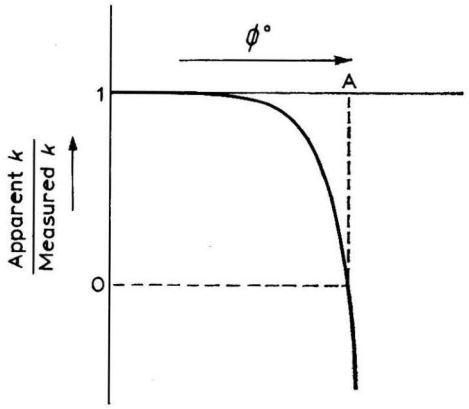

Fig. 1. Variation of measured rate constant as a function of potential across the diffuse double layer (ϕ^0) for attraction of the depolarizer (schematically, after MATSUDA AND DELAHAY[11]). "A" represents the "critical" value of ϕ^0: when $\phi^0 < A$, the measured rate constant is too large but the phase angle in faradaic-admittance studies is normal ($< 45°$); for $\phi^0 = A$, the measured rate constant is infinite, phase angle $= 45°$ at all frequencies; for $\phi^0 > A$, the measured rate constant is negative, the phase angle exceeds 45°.

ϕ^0 can be at or close to this critical value, the reduction of a positively-charged species may be expected to show the following characteristics:

(1) Increasingly negative values of ϕ^0 will lead to large, infinite, and, finally, negative measured rate constants; *e.g.*, the use of supporting electrolytes containing anions of increasing surface activity will produce such a progression.

(2) At a fixed value of ϕ^0, changes in the true exchange-current-density can produce similar effects; *e.g.*, changes in depolarizer concentration, or in the ratio of oxidant to reductant, can change the measured value of k and even produce—or cause to disappear—"anomalies" such as phase angles greater than 45°.

(3) Since variations of ϕ^0 of the order of millivolts or even less, or corresponding variations in the exchange-current-density, can have such profound effects (steep slope of the curve in Fig. 1 at the critical value of ϕ^0) it will be difficult to obtain reproducible results; experimental conditions may need to be exceedingly closely controlled although experience gained with other systems has not provided grounds for quite such careful control.

Application to the Cd(II)/Cd(Hg) system

The reported behaviour of cadmium fits the expectations for mass transport influenced by electrical migration as enumerated above. It remains to show that the critical value of ϕ^0 may be reached or exceeded with this system, and to give possible reasons for small differences of ϕ^0 and/or of exchange-current-density in experiments that have been performed at various times.

Negative values of k have been reported (*e.g.*, in 1 *M* potassium chloride and potassium nitrate solutions[4]) but never in sulphate solutions. Measurements have shown that ϕ^0 in 1 *M* potassium chloride is $\geqslant 34$ mV (GRAHAME AND PARSONS[14]; the relevant data is not given explicitly in this reference, but supplied by the authors as a supplement to reprints of the article); this represents the "critical" value if the true exchange-current-density is of the order of 1 A cm^{-2} (RANGARAJAN[12]). Since some reported values for the speed of the Cd(II)/Cd(Hg) system are too fast to be measured by faradaic-impedance techniques (SLUYTERS-REHBACH AND SLUYTERS[5], BIEGLER AND LAITINEN[3]; in some supporting electrolytes, BAUER *et al.*[4]) it is reasonable to conclude that in the reduction of cadmium ions, the critical value of ϕ^0 can be approached, reached, or exceeded.

Therefore, a plausible explanation exists for:

(1) "Anomalies" in the Cd(II)/Cd(Hg) system.

(2) Consistently higher measured values of k in chloride and nitrate solutions than in sulphate[6] or values of k that are negative in chloride and nitrate but positive in sulphate[4], since it is known that ϕ^0—at the relevant potential—is more negative in chloride and nitrate than in sulphate[15].

(3) The influence of reactant concentrations on measured rate-constant values: different exchange-current-densities correspond to different critical values of ϕ^0.

(4) Lack of accord between various reports. Variations in drop-time, minor differences in supporting-electrolyte composition (potassium chloride acidified[6] to pH 2 as compared to unacidified solutions[2]), small differences in temperature, the presence of various sorts of trace impurities—all these may be expected to produce in a system that is close to the critical point, effects so marked that such an explanation would not otherwise be plausible.

These points cover all the essential features reported in the literature for the Cd(II)/Cd(Hg) system, and it seems that the mechanism of reduction can thus be regarded as that of a fast electron-transfer with mass transport occurring by diffusion together with electrical attraction within the diffuse double layer (*i.e.*, the "Levich correction" or "dynamic ϕ effect").

It is also worth noting that systems of this sort provide a means for obtaining information about the double-layer structure (*e.g.*, ϕ^0) from measurements on faradaic processes (a possibility earlier noted by GIERST[16], and by BREYER *et al.*[17]) and that in certain cases this approach could be by far the most sensitive technique for such investigations.

Faculty of Agriculture, H. H. BAUER
The University of Sydney (Australia)

1 B. BREYER AND H. H. BAUER, *Alternating Current Polarography and Tensammetry*, Interscience/John Wiley, New York, 1963, pp. 64 ff. and 149 ff.
2 J. E. B. RANDLES in E. YEAGER (editor), *Transactions Symposium Electrode Processes, Philadelphia, 1959*, Wiley, New York, 1961, p. 209.
3 T. BIEGLER AND H. A. LAITINEN, *Anal. Chem.*, 37 (1965) 572.
4 H. H. BAUER, D. L. SMITH AND P. J. ELVING, *J. Am. Chem. Soc.*, 82 (1960) 2094.
5 M. SLUYTERS-REHBACH AND J. H. SLUYTERS, *Rec. Trav. Chim.*, 82 (1963) 535.
6 G. C. BARKER, *Anal. Chim. Acta*, 18 (1958) 118.
7 H. H. BAUER, *J. Sci. Ind. Res., India*, 24 (1965) 372.

8 D. E. SMITH, *Anal. Chem.*, 35 (1963) 1811.
9 H. H. BAUER AND D. C. S. FOO, unpublished work.
10 H. MATSUDA, *J. Phys. Chem.*, 64 (1960) 339.
11 H. MATSUDA AND P. DELAHAY, *J. Phys. Chem.*, 64 (1960) 332.
12 S. K. RANGARAJAN, *Canadian J. Chem.*, 41 (1963) 983, 1007.
13 K. NARAYANAN AND S. K. RANGARAJAN, *Australian J. Chem.*, 16 (1963) 565.
14 D. C. GRAHAME AND R. PARSONS, *J. Am. Chem. Soc.*, 83 (1961) 1291.
15 D. C. GRAHAME AND B. SODERBERG, *J. Chem. Phys.*, 22 (1954) 449.
16 L. GIERST in E. YEAGER (editor), *Transactions Symposium Electrode Processes, Philadelphia 1959*, Wiley, New York, 1961, p. 109.
17 B. BREYER, H. H. BAUER AND J. R. BEEVERS, *Australian J. Chem.*, 14 (1961) 479.

Received September 29th, 1965

Clarification of a supplementary polarographic device for automatic recording of capacitance

An electronic circuit auxiliary to a pen-recording polarograph has been described by KOWALSKI AND SRZEDNICKI[1,2] for rapid, continuous and automatic recording of double-layer capacity. This device has been claimed to be useful in investigations of electrochemical adsorption of organic compounds. There are, however, certain errors in the circuitry previously published[1] such that the device cannot function properly if constructed as described. Accordingly, the circuit has been modified[3], and the details are shown in Fig. 1. For convenience, we have incorporated Philips-

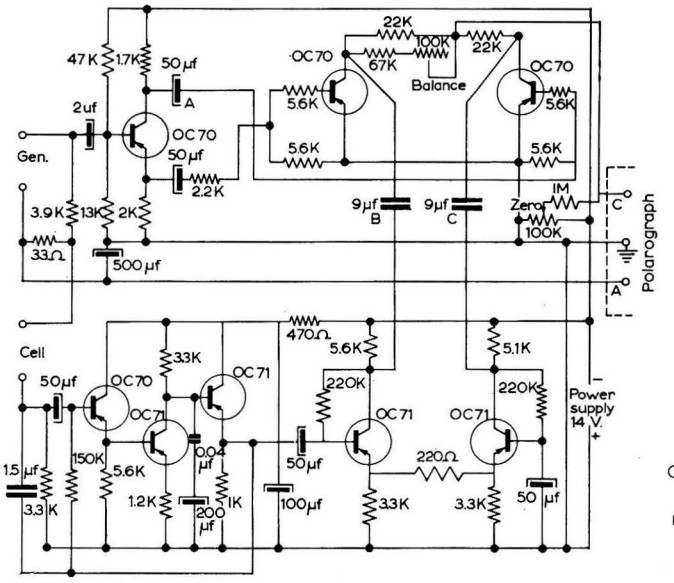

Fig. 1.

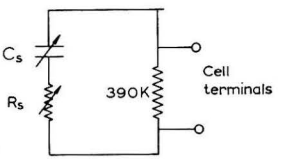

Fig. 2.

type transistors into the system, and added a variable resistor to balance oscillographically the two outputs of the phase detector. The important omissions in the circuit originally published are the capacitors A, B and C, without which the associated transistors are not biased correctly.

The entire assembly was tested by connecting an analogue circuit (Fig. 2) across the cell terminals (*cf.* refs. 4 and 5). It was found that when R_s and C_s, which simulate the solution resistance and double-layer capacitance, respectively, were varied, the Polariter PO-4 polarograph recorder deflection was linearly dependent on the magnitude of C_s at frequencies from 20 c/sec to an upper limit determined by the magnitude of R_s. Frequencies below 20 c/sec are restricted by mechanical problems arising from pen vibrations of the recorder. Frequencies up to 1200 c/sec were investigated for various values of R_s and C_s. For increments of 0.1 μF in the range $C_s = 0$–1.0 μF, equal pen deflections were observed provided that the condition $(\omega R_s C_s)^2 \ll 1$ (derived from eqn. (4), ref. 1) is fulfilled. The capacity–potential relationship was recorded using a hanging mercury-drop electrode[6] with an area of 0.2 cm^2, for an aqueous 1.0 *N* potassium chloride solution. The area of the electrode was estimated by comparing the total capacity recorded at −1.0 V (S.C.E.) with the data of GRAHAME AND PARSONS[7]. The solid line in Fig. 3 represents the results obtained for the 1.0 *N* KCl solution, and the circular points are the data of GRAHAME AND PARSONS[7] added for

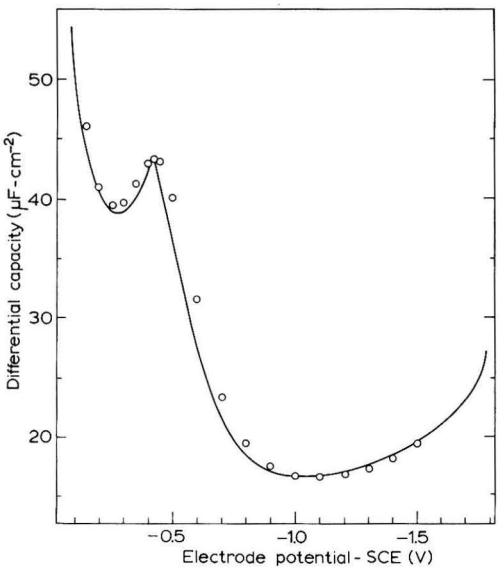

Fig. 3.

purposes of comparison. It is important to emphasize that our results shown in Fig. 3 are reproducible and require only 2 min to record. The order of agreement illustrated by Fig. 3 is much better than that obtained for various inorganic electrolytes using a square-wave charging technique[5]. The method seems to be more advantageous than the Lippmann electrocapillarometer or polarographic drop-time method[8] for studying the adsorption of highly surface-active organic compounds.

Acknowledgements

This work has been supported by a financial grant and a studentship (to E.M.L.V.) from the National Research Council of Canada. Valuable discussions and helpful suggestions from Z. KOWALSKI and P. T. VALERIOTE are gratefully acknowledged.

Lash Miller Chemical Laboratories,
Department of Chemistry,
University of Toronto,
Toronto 5, Ontario (Canada)

E. M. L. VALERIOTE
R. G. BARRADAS

1 Z. KOWALSKI AND J. SRZEDNICKI, *J. Electroanal. Chem.*, 8 (1964) 399.
2 Z. KOWALSKI AND J. SRZEDNICKI, *Roczniki Chem.*, 36 (1962) 565.
3 Z. KOWALSKI, private communication.
4 J. J. MCMULLEN AND N. HACKERMAN, *J. Electrochem. Soc.*, 106 (1959) 341.
5 R. G. BARRADAS AND E. M. L. VALERIOTE, *J. Electrochem. Soc.*, 112 (1965) 1043.
6 R. NARAYAN, *J. Electroanal. Chem.*, 4 (1962) 123.
7 D. C. GRAHAME AND R. PARSONS, *J. Am. Chem. Soc.*, 83 (1961) 1291.
8 R. G. BARRADAS AND F. M. KIMMERLE, *J. Electroanal. Chem.*, 9 (1965) 483.

Received November 15th, 1965

J. Electroanal. Chem., 12 (1966) 67–69

Oscillopolarographic analysis of phenols

TICHÝ[1], DOLEŽAL *et al.*[2] and MATYSIK[3,4] have recently shown that the analysis of phenols can be carried out using an oscillographic polarography method with alternating current as well as the well-known colorimetric, chromatographic and volumetric methods. The present work is concerned with the study of the oscillopolarographic behaviour of phenols in various supporting electrolytes, including acids, bases and salts over a wide range of acidity. The effect of bromine, and cations that form complexes with phenols, on the oscillopolarographic activity of phenol and cresols, was also investigated.

Experimental

The qualitative and quantitative determinations were carried out using a Krizik Type P576 Polaroscope. The phenol was dissolved in water to obtain a 10-m*M* stock solution. This solution was added to the base solution so that the final phenol concentration did not exceed 1 m*M*. Chemicals were Merck p.a. and water was doubly-distilled.

Results and discussion

The behaviour of some phenols in various base solutions is given in Table 1, where the position of each incision is described by means of the Q-value. From Table 1, it can be seen that phenol forms incisions only in Na_2HPO_4 and KH_2PO_4 although the cresols show activity in all these solutions, but the incisions in all cases are slight. The

TABLE 1

DETECTION OF PHENOLS AND CRESOLS

Supporting electrolyte	*pH*	*Compound*	*Incisions*	
			Q	*pD*
0.1 *M* HCl	1	phenol	—	—
		o-cresol	0.68	4.97
		m-cresol	0.68	4.97
1 *M* $KHSO_4$	1	phenol	—	—
		o-cresol	0.71	4.97
		m-cresol	0.71	4.97
0.01 *M* HCl	2	phenol	—	—
		o-cresol	0.68	4.97
		m-cresol	0.68	4.97
saturated KH_2PO_4 soln.	5	phenol	0.50	4.60
		o-cresol	0.57	4.97
		m-cresol	0.57	4.97
0.1 *M* $AlCl_3$	5	phenol	—	—
		o-cresol	0.51	4.97
		m-cresol	0.51	4.97
saturated sodium oxalate soln.	7	phenol	—	—
		o-cresol	0.47	4.97
		m-cresol	0.47	4.97
0.1 *M* sodium and potassium tartrate	7	phenol	—	—
		o-cresol	0.47	4.97
		m-cresol	0.47	4.97
saturated $NaHCO_3$ soln.	8	phenol	—	—
		o-cresol	0.52	4.97
		m-cresol	0.52	4.97
saturated Na_2HPO_4 soln.	9	phenol	0.44	4.98
		o-cresol	0.51	4.97
		m-cresol	0.51	4.97
0.1 *M* $Na_4P_2O_7$	9	phenol	—	—
		o-cresol	0.47	4.97
		m-cresol	0.47	4.97

phenol incisions are insufficient for its identification, and those of the cresols although enabling them to be identified as cresols, are insufficient to distinguish between *o*-cresol and *m*-cresol.

Solutions of KOH, NaOH, and citric acid and saturated solutions of $KClO_3$ and potassium biphthalate were also tried as supporting electrolytes (Group I). Other solutions tried were LiCl, KBr, $NaNO_3$, K_3PO_4, potassium hydrogen tartrate, H_3PO_4, $Al(NO_3)_3$, H_2SO_4 and $HClO_4$ (Group II). The cresols and phenol did not give incisions with Group I but in the electrolytes of Group II, the cresols gave even weaker incisions than those described in Table 1, and phenol showed no activity.

Small volumes (0.1–0.2 ml) of $FeCl_3$ and $AlCl_3$ solutions were added to improve the depolarizing activity as these cations form complexes with phenols. The Fe^{3+} ion forms complexes with phenols: these have been described by GORE AND NEWMAN[5]. However, no appreciable improvement in the sensitivity of the reaction was obtained, and no better incision in the curve $dE/dt = f(E)$. Similar results were obtained with the Al^{3+} ion.

With the same aim the effect of bromine on the incisions was studied; 0.5 ml of bromine water was added to the electrolyte solutions. Where necessary, the pH was first adjusted to fall in the range 0–4 to prevent the dismutation of the bromine. In

some instances, the addition of bromine water caused a deformation in the oscillopolarogram of the supporting electrolyte ($KHSO_4$, H_3PO_4). In others, the form of the oscillopolarogram remained unchanged. The latter cases showed, on one hand, the increased depolarizing activity of the cresols, and, on the other hand, the appearance of activity of phenol which was not observed in the absence of bromine water (0.1 *M* HCl, 0.1 *M* $AlCl_3$, 0.01 *M* HCl). With increasing acidity, the position of the incisions of phenol and the cresols is displaced towards the more negative potential values, and *Q*-values are very near to 1 when the pH of the solution is zero (1 *M* HCl).

Similar results to those obtained in HCl and $AlCl_3$ were obtained with a 0.5-*M* solution of LiCl acidified to pH 2 with hydrochloric acid. The *Q*- and p*D*-values are the same in both cases, but the oscillopolarogram is more stable with LiCl.

Figures 1, 2 and 3 show the oscillopolarograms for phenol, *o*-cresol and *m*-cresol in a supporting electrolyte composed of 5 ml of 0.5 *M* lithium chloride, pH 2. and 0.5 ml of bromine water (Fig. 4).

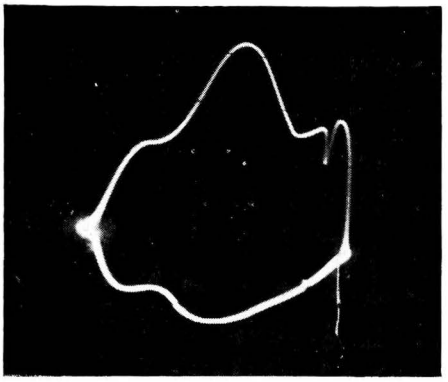

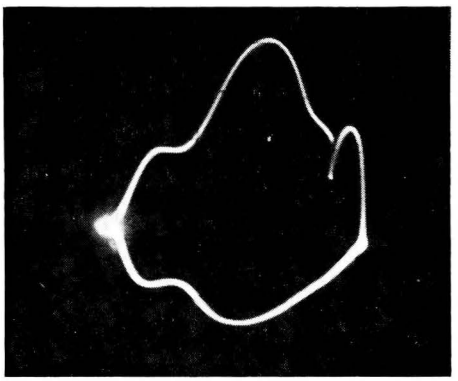

Fig. 1. The curve $dE/dt = f(E)$ in the determination of phenol, 16.7 μg/ml in 5 ml of 0.5 *M* LiCl and 0.5 ml of bromine water (pH 2). AC = 0.1 mA, DC = 3.0 mA.

Fig. 2. The curve $dE/dt = f(E)$ in the determination of *o*-cresol, 19.2 μg/ml; supporting electrolyte, see Fig. 1.

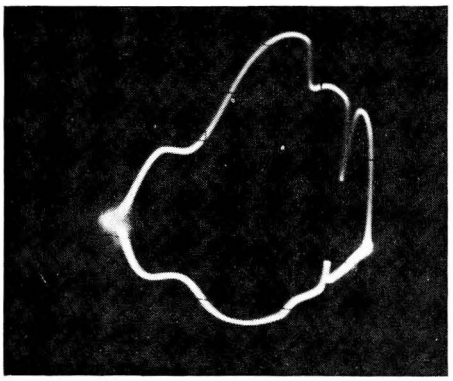

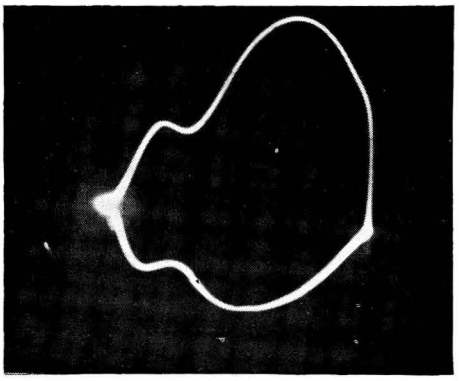

Fig. 3. The curve $dE/dt = f(E)$ in the determination of *m*-cresol, 9.6 μg/ml; supporting electrolyte, see Fig. 1.

Fig. 4. Supporting electrolyte, see Fig. 1.

Table 2 shows that all the phenols studied, except hydroquinone, catechol and pyrogallol, show activity under these conditions. Pyrogallol, catechol and hydroquinone do not produce incisions even at concentrations of 0.1 mg/ml. Phenol and *m*-cresol both produce a cathodic and an anodic incision. In both cases the anodic inci-

TABLE 2

DETECTION OF PHENOLS

Supporting electrolyte	*pH*	*Compound*	*Incisions*	
			Q	*pD*
5 ml 0.5 *M* LiCl with 0.5 ml bromine water	2	phenol	C: 0.85	5.72
			A: 0.85	4.70
		o-cresol	C: 0.82	5.01
		m-cresol	C: 0.86	6.01
			A: 0.86	5.70
		hydroquinone	—	—
		catechol	—	—
		resorcinol	C: 0.22	4.70
		pyrogallol	—	—
		phloroglucinol	C: 0.70	4.64

sion is slight. *o*-Cresol ($Q = 0.82$) only gives an anodic incision at concentrations greater than 50 μg/ml. Resorcinol also produces a decrease in the most negative region of the cathodic curve. The cathodic incision of phloroglucinol is slight.

Identification of one phenol in the presence of others

The characteristics of the incisions and the Q-values made possible:

(a) The identification of phenol in the presence of hydroquinone, catechol, resorcinol and pyrogallol.

Cresols will interfere with this, owing to the similarity of their anodic and cathodic Q-values. Phloroglucinol, although having a different Q-value, interferes because of the shape of the incision and also because of its greater reactivity with bromine. In the presence of a high concentration of phloroglucinol, phenol might not produce an incision. Resorcinol does not interfere notably, in spite of the decrease of the curve.

(b) The identification of *o*-cresol in the presence of hydroquinone, catechol and pyrogallol.

For the same reasons as above, phenol and *m*-cresol interfere. In this case, resorcinol interferes because of its lower pD value. Phloroglucinol interferes for the same reasons as above.

(c) The identification of *m*-cresol in the presence of hydroquinone, catechol, resorcinol, pyrogallol and phloroglucinol.

Phenol and *o*-cresol interfere. The high sensitivity of the activity of *m*-cresol minimises the interference of resorcinol and phloroglucinol.

(d) The identification of resorcinol in the presence of all the phenols tested.

It can be seen from the Q-values, that none of the phenols mentioned will interfere with the cathodic incision ($Q = 0.22$) of resorcinol.

Quantitative determinations

The depth of the incision was measured with reference to a luminous axis. A study was made of the relation between the "*h*"-value (the distance between the top of the incision and the potential axis) and the concentration of phenol in the cell with the intention of obtaining a quantitative relation. The graphs in Figs. 5 and 6 show that it is possible to make a calibration curve for the determination of *o*-cresol and *m*-cresol in the ranges 20–80 μg/ml and 4–9 μg/ml, respectively.

During these measurements it was observed that the depth of the incision decreased with time. However, it was proved that if the measurement of "*h*" was

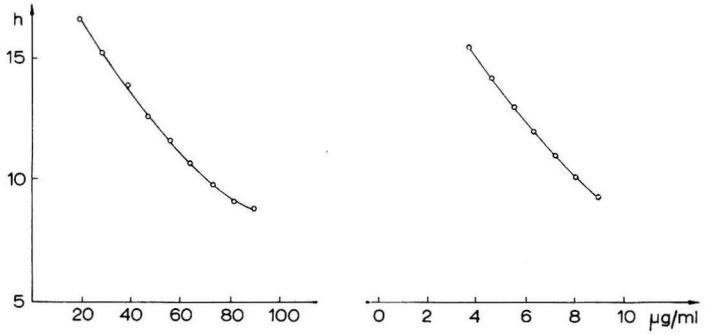

Fig. 5. Relation between the concn. and the depth of the incision of *o*-cresol, in a medium of 0.5 *M* LiCl at pH 2, and bromine water. AC = 0.15 mA, DC = 6 mA.

Fig. 6. Relation between the concn. and the depth of the incision of *m*-cresol, for medium see Fig. 5.

carried out as quickly as possible after the electrochemical reaction, good results were obtained. The "*h*"-values of the curves were measured in the first 6 sec. In spite of all these precautions the results obtained for phenol were not good.

The error in the determination of *o*-cresol and *m*-cresol was calculated to be $\pm 7\%$ and $\pm 10\%$, respectively. The error has not been calculated for the determination of a cresol in the presence of a non-interfering phenol.

Instrumental Laboratory, Department of Science, PATRICIA REYES G.
Faculty of Philosophy and Education, RICARDO AROCA M.
University of Chile, Santiago (Chile) ALFONSO MORALES B.

1 M. TICHÝ, Thesis No. P7, Charles University, Prague, 1961.
2 J. DOLEŽAL, V. KOPRDA AND J. ZÝKA, *Talanta*, 10 (1963) 621.
3 J. MATYSIK, *Ann. Univ. Mariae Curie-Sklodowska, Lublin-Polonia*, AA 16 (1961) 29.
4 J. MATYSIK, *Ann. Univ. Mariae Curie-Sklodowska, Lublin-Polonia*, AA 16 (1961) 37.
5 P. H. GORE AND P. J. NEWMAN, *Anal. Chim. Acta*, 31 (1964) 101.
6 J. MLODECKA, *Rev. Chim. (Bucharest)*, 10 (1959) 343.
7 C. O. HUBER AND J. M. GILBERT, *Anal. Chem.*, 34 (1962) 247.
8 Y. MIZUNOYA, *Japan Analyst*, 11 (1) (1962) 87.
9 N. T. CRABB AND F. E. CRITCHFIELD, *Talanta*, 10 (3) (1963) 271.
10 J. HEYROVSKÝ AND R. KALVODA, *Oscillographische Polarographie mit Wechselstrom*, Akademie-Verlag, Berlin, 1960.

Received August 10th, 1965

BOOK REVIEWS

Elementary Electrochemistry by A. R. DENARO, Butterworths, Washington, 1965, pages viii+222, $4.50 or 22s.6d.

This little book is "aimed primarily at students who propose to take the Part 1 examination of the Royal Institute of Chemistry but should prove useful... in degree courses". That is, it follows the pattern of most electrochemistry textbooks of the last thirty years, but in a condensed form which has led to the introduction of a number of misleading statements. Little attempt has been made to bring the material up to date, except in the short chapter on electrolysis, and this has resulted in a treatment that is divorced from modern practice.

In the preface one is first surprised to find that sign conventions for cells are relegated to an appendix, but on reading in the latter that the "European" convention is "characterized by the lack of any convention other than the adoption of the standard hydrogen electrode as the arbitrary zero of potential" (p. 206), one is relieved that the student is not muddled on this point in the text. The preface also makes a point that dimensions of quantities are specially considered and yet the dimension (as distinct from the units) of no electrical quantity is mentioned. The relation between absolute and international units is quoted to 6 figures (p. 7), yet the faraday is given as 96,500 C (p. 8), while there is no mention of the fact that most tabulated conductances are based on Jones and Bradshaw's data and are therefore in international units; it is indeed "possible that international units may be encountered in some accounts of electrochemistry" (p. 7).

Some of the diagrams are very unsatisfactory. The conductance cells on p. 15 are drawn in a way which suggests that the electrodes in the dip-type cell have no support other than the electrical connection and if the other cell were immersed in a thermostat the contacts would be submerged. There seems no need to perpetuate Figs. 2, 7 and 8, which neither represent present practice nor help understanding. In fact, there are many points in the text where it is unclear as to the way in which experiments are actually done, *e.g.*, it is not stated how an electrolyte of accurately known specific conductance is obtained (p. 17) nor how this was measured in the first place.

The only numerical values given for transport numbers are those for CdI_2 (p. 44)! The discussion of Washburn's experiments (p. 42) could well be omitted in an elementary book, but to quote the assumption that the proton is hydrated with one molecule of water without comment is inexcusable. The description of the electrophoretic effect (p. 25) is incorrect.

This list of comments could be continued, but enough has been said for the reader to assess the quality of the book. The cautious student with an able teacher *could* learn from it, but he could learn so much better elsewhere.

ROGER PARSONS, University of Bristol

Flame Spectroscopy, by RADU MAVRODINEANU AND HENRI BOITEUX, Allen Series, Wiley Series in Pure and Applied Spectroscopy, J. Wiley and Sons, Inc., New York, 1965, xiv+720 pages, 315s.

This treatise describes and discusses the basic knowledge necessary for the practice of flame emission and atomic absorption spectroscopy, and is one in the series covering pure and applied spectroscopy. This book is to be regarded as a "mod" version of the original *L'Analyse Spectrale Quantitative par la Flamme* which was originally published in France in 1954 by Masson. Needless to say, the book is true to the tradition already set by the previous numbers of this series. It is excellently produced both in printing and presentation, and is lavishly illustrated with photographs and diagrams of highest quality and commendable clarity. However, one should expect such a treatment for the price that has to be paid for it. Discussions of practical laboratory methods for the determination of elements are deliberately avoided. However, extensive references are given to published papers of this type.

The book is divided into three parts, 1 and 3 by MAVRODINEANU, and 2 by BOITEUX, and extends over 22 chapters. The titles of the parts are:

(1) Properties of the Flame. Construction and Use of the Excitation Source.
(2) Description of Flame Spectra and Analysis of the Excitation Conditions in the Flame.
(3) Flame Spectra Reproductions. Wavelength Tables. Complementary Bibliographies.

The first part describes in a most detailed manner the fundamental principles of flame production, inflammability, burning velocity, temperature contours, especially in relation to acetylene–oxygen flames. The coverage of the instruments available commercially is truly international, and construction and performance of machines are accurately but briefly described. Properties of the less common but very effective flames such as cyanogen–oxygen, hydrogen–perchloryl fluoride, are described. Even such recent developments as the plasma jet (both direct-current and high-frequency), atomic hydrogen, and augmented flames are given detailed treatments. The section continues with discussions of the regulation and measurement of gas flow and pressure, burners and atomizers from the original to most modern types. A chapter describing interferences occurring in radiations from the flame is also included, although "interferences" is not the correct term to use for some of the phenomena discussed, *e.g.* effect of variation of gas pressure on flame emission intensity. Finally, the section is completed with a discussion of atomic absorption spectroscopy, probably the fastest growing area of this field; consequently the chapter is a little dated.

Part 2 attempts to describe with a fundamental and theoretical treatment, atomic and molecular spectroscopy. Thus, the modern theories of molecular spectroscopy are related to the values of emission frequencies. The emission spectrum of unsalted air–acetylene flames, and acetylene–oxygen flames is given for all conditions, from very rich to very lean mixtures. Considerations regarding thermal equilibrium in flames, together with intensities and shapes of spectral lines complete this section. This section is the analysts' answer to those who say no mathematics is required for analytical work, for here it abounds. However, one must be honest and ask how many readers will use this section in their analytical studies; many less than there should be, would be a very safe assumption.

In Part 3 of the book, the wavelength tables are accompanied by excellent photographic reproductions of typical spectra and provide valuable reference works, but one feels that reproduction as traces from a densitometer (surely the usual manner today), would have been more appropriate. The wavelength tables cover about sixty pages, arranged in increasing wavelength numbers. The book is completed by a bibliography of the earlier works on flame spectroscopy, and an index of a quite detailed nature.

Thus, this book should provide an extremely powerful teaching aid and reference manual for flame spectroscopy. Certainly, it should be in most good libraries, but the price will keep its circulation down to a minimum, especially to the private individual.

G. NICKLESS, University of Bristol

J. Electroanal. Chem., 12 (1966) 75–76

CONTENTS

SUBMICRO METHODS OF ORGANIC ANALYSIS

by R. BELCHER
Professor of Analytical Chemistry,
The University of Birmingham, Great Britain

6 × 9″, ix + 173 pages, 12 tables, 35 illus., 186 lit. refs., 1966, Dfl.27.50, 55s., $10.00

Contents: 1. Introduction. 2. The balance. 3. General apparatus. 4. The determination of nitrogen. 5. Carbon and hydrogen. 6. Chlorine. 7. Bromine and iodine. 8. Fluorine. 9. Sulphur. 10. Phosphorus and arsenic. 11. Carboxyl groups. 12. Organic bases in non-aqueous media. 13. Alkoxyl and N-methyl groups. 14. Acetyl groups. 15. The carbonyl group. 16. Olefinic unsaturation. 17. Oxidation with periodate. 18. The determination of nitro and nitroso groups. 19. Thiol groups. 20. The cryoscopic determination of molecular weight. Index.

TECHNIQUES OF OSCILLOGRAPHIC POLAROGRAPHY

Second Edition, completely revised and enlarged
by R. KALVODA
Institute of Polarography, Czechoslovak Academy of Sciences, Prague, Czechoslovakia
with a preface by Professor J. Heyrovský

6 × 9″, 213 pages, 3 tables, 90 illus., 263 lit. refs., 1965, Dfl. 30.00, 60s., $11.00

Contents: Preface (J. Heyrovský); Author's Preface; 1. Introduction. 2. Examples of application of the oscillopolarographic method. 3. Practical oscillopolarographic exercises. 4. Maintenance of apparatus and construction of auxiliary electrical circuits. Index.

TABLE OF META-STABLE TRANSITIONS FOR USE IN MASS SPECTROMETRY

by J. H. BEYNON, R. A. SAUNDERS AND A. E. WILLIAMS
Research Department, Imperial Chemical Industries Ltd.,
Manchester, Great Britain

9½ × 6½″, xix + 392 pages, 1965, Dfl. 45.00, 90s., $16.50

These tables are intended to make it easy to determine the ionic reaction which gives rise to any meta-stable peak in a mass spectrometer, and will prove indispensable to any laboratory possessing this equipment. The introduction is given in English, German, French and Russian, to make the tables more generally useful.

STATIONARY PHASE IN PAPER AND THIN-LAYER CHROMATOGRAPHY

Second International Symposium organized by the Chromatography Group of the Czechoslovak Chemical Society, at Liblice
by K. MACEK AND I.M.HAIS

7 × 10″, 358 pages, 69 tables, 135 illus., 494 lit. refs., 3 coloured plates, 1965, Dfl. 42.50, 85s., $16.00

Contents: List of participants in the discussion. Introduction. Opening speech. I. Chromatography papers. II. Thin-layer materials. III. Stationary liquids and adsorbents in paper chromatography. IV. Stationary liquids and impregnations for thin layers. V. General problems of the stationary phase. Discussion. Closing remarks. Author index. Subject index.

ELSEVIER PUBLISHING COMPANY
AMSTERDAM LONDON NEW YORK